Skolkovo Institute of Science and Technology

DEVELOPMENT OF KW SCALE HYDROGEN ENERGY STORAGE SYSTEM

Doctoral Thesis

by

ALIYA GLAGOLEVA (KHAYRULLINA)

DOCTORAL PROGRAM IN MATERIALS SCIENCE AND ENGINEERING

Supervisor
Keith J. Stevenson

Co-Supervisor
Vasily I. Borzenko

Moscow - 2018

Abstract

Low-pressure metal hydride (MH) hydrogen energy storage is a new developing technology predominantly present in laboratory scale theoretical and experimental investigations, having a potential to couple renewable sources of energy (RES) and fuel cells (FC) in stand-alone generation systems due to the absence of the loss of capacity and maintenance. This dissertation introduces the tailored design, development, and experimental investigations of four different energy storage systems that comprise the foundation for system integration, intermetallic compounds composition, and heat and mass transfer intensification. The studies presented herein focus on two experimental systems that function as the foundation for low-pressure MH energy storage system integration and scalability: 1) the 175 W H2Bio system with two MH storages 140 l each and 2) the 1 kW H2Smart system, which is the primary focus of this dissertation, with one 1000 l MH storage, electrolyzer, and a PEM FC. These specially designed systems have helped to overcome significant fundamental limitations associated with heat and mass transfer in a porous intermetallic compound and thus improve efficiency rate of the system by utilizing exhaust heat from the FC. In the first chapter, state-of-the-art energy storage systems, hydrogen storage systems, and MH storage systems are described as well as the Batamai village case is presented. In the second chapter, an experimental system H2Bio of the power scale of 175 W is created to overcome initial system integration difficulties, test the concept, and obtain working regimes. In the third chapter, a novel energy storage simulation technology integrated into a physical environment is created to enable physical hardware-in-the-loop tests for a comparative analysis of different energy storage systems based on the electrical parameters. The fourth chapter focuses on preliminary kW scale qualitative and quantitative experiments that prove the

possibility of utilizing waste heat from the FC to maintain a desorption process in MH storage. The fifth chapter highlights the design, development, and system integration of a 1 kW H2Smart system with the novel type of air-heated MH storage, PEM FC, electrolyzer, and a regular 220 V output through an inverter. Also, the design, composition, and PCT diagram investigation of an intermetallic compound suitable for the design requirements obtained in the previous chapters are presented in this chapter. The dissertation concludes with an economical comparison of different energy storage systems suitable for the case of Batamai village, where the advantage of low operational costs and the absence of memory effect of MH storage systems bring proposed system to the comparable level of costs with regular Lead Acid batteries over the 10-15 years period of time. The novel methodologies and experimental systems described in this dissertation provide an experimental blueprint to help establish a solid physical/analytical foundation of this environmentally friendly energy storage technology.

Publications

1. A Khayrullina, V Borzenko. Air heated metal hydride energy storage system design and experiments for microgrid applications. *International Journal of Hydrogen Energy*. 2018. DOI: 10.1016/j.ijhydene.2018.05.145

2. A Khayrullina, D Blinov, V Borzenko. Novel kW scale hydrogen energy storage system utilizing fuel cell exhaust air for hydrogen desorption process from metal hydride reactor. *Proceedings of the 31st International Conference on Efficiency, Cost, Optimization, Simulation and Environmental Impact of Energy Systems ECOS 2018*. ISBN: 978-972-99596-4-6

3. A Sveshnikova, K Abrosimov, A Khayrullina, A Ustinov. Effect of ambient air conditions on PEM fuel cell performance. *Journal of Renewable and Sustainable Energy* 9, 044301 (2017). DOI: 10.1063/1.5001138

4. A Ustinov, A Khayrullina, V Borzenko, M Khmelik, A Sveshnikova. Development method of Hybrid Energy Storage System, including PEM fuel cell and a battery. *Journal of Physics: Conference series 745*, 032152 (2016). DOI: 10.1088/1742-6596/745/3/032152

5. A Jenkins, C Patsios, P Taylor, A Khayrullina, V Chirkin. Optimising virtual power plant response to grid service requests at Newcastle Science Central by coordinating multiple flexible assets». IEEE Xplore (2016). DOI: 10.1049/cp.2016.0812

Acknowledgements

Skoltech people (professors, students, researchers, and staff) have made an incredible impact on all aspects of my life. Coming from all corners of the world, showing me different edges of thinking they have continuously challenged my views and broadened my horizons. First I thank Professor Keith Stevenson for taking me in the last years of Ph.D. and helping me through them with his guidance, knowledge, and support. He has made himself available regardless of his duties; he always provided valuable feedback and taught me to think strategically, looking at a bigger picture.

Second, hydrogen laboratory director of our partner institution JIHT RAS Dr. Vasily Borzenko warmly welcomed me into his research group and guided my research all four years of the program from the very beginning to the last days of the process as my co-advisor. Without him, his guidance, and teaching skills, this thesis would not have been possible. I want to wholeheartedly acknowledge how grateful I am for his continuous time and effort he has put in my thesis and me.

Third, I thank Dr. Alexander Ustinov for giving me the opportunity to join Skoltech and start my journey of a Ph.D. student.

I want to also express my gratitude to the members of the CES group. Anna Sharova and Polina Rumyantseva you have always been at the forefront of the changing environment of Education system at Skoltech and helped us through. I thank all our collaborators and my co-authors for their experience and patience. There are a lot of professors who became genuine mentors and continue to be dear friends. There are also current and former students who have made an impact on my work and life at Skoltech. And there are people from the Education office who were always there to explain the procedures and help through the changing environment with their countless hours of selfless work. I cannot imagine Skoltech without any of them.

And, I owe my deepest gratitude to my husband, Maksim, who has always been there by my side, continually supporting me at each and every step I took, inspiring me at the times when I lost the way, helping me to believe in myself when I felt low, and just being there for me every day.

Table of Contents

List of Symbols, Abbreviations

AL-TES – aquiferous low-temperature thermal energy storage

CAES – compressed air energy storage

CAPEX – capital expenditures

CES – cryogenic energy storage

DER – distributed energy resources

DG unit – distributed generation unit

EDLC – electric double layer capacitor

ES – energy storage

ESS – energy storage system

FC – fuel cell

H2BS – hybrid hydrogen/batteries backup system

HT-TES – high-temperature thermal energy storage

IMC – intermetallic compound

MG - microgrid

MH – metal hydride

OPEX – operational expenditures

PCT diagram – pressure-concentration-temperature diagram

PEM – proton exchange membrane

PHS – pumped hydroelectric storage

PSB – polysulphide bromide battery

RES – renewable sources of energy

SMES – superconducting magnetic energy storage

SOC – state of charge

VRB – vanadium redox battery

List of Figures

List of Tables

Introduction

The wind, as a direct motive power, is wholly inapplicable to a system of machine labor, for during a calm season the whole business of the country would be thrown out of gear. Before the era of steam engines, windmills were used for draining mines; but though they were powerful machines, they were very irregular, so that in a long tract of calm weather the mines were drowned, and all the workmen thrown idle.

William Stanley Jevons, 1865 [1]

In the second half of the 19th century, people could only observe instability issues accompanying renewable energy sources (RES). Nowadays, it gets more evident that the technology for RES enters the market and has the potential to play a significant role in the overall energy production of the future. As an answer to the problem stated by Mr. Jevons in 1865, replacing fossil fuels with renewables or with the mix of renewable and nuclear energy sources people strive to solve instability issues by Energy Storage (ES) systems. Since most of RES are highly dependent on the uncontrollable external conditions, such as solar or wind, it is important to balance consumption and production adding some sources of power that can compensate for the fluctuations.

Current energy storage technology offers a variety of solutions for different situations, the first chapter of the current thesis starts with a comparative analysis of the energy storage technology applicable for Microgrids (MG) with an outcome that a case-based approach is necessary to determine suitable energy storage technology. For the purpose of this thesis, the description of the case of a typical Far East settlement is presented. Batamai and many other villages are located outside the centralized grid and experience high cost of energy due to diesel transportation issues. The first chapter then continues with a technology concept proposal for the case and current state-of-the-art in the chosen technology of hydrogen energy storage.

The research presented in this dissertation is a part of a collaborative effort of bringing metal hydride (MH) hydrogen energy storage systems to the kW scale system integration level as a viable technology for stand-alone applications where the absence of the loss of capacity is crucial for the operation. Our research team realized that a smaller power system must be experimentally tested to prove the proposed concept as well as to enable the investigation of electrochemical parameters of the hydrogen

storage reactor, electrical parameters of the system integration, pressure-concentration-temperature (PCT) diagrams of intermetallic compounds, heat and mass transfer processes in the reactor and the fuel cell (FC). This dissertation presents four different experimental systems designed for the aforementioned purposes, primary focusing on the MH storage system design and development using an experimental approach due to the limited amount of theoretical information available for kW scale MH storage system electrochemical parameters. Experimental setups were designed and developed to test the main elements of the concept, carrying out experimental research of heat and mass transfer processes in MH porous media during the sorption/desorption of pure hydrogen, as well as in the presence of impurities in the incoming gas.

The analytical review of modern scientific, technical, and methodological literature from the first chapter showed that for the conditions of the Far East settlements of Russia, the utilization of heat losses from the FC for the heat supply of MH reactors, the efficiency of the use of primary renewable energy can reach 60% and the energy recovery factor - 35-40%. It was also shown that MH hydrogen systems for storage and uninterrupted power supply are considered as an alternative to diesel generators and storage batteries. The primary scientific and technical goal of the project was to develop a safe low-pressure energy technology for the uninterrupted operation of stand-alone power generation unit by accumulating energy in hydrogen using excessive renewable energy and producing electricity in FCs. The first chapter concludes with goals and technical requirements for the storage system design and development.

Chapter two starts with the first system integration of the main elements of the proposed concept: MH storage and the PEM FC. The working regimes are investigated as well as a significant number of system integration errors and difficulties were maintained throughout the creation of the setup. Additionally, the chapter discusses the influence of ambient conditions, such as temperature and relative humidity, on the FC performance. The system integration points for improvement include (i) the need for backup supply (investigated in Chapter three); (ii) the presence of additional heat carrier that limits autonomous application of the technology (the new concept of internal excessive heat utilization was qualitatively assessed in Chapter four); (iii) the need for higher power output (new kW scale system was designed and developed in Chapter five using all outcomes of Chapters three and four); (iv) economical feasibility

of the concept (assessed in Chapter six).

The structure of the Thesis is presented in Figure 1.

Introduction	
Chapter One:	- technical comparison of ES technologies formulated the need for case-based approach - case introduction - technology proposal and state-of-the-art - goal of the research
Chapter Two:	- low-power proof of concept - the influence of ambient conditions - need for back-up supply (investigated in Ch.3) - the presence of additional heat carrier limiting autonomous operation (qualitatively assessed in Ch.4, heat carrier replaced in Ch.5) - the need for higher power output (Ch. 5)
Chapter Three:	- novel energy storage simulation methodology
Chapter Four:	- experimental investigations of an external heat carrier replacement by excessive FC heat output utilization
Chapter Five:	- design and development of a kW scale system utilizing proposed concept of external heat carrier replacement - working regimes of the system
Chapter Six:	- economical analysis and comparison with existing technologies and practical alternatives
Conclusion	

Figure 1. Structure of Thesis

Chapter three discusses the creation of a novel energy storage simulation methodology that enables a comparative analysis of the electric parameters of different types of energy storage systems. The system uses a battery emulator Regatron GSS coupled with the Triphase controller with integrated current demand from the simulated storage. For the purpose of this dissertation, four different types of batteries were tested with current demand from the 175 W PEM FC installed in the first experimental setup. As the outcome, a Lead Acid battery proved to be a suitable backup supply for the FC. The created concept gives a unique opportunity for physical testing without an expensive creation of separate experimental setups for each energy storage system.

Chapter four focuses on preliminary investigations of a kW scale hydrogen storage system. The experiments included internal and external temperatures measurement inside and outside the FC, the qualitative investigation of the hydrogen flow level during the desorption process maintained by an exhaust heat simulated to the

parameters of a real 1 kW PEM FC output heat.

In chapter five, the proposed technology is proved to be feasible for the design of hydrogen energy storage systems. The experimental setup H2Smart can be used to demonstrate the performance of the technology (as a proof-of-concept) for further commercial development. It can also serve as experimental equipment for research and development, a pilot zone for the development of regulatory and methodological documentation, and educational process equipment.

In chapter six, a financial analysis of the 30 kW system installed in the case of Batamai village shows that the absence of capacity loss and maintenance for MH systems brings the OPEX of the proposed systems to the comparable level with the same capacity Lead Acid batteries in a 10-15 year timeframe. Also, capital investments in MH hydrogen storage systems can reach 50-60 $ / kWh.

Experimental investigations have also proved that each hydrogen absorbing material needs to have experimental investigations due to the absence of proper modeling of fine disperse beds with chemical characteristics.

This dissertation, however, does not include theoretical investigation of the challenges but willingly focuses on the strategies of overcoming these challenges from one experimental setup to another, and provides valuable experimental insight to aid ongoing theoretical and experimental efforts towards transforming this laboratory level technology into real-world application.

Chapter 1 Energy Storage (ES) technologies and Case-based approach

Microgrid (MG) plays the role of the small electric power system that can be both interconnected with the utility grid as well as operate autonomously (island mode) [2],[3]. It usually consists of multiple energy sources, customers and energy storage units. When running in an islanded mode possible malfunction of an energy source will cause immediate active and reactive power shortage, which must be instantly compensated. ES technology for MG lowers the level of power fluctuations and deals with imbalance challenges between the demand side and the supply side. ES is the process of converting electrical energy from a power network to the form of energy that can be stored and easily converted back to the network when needed [4].

Electrical energy can be converted to many different forms of storage [5]: gravitational potential energy with water reservoirs, compressed air, electrochemical energy in batteries and flow batteries, chemical energy in fuel cells, kinetic energy in flywheels, magnetic field in inductors, electric field in capacitors.

Ever increasing reliance on electricity in industry, commerce, and home, power quality requirements, and the growth of RES brought technological development of ES to a new level. Many scientists reviewed the great variety of ES technologies, including Ibrahim et al. [6], Chen et al. [7], Huggins et al [8]. The necessity of such systems especially highlighted when an isolated area can not connect to the grid and has an intermittent energy source. Many examples of hybrid ES systems for residential MG are shown in the literature, with one of the most recent publications by Traore [9]. Additionally, Edison Electric Institute in 2017 released a report on different ES technologies [10], including pumped hydro, batteries, compressed air energy storage (CAES), thermal, etc. The report states that even in 2017 pymped hydro in US accounts for 95% of the installed storage capacity with thermal storage in the second place [11].

Current chapter starts with introducing great variety of ES technologies and functions with a note on latest developments in the field from systematic point of view. Then continues with techno-economic comparison of different ES technologies and concludes that a case based approach is necessary. In the section 1.5, a case of a small village in Yakutia is presented as a reference and a real pilot settlement for the introduction of RES, however, current thesis and research is dedicated for the

development of a technology feasible for application in many villages like the one presented. Following sections of chapter 1 propose an ES technology and introduce state-of-the-art in the chosen technology. The chapter concludes with the formulation of goals for the research.

1.1 ES as an essential part of each step in traditional electricity value chain

Due to the producer-consumer system that always goes in one direction the electricity must be fully used when produced. The demand, on the other side, varies every hour, every day, and every season. In order to meet short seasonal demand, large power plants are designed to meet peak level requirements and run inefficiently for the rest of the operational time. If energy storage is available for peak hours, power plants can operate on an average electrical demand level. That means that ES can follow the load changes, meet the peak hours, and work as a standby reserve. Thus, it enters the value chain of the electricity network and brings clear benefits. Electricity value chain has five components: energy source, generation, transmission, distribution, and customer-side energy service. Clear definition of the role of ES can be determined from an assumption that it is a separate sixth part of the chain.

In this case, it is a complex task to determine whether it should be connected in parallel to an energy source or included to the distribution line close to the consumer side for balancing the load. ES is the technology that is designed to be used in various applications and different ways, which is why it is not the sixth component of the value chain but an essential part of every step (depending on individual cases) as shown in Figure 2.

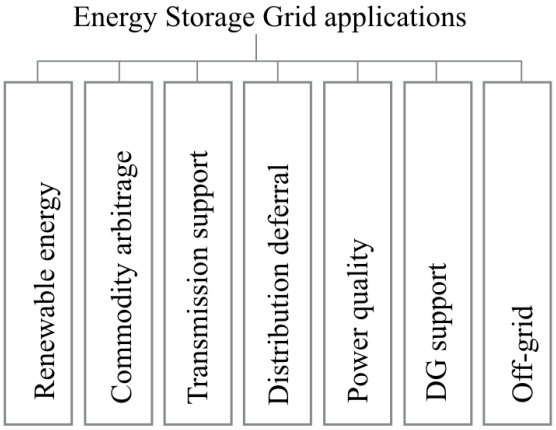

Figure 2. Applications of ES on the grid [13]

Primary functions of ES suitable for each of the five steps of electricity value chain form a broad range of possible applications [2]-[4], [6]-[14]. One of the examples of generation step applications is commodity storage that stores bulk energy generated at night and uses it for the peak demand periods during the day. It also allows arbitraging a production price of the two periods and uniforms load factor for the generation, transmission, and distribution systems. Other examples of generation step applications include contingency service for compensating power facility falls, area control for the prevention of unplanned transfer of power, frequency regulation for maintaining a state of frequency equilibrium during regular and irregular grid conditions, and energizing transmission system or assisting other facilities to start-up and synchronize to the grid. During the step of transmission and distribution, ES can ensure system stability by maintaining a synchronous operation of all components. Also, ES can stabilize voltage between each end of all power lines or eliminate additional transmission facilities to save capital that otherwise goes underutilized for years.

On the side of a customer, ES ensures energy service by shifting energy demand to reduce charges, eliminates secondary oscillation and disruptions, and bridges power during the times of disruption. For renewable sources of energy, ES can mitigate power delivery constraint present after insufficient transmission capacity. However, more importantly, ES can shape energy curve to fit the needs of a consumer. ES stores energy during the off-peak time of the day and discharges during the hours of maximum consumption when energy production from renewable sources is not available. ES can also meet shorter-term needs of the consumer by mitigating shortfalls in wind energy generation, supporting grid frequency during sudden decreases in wind generation, and suppressing fluctuations by absorbing and discharging energy during small variations.

ES has a broad range of different functions for all the major parts of an electricity value chain. As well as these functions, ES has a great variety of different technologies that form a complex task of finding a proper ES technology suitable for each case. Scientists and companies are often limited to the ES systems they research and work with, eliminating themselves from the great variety of other ES systems available.

1.2 MicroGrid-based applications benefiting from ES systems

Even though there are some similarities between ES systems for grid applications and

ES systems for MG applications they have fundamental differences as ES plays an essential role in MG. It maintains stability, integration of RES and power quality. ES is profitable to use in MG due to small capacity and small investments, besides that, MG benefits from using ES in the following ways: short term power supply, facilitating integration of RES, arbitrage, optimization of microsource in MG, power quality improvement.

"Energy buffer" concept has many similarities in the way grid-scale ES systems work towards integration of RES. In the Figure 3, a PV plant performance with the NaS battery storage is shown [15], without ES, the power output would not be stable. However, in order to use ES as RES integration tool, the technology must develop towards the immediate start and fast response time of ES. Many countries have different tariffs for peak and outside of peak hours. It is a great investment potential for ES start-ups to buy energy when peak hour is not present and to sell it back when the peak is reached. However, it is still extremely challenging to perform this investment as the ES system installation and maintenance costs are still considerably high.

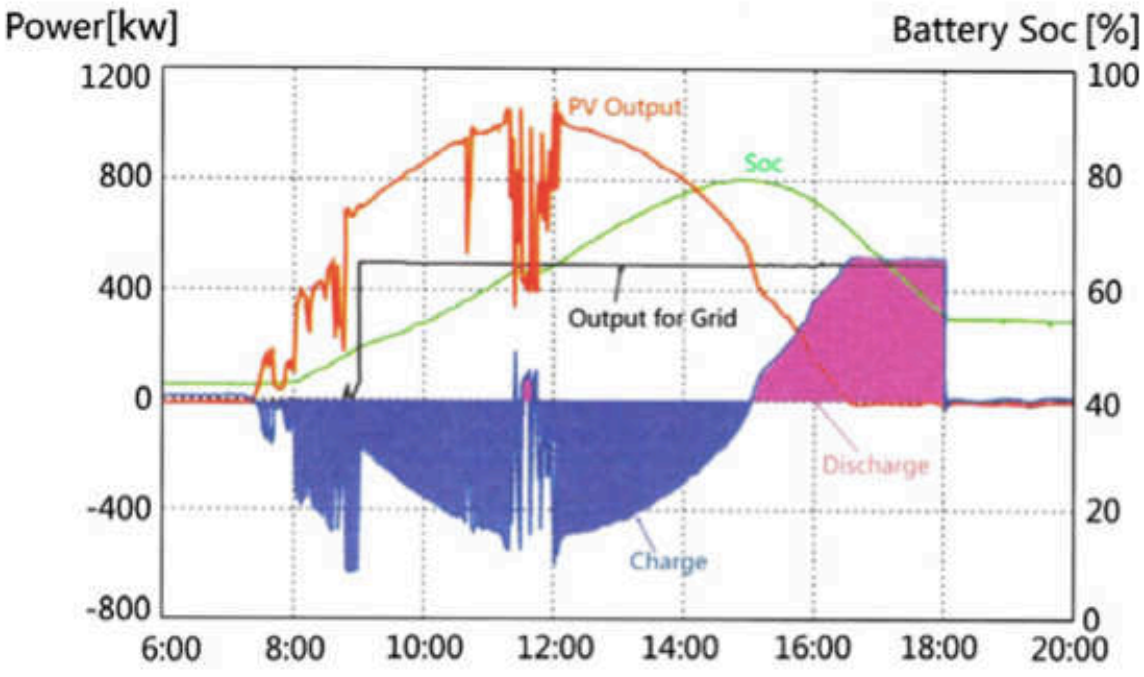

Figure 3. Performance of a PV plant with ES [15]: blue line is battery power, red line is PF output, black line is the output for the grid, green line is a SOC of the battery

Besides failures in the grids, there is an abnormal operation that might appear in the MG among the DG units. If some of the DG is experiencing shortage or fuel losses or low fuel pressure rates, ES will play a role of standby microsource to keep the level of

output power at the expected value. Since MG might be integrated into the utility grid, high power quality is needed. ES works as the regulator to provide specified active or reactive power for customers. For example, supercapacitor or FESS can resolve transient issues like system failures very fast.

Possible ES integration configurations include two ways: aggregated and distributed. In the Figure 4, all of the ESs are kept in one place, and the whole system integrated to MG as one piece. All the capacity can be used to balance power flow fluctuations [16,17]. It proved to show better performance over distributed ESs having the same capacity. Aggregated ES configuration connects to AC bus of an MG through an inverter. For an FES unit charging and discharging power by an induction machine at a variable speed, an AC/DC/AC converter interface is thereby compulsory, while for a SMES unit or capacitor storage, a DC/DC chopper is required before the voltage source converter (VSC) [18].

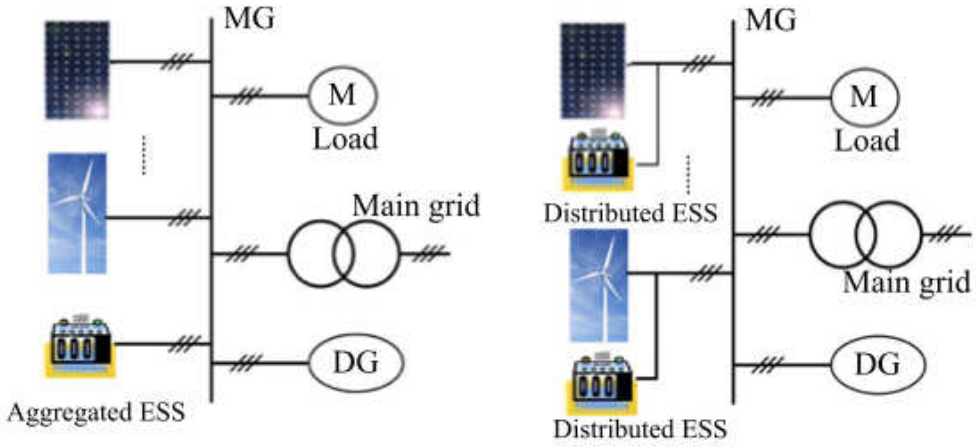

Figure 4. Typical aggregated (a) and distributed (b) ES configuration [16,17]

However, the capacity increase for aggregated ESS is associated with an increased capital costs. Thus, the advantages of distributed ESS are also significant due to being more flexible, efficient and easier to manufacture.

The optimization of the performance and the reduction of cost are less complex while distributed energy resources (DER) and ES pair is connected separately to the MG. The configuration of these pairs is also simpler as there is only one type of source. However, the power produced by the DERs has to be carried by the transmission lines before being stored in ESS. Though the power electronics interfaces might be individually optimized for both DER and ES, the storage will still experience losses. In

future MG, a mixture of the aggregated and distributed ES systems would be a preferable solution.

1.3 Advances and issues of ESS

1.3.1 Optimization issues (modeling and software)

Recent 20 years break-through in IT technology, such as modeling software and tools, made it possible to try most of the ideas in the digital world before going to the real testing mode. However, the field of ES still lacks necessary optimization tools and software. One of the most significant points to develop ES modeling further is the fact that little investigation is done in the field of mutual effects from ES to MG and back. The models might also work on the impact ES makes in the overall cost (both installation and maintenance), emissions, materials, efficiency, system lifetime, cycle life, etc. Models should also demonstrate an ES performance under varying load conditions, critical situations included.

Currently, there are both non-commercial and commercial models available; some typical non-commercial models include HOMER; ReEDS; NEMS; RETScreen, and EnergyPlus. Commercial models include GE MAPS; the Ventyx-ProMod and System Optimizer; Power World; Energy2020; IPM, and Dynastore [16]. By comparison, no model or software package could combine all of the characteristics to assess energy storage in the smart grid. Additionally, no model is specifically focused on the issues of optimization of storage. They are used for calculating system capacity, transmission modeling, and generation source placement.

Many available algorithms and models aim to predict ESS performance and lifetime, but these models still need to be further verified [19],[20]. For example, to evaluate the reliability of ESS, a system risk model must be established before the system can be quantitatively assessed with appropriate risk indices. The risk indices, such as loss of load expectation and loss of energy expectation [19], must be carefully chosen and quantized. So the modeling task is not just confined to ESS itself but a systematic methodology, involving accurate modeling and software analysis.

Maxwell Technologies and Ansoft have jointly developed a model of the supercapacitor for the Ansoft product Simplorer. EPRI has funded Power Technologies International to develop SMES and battery models for PSS/E. EPRI has also produced a bespoke model for evaluating the benefit of employing energy storage called

DYNATRAN (Dynamic Analysis of Interconnected Systems with Energy Storage), which uses Monte Carlo simulation to study unit commitment/dispatch [20].

The state-of-the-art simulation tools applied in feasibility studies worldwide include ES-Select, PLATOS Hybrid2, Homer, IPSYS and MATLAB/Simulink, and other. For example, ES-Select is a sophisticated, highly interactive, decision-support model that handles uncertainties in cost, benefits, efficiency, cycle life, and other parameters [21]. PLATOS has been developed to optimize the application of storage systems in electrical distribution networks with distributed energy resources [22]. Having diverse options, ES field still has no full ES environment model where all the existing technologies could be modeled manually solving a complex issue of sizing and locating ES in the MG.

1.3.2 Hybrid ES

Many ES technologies have different characteristics. Combination of the advantages of the few ES technologies successfully overcomes disadvantages of a specific technology. Few hybrid structures were presented and tested, some of them include a battery with EDLC, FC with battery or EDLC, CAES with battery or EDLC, battery with FESS and a battery with SMES. A hybrid ESs coordinated together with DGs in the MG will give higher efficiency than in the separate operation. However, hybrid ES requires a careful configuration and control (charge/discharge control, power flow optimization, etc.) otherwise the possibility of an unbalanced effect on MG occurs. Currently, an "if-then-else" strategy is widely used in engineering design, while cascaded control, fuzzy control, and knowledge-based advanced control are still under research [23].

1.3.3 Smart ESS

There is no clear definition of Smart storage, though some researchers describe smart storage system as the system with Stochastic Source Module, Short Term Storage Module, and Medium/Long Term Storage Module [24]. This definition aligns with the definition of Hybrid ES thus needs to be revised. Expectations towards Smart ES include power electronics interfaces, high efficient energy management systems, control systems, HMIs (human machine interface), and communication interfaces for interconnection with upper controllers, all of these technologies are expected to be incorporated [25]. Also, flexibility and "plug & play" equipment with PC are needed.

The system proposed by the U.S. DOE Solar Energy Program [26], which includes inverters, energy management systems, control systems and provisions for ES, can be called as a first "Smart ES rudiment" [23].

Correct integration of ESs with other smart grid devices, such as FACTS (Flexible AC Transmission Systems) and DERs, can provide independent active and reactive power absorption into the grid or injection to the grid, which leads to an economical and flexible transmission controller [18]. The independent control of power with an ESS/FACTS system makes it an ideal candidate for many types of power system applications, including voltage control and oscillation damping [23]. FACTS being integrated with ESS becomes an enhanced ESS equipment to provide advanced power regulation.

1.4 Comparative analysis of ES technologies

1.4.1 Technical maturity

PHS and lead-acid battery are mature technologies and have been used for over 100 years. CAES, NiCd, NaS, ZEBRA Li-ion, Flow Batteries, SMES, flywheel, capacitor, supercapacitor, AL-TES, and HT-TES are considered as technologies in the developed stage, which means that they are technically developed and available on the commercial market. However, the number of large-scale applications of these technologies are still insufficient in number. The issues of reliability are still open for the electricity industry [7],[27]-[43].

The rest of the technologies, such as Solar Fuel, CES, Metal-Air battery, and Fuel Cells [35],[37]-[42], are currently under development. They are not fully present on the market regardless of the investigation level of various institutions. These technologies still have some potential to lower energy costs and mitigate environmental concerns in the future.

1.4.2 Power scale and discharging time

The power ratings of various ESS are compared in Table 1. The ESs can be divided into three categories based on their applications: energy management, power quality, bridging power.

CAES, CES, and PHS are more suitable for energy management purposes in the scales above 100MW of power output [7],[30],[42]; they can serve for load leveling,

ramping, spinning reserve. Large batteries, flow batteries, fuel cells, solar fuels, CES and TES, are suitable for medium scale applications in the range from 10 to 100 MW [31],[35],[39]-[43].

Power quality issues, such as instantaneous voltage drop, short duration UPS, require a high-speed response (sometimes, milliseconds). Flywheel, batteries, capacitors, SMES, and supercapacitors ensure fast response [27],[29]-[31]. These types of applications usually do not exceed 1 MW.

Batteries, flow batteries, fuel cells, and Metal-Air cells have both a relatively fast response (<1 s) and a long time of discharge (hours) [27],[28],[33]-[35]. Therefore, they can be used for the bridging power. The scale of such applications typically in the range of 100kW to 10 MW.

Table 1. Comparison of technical characteristics of ES systems [7]

Systems	Power rating and discharge time		Storage duration		Capital cost		
	Power rating	Discharge time	Self discharge per day	Suitable storage duration	$/kW	$/kWh	cent/kWh-Per cycle
Fuel cells	0-50 MW	Seconds-24 h+	Almost zero	Hours-months	10,000+		6000-20,000
PHS	100-5000 MW	1-24 h+	Very small	Hours-months	600-2000	5-100	0.1-1.4
CAES	5-300 MW	1-24 h+	Small	Hours-months	400-800	2-50	2-4
Li-ion	0-100 kW	Minutes-hours	0.1-0.3%	Minutes-days	1200-4000	600-2500	15-100
Lead-acid	0-20 MW	Seconds-hours	0.1-0.3%	Minutes-days	300-600	200-400	20-100
NiCd	0-40 MW	Seconds-hours	0.2-0.6%	Minutes-days	500-1500	800-1500	20-100
NaS	50 kW-8 MW	Seconds-hours	~20%	Seconds-hours	10003000	300-500	8-20
ZEBRA	0-300 kW	Seconds-hours	~15%	Seconds-hours	150-300	100-200	5-10
Metal-Air	0-10 kW	Seconds-24 h+	Very small	Hours-months	100-250	10-60	
VRB	30 kW-3 MW	Seconds-10 h	Small	Hours-months	600-1500	150-1000	5-80
ZnBr	50 kW-2 MW	Seconds-10 h	Small	Hours-months	700-2500	150-1000	5-80
PSB	1-15 MW	Seconds-10 h	Small	Hours-months	700-2500	150-1000	5-80
Solar fuel	0-10 MW	1-24 h+	Almost zero	Hours-months	-	-	-
SMES	100 kW-10 MW	Milliseconds-8 s	10-15%	Minutes-hours	200-300	100010,000	
Flywheel	0-250 kW	Milliseconds- 15 min	100%	Seconds-minutes	250-350	1000-5000	3-25
Capacitor	0-50 kW	Milliseconds - 60 min	40%	Seconds-hours	200-400	500-1000	
Super-capacitor	0-300 kW	Milliseconds - 60 min	20-40%	Seconds-hours	100-300	300-2000	2-20
AL-TES	0-5 MW	1-8 h	0.5%	Minutes-days		20-50	
CES	100 kW- 300 MW	1-8 h	0.5-1.0%	Minutes-days	200-300	3-30	2-4
HT-TES	0-60 MW	1-24 h+	0.05-1.0%	Minutes-months		30-60	

1.4.3 Storage duration

Among significant characteristics of ES technologies, every day self-discharge is a limiting factor of energy storage. Table 1 illustrates that Fuel Cells, Metal-Air Cells, solar fuels, CAES, PHS, and flow batteries can be used for long periods of storage due

to very low energy dissipation on a daily basis. For the period that does not exceed ten days NiCd, Li-ion, TESs, Lead-Acid, and CES are the better option with a medium level of self-discharge [32],[33],[42],[43]. NaS, ZEBRA, SMES, capacitor, and supercapacitor have a very high self-charge ratio of 10–40% per day. They can only be implemented for short cyclic periods of a maximum of several hours. High working temperatures can explain high self-discharge rates of NaS and ZEBRA as they need to maintain self-heating through the use of stored energy [7].

Shortest reasonable period of storage does not exceed tens of minutes for flywheels. They discharge all the amount of stored energy within a day.

1.4.4 Capital cost

Capital cost is one of the major factors for ES systems to enter an industrial market. Capital cost is shown in Table 1, in the following dimensions: cost per kWh, per kW and per kWh per cycle. All the costs per unit energy are shown in the table. The division used the storage efficiency to obtain the cost per output (useful) energy. The cost per cycle is obtained using the cost per unit energy and the cycle life. It is one of the practical ways to evaluate the cost of energy storage in the situation of frequent charging and discharging regimes.

The capital cost of lead-acid batteries is comparatively low. However, they are not the least expensive possibility for energy management applications because they have a short life cycle for this type of use. In this type of calculation, the costs of maintenance, disposal, and operation are not considered due to a low amount of available information for the emerging technologies.

The division, shown in Table 1, shows that CAES, Metal-Air battery, PHS, TESs, and CES are in the low range of the capital cost per kWh. While the Metal-Air batteries show high energy density and relatively low cost they have an unsatisfactory life cycle and are currently under development. Speaking about more developed technologies, CAES has the lowest capital cost compared to all the other systems. The capital cost of batteries and flow batteries is still higher than the break-even cost upon the PHS, but the difference is slowly closing. For high power and relatively short working time applications the SMES, flywheel, supercapacitors, and capacitors are the best option due to cheap high output power even though their storage energy capacity is more expensive. PHS and CAES show the lowest costs per cycle among all the ES

technologies. Batteries and flow batteries have higher costs per cycle, but the decrease in the latest is expected with the development of the technologies. CES considered as a promising technology with some potential for lowering cycle costs, but it is not yet present on the market. Among the highest costs per cycle are the fuel cells and no information is available to estimate these costs for the solar fuels as they are at the development stage.

It is also useful to highlight that capital cost of different energy storage technologies and systems can differ from current estimations predominantly due to recent breakthroughs, system building locations, countries, sizes of the system.

1.4.5 Efficiency issue

The cycle efficiency is the ‘‘round-trip” efficiency defined as $g = E_{out}/E_{in}$, with g, E_{out} and E_{in} being the cycle efficiency, electricity input and electricity output, respectively. The self-discharge loss during the storage is not considered. Regarding efficiency, ES systems can be divided into three big groups:

SMES, flywheel, supercapacitor, and Li-ion battery have a very high cycle efficiency of > 90% [27],[29],[30],[33]. PHS, CAES, batteries (except for Li- ion), flow batteries and conventional capacitor have a cycle efficiency of 60–90% [7],[28],[30],[31]. Storing electricity by compression and expansion of air is more often less efficient than pumping water, since rapid compression increases the temperature of gas, increasing its pressure thus making further compression more energy- consuming. Hydrogen, DMFC, Metal-Air, solar fuel, TESs, and CES have efficiency rates less than 60% predominantly due to large losses during the conversion from the AC side to the storage system [35],[43]. Hydrogen storage of electricity has relatively low energy efficiency (20– 50%) due to the combination of electrolyzer efficiency and the efficiency of re-conversion back to electricity. There is a trade-off between the capital cost and round-trip efficiency. Low capital cost with a low efficiency can compete with high cost and high-efficiency level.

Table 2. Comparison of technical characteristics of ES systems_2 [7]

Systems	Energy and power density				Life time and cycle life		Influence on environment	
	Wh/kg	W/kg	Wh/L	W/L	Life time (years)	Cycle life (cycles)	Influence	Description
Fuel cell	800-10.000	500+	500-3000	500+	5-15	1000+		Depends on the fuel
PHS	0.5-1.5		0.5-1.5		40-60		Negative	Destruction of trees and green land for building the reservoirs
CAES	30-60		3-6	0.5-2.0	20-40		Negative	Emissions from combustion of natural gas
Li-ion	75-200	150-315	200-500		5-15	1000-10.000+		
Lead-acid	30-50	75-300	50-80	10-400	5-15	500-1000	Negative	Toxic remains
NiCd	50-75	150-300	60-150		10-20	2000-2500		
NaS	150-240	150-230	150-250		10-15	2500		
ZEBRA	100-120	150-200	150-180	220-300	10-14	2500+		
Fuel cell	800-10.000	500-	500-3000	500-	5-15	1000+		Depends on the fuel
Metal-Air	150-3000		500-10,000			100-300	Small	Little amount of remains
VRB	10-30		16-33		5-10	12,000+	Negative	Toxic remains
ZnBr	30-50		30-60		5-10	2000+		
PSB	-	-	-	-	10-15			
Solar fuel	900-100.000		500-10,000		-	-	Benign	Usage and storage of solar energy
SMES	0.5-5	500-2000	0.2-2.5		20+	100,000+	Negative	Strong magnetic fields
				1000-4000				
Flywheel	10-30	400-1500	20-80	1000-2000	15	20,000+	Almost none	
Capacitor	0.05-5	-100.000	2-10	100,000+	5	50.000+	Small	Little amount of remains
Super-cap			2.5-15	500-5000	10-30	100,000+	Small	Little amount of remains
AL-TES	80-120		80-120		10-20		Small	
CES	150-250	10-30	120-200		20-40		Positive	Removing contaminates during air liquefaction
HT-TES	80-200		120-500		5-15		Small	

1.4.6 Energy and power density

The power density (W/kg or W/liter) is calculated by the output power divided by the volume of the storage. Moreover, the energy density equals to stored energy divided by the volume. In Table 2, the FC, Metal-Air battery, and Solar fuels have a notably high energy density (typically 1000 Wh/ kg), although, as mentioned above, their cycle efficiencies are quite low. Batteries, TESs, CES, and CAES, have medium level energy density [7].

The energy density of PHS, SMES, Capacitor/supercapacitor, and flywheel are below 30 Wh/kg, which puts them in the lowest positions. Nonetheless, the power densities of SMES, capacitor/supercapacitor, and flywheel are very high which is suitable for some applications with significant discharge current and realtively fast response. Li-ion and NaS have higher energy density compared to other conventional batteries. The energy density of flow batteries is slightly lower than those of conventional batteries. Also, there are differences present in the energy density of the ESS made by different manufacturers but representing the same type of ES.

1.4.7 Lifetime

Lifetime and cycle life for various ESs are compared in Table 1. The cycle lives of ES systems with electrical technologies are very long, usually greater than 20,000.

Examples include SMES, capacitor, and supercapacitor.

Thermal and mechanical energy storage systems, including CAES, flywheel, PHS, AL-TES, CES, and HT-TES, also have long cycle lives. Since these technologies base on conventional mechanical engineering, their life time is limited by the life time of the mechanical components.

The cycle abilities of batteries, flow batteries, and fuel cells do not show high results as chemical processes affect operating time. Some of the technologies, for example, a Metal-Air battery has only few hundred cycles, and it needs to be further improved.

1.4.8 Influence on the environment

Regarding positive influences, solar fuel and CES are on the front of the technologies. Solar fuels produce electricity from renewable energy and store it in hydrogen, which decreases the use of fossil fuels. CES removes contaminates during the charging process of liquefaction, which mitigates the results of the burning of fossil fuels.

PHS, CAES, batteries, flow batteries, fuel cells and SMES have negative influences on the environment due to different reasons [29],[31],[34],[35]. The construction of PHS systems inevitably involves the destruction of trees and green lands for building reservoirs. This type of construction changes the local ecological system, which may have environmental consequences. The major drawback of PHS lies in the scarcity of available sites for two large reservoirs and one or two dams. CAES is based on conventional gas turbine technology and involves combustion of fossil fuel hence emissions can be an environmental concern. Also, a great limitation of the available landscape possesses the main disadvantage for CAES as it is only economically feasible for power plants with rock mines, salt caverns, aquifers or depleted gas fields in the close distance. In addition, CAES is not an independent system and has to be associated with a gas turbine plant.

Batteries and flow batteries have toxic remains/wastes. The major environmental of the implementation of SMES is a strong magnetic field that can be harmful to human health. Other ES systems have relatively small influences on the environment, as they do not involve fossil combustion, landscape damage, and toxic remains.

To sum up, energy storage technologies cover a wide range of different criteria that differ from case to case: power scale, discharge time, self-discharge, capital and operational costs, efficiency, energy and power density, environmental effect. The

choice of energy storage technology must be conducted on a case-to-case basis. The case that initiated this thesis is described below.

1.5 Case description: power production in Far East Settlements of Russia

More than 900 settlements in Russia are not connected to the centralized grid. These settlements are powered up by diesel engines built in the last century. The cost of one kWh is high due to diesel fuel transportation costs, which normally occurs only in the winter period, as there are no roads except for winter trails upon frozen rivers, and low efficiency rate of these engines. It is needed 30 times more Russian rubles to generate 1 kWh than the average in Russia, and this price difference is fully subsidized from the state budget. The need for sustainable energy in these areas is estimated at 2,54 bln kWh per year [44]. According to the solar energy potential map, most of the decentralized areas have 3,5 to 4,5 kWh per m2/day [45].

Typical daily load of a small town (Figure 5) from this area has been studied in order to identify the peak consumption for the periods of maximum load. This case particularly describes Batamai town with the population of 233 people, located at 63°31’00’’N 129o26’00’’E. Maximum daily load reaches 65-70 kW, minimum - 3 kW. In the Figure 5, only January and October daily loads are shown due to the presence of peak consumption rates during these months.

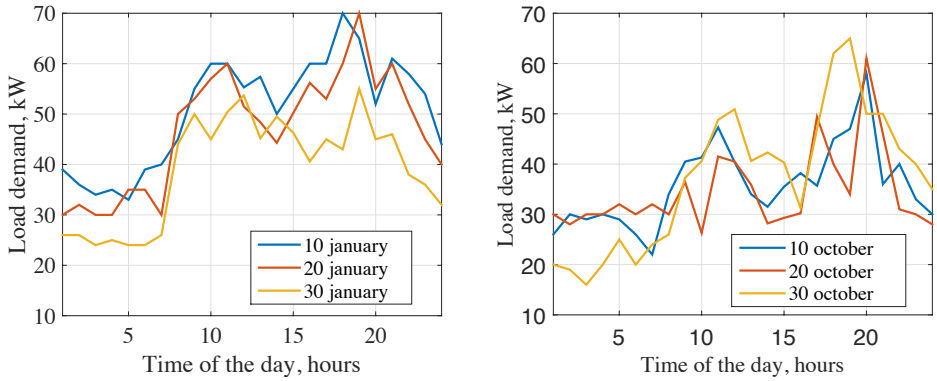

Figure 5. Batamai village demand (January 3 days, October 3 days) [46]

The replacement of diesel engines with autonomous power generation systems that include solar panels and energy storage systems has an opportunity to reduce the price for energy in these regions. A system of solar panels was installed in Batamai town (Figure 6).

Figure 6. Batamai village solar PV system [47]

The installed system consists of 52 units of JRM-195 solar PVs (China) covering 10140 W, 73 units of FSM-230 (Russia) covering 16790 W, 13 units FSM-250 (Russia) covering 3250 W, 120 units of ECS-250M60 (China) covering 30 000 W. Besides solar PVs, 3-phase invertors 10 kW each were installed in the following quantity: 3 units of SMA Sunny Tripower STP 10000TL-10 (Germany) and 3 units of SMA Sunny Tripower STP 10000TL-20 (Germany) [47].

As the result of installation, solar panels in different years were installed in different capacity, steadily growing to reach 60 kW of total capacity installed. In the years 2011-2014, 132,100 kWh of electricity was produced, saving 40.43 tons of diesel, and, as a result, saving 1,541,800 rub. The year 2015 alone had 48,840 kWh of produced electricity, saved 14.45 tons of diesel and 584,010 rub [47].

Table 3. Electricity production from solar panel PVs in Batamai town [47]

	Electricity generation, thousand kWh	Diesel fuel saving, tons	Savings, thousand rubles
2011-2014	132.10	40.43	1,541.80
2015	48.84	14.45	584.01
2016 (10 months)	49.00	13.62	593.59
Total:	**229.94**	**68.50**	**2,719.40**

If energy storage systems would be installed together with solar panels in the cities like Batamai, the higher diesel engine replacement percentage could be achieved. The proposed technology should function as an energy storage technology to be coupled with solar panels. Prefferably, the proposed concept should have a modular design as villages across far east settlements can differ in number and load needs. Additionally, the concept should be easy-to-use "black box" solution to avoid high maintenance cost and high qualification needed from the personnel. In the next subsection, a proposed technology will be compared to existing solution of diesel engines and another proposed technology – lead acid batteries.

1.6 Proposed ES technology

Since the limitation of a specific case of Far East Settlements in Russia includes the low availability of engineers to provide maintenance and higher reliability risks, the proposed technology has both low maintenance need and higher reliability compared to diesel engines. Additionally, compared to battery systems, proposed hydrogen energy storage (Figure 7) has no loss of capacity over time and stable to temperature differences. It is easily scalable as it can be designed in modules. Even though capital costs are high at this stage of research and development, present thesis aims to make a step towards connecting laboratory discoveries to practical applications through the creation of full cycle system prototypes of different scale.

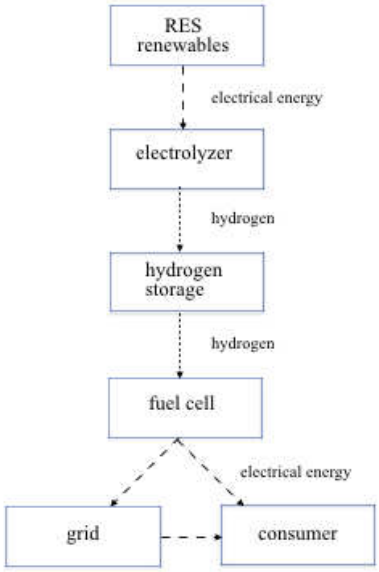

Figure 7. General Idea of the proposed technology

In the variety of fuel cells, the case of Far East settlements of Russia again provides limitations that a fuel cell needs to have working regimes at the near ambient temperatures, eliminating high-temperature fuel cells (SOFC, PAFC, MCFC). PEM fuel cell has high maneuverability characteristics. It can be integrated to modular design of a proposed technology as different sizes of settlements have different demand and cannot afford to have different solutions for each settlement separately. There is also a very low environmental intrusion due to the byproducts produced with the absence of combustion and vibration, with no moving parts and working in silence. PEM fuel cell proved to be reliable also in terms of the development of technology with the presence of commercial products and being present on the market as a back-up power supply for a long time.

Theoretically, a solution with low temperature MH storage system with an air-cooled PEM fuel cell for kW scale stationary application has been proposed [48],[49]. The system has zero CO2 emissions, low operational costs (OPEX), and no loss of capacity over time compared to batteries. Even though the capital costs (CAPEX) are still hardly comparable with the same cost category for batteries, the research in [50] shows that the operation period of 10 years and higher make it considerable for the proposed system to be investigated. In the proposed scheme, hydrogen energy storage technology is a so-called “green” technology. The variety of different hydrogen storage system is investigated in the next section.

1.7 Hydrogen storage technology

A critical component of the development of hydrogen energy and hydrogen economy is the search for economically justified methods for storage and transportation [51]-[56]. Principal concerns of hydrogen usage are regarding the low density (0.0899 kg / m3), the low temperature of liquefaction, high explosiveness, an adverse effect on the properties of structural materials [57],[58]. Currently, a case-based approach is applied to the hydrogen technology justification. For example, transport applications [59],[60], where mass characteristics are a limiting factor, the high-pressure tank system is the best choice, and for stationary applications, cryogenic or underground storage is more suitable, depending on the scale of the project. Depending on the physical essence, hydrogen storage technologies include [58],[61]:

- physical methods;

- adsorption;

- chemical methods;

- in the form of metal hydrides or intermetallic compounds (IMC).

For an effective fuel supply system for an FC, these technologies need to be compared from the viewpoint of the operating conditions (temperature, pressure) and the possibility of synthesizing hydrogen-containing materials that are sufficient for specified amounts of hydrogen storage.

1.7.1 Physical methods of hydrogen storage

The most traditional method of hydrogen storage is the storage in a gaseous state in the cylinders of standard pressure and volume (40 liters, 15.0 MPa). The process does not have sufficient differences from the storage and transportation methods of other gases. Additionally, gasholders, natural and artificial underground reservoirs are also used [62]. To increase the efficiency of this technology the hydrogen pressure needs to be increased as well. Modern high-pressure composite cylinders allow 6% mass content of hydrogen and higher (pressures up to 70 MPa) (Figure 8). Various types of hydrogen storage cylinders present different mass content and bulk density characteristics [61].

Figure 8. 700 bar hydrogen storage type IV vessel; mass: 28 kg, storage capacity 5.2%wt (21^{o}C)

The disadvantages of this technology include hydrogen corrosion of structural materials and the need for expensive hydrogen compression, which is a complex procedure due to a high leakage rate of hydrogen through movable seals. Also, the safety issues of such systems present difficulties for the technology to be utilized on the market, especially in transport applications.

The storage of hydrogen in the liquid state is characterized by a high mass density at a bulk density of 70 kg / m3 as the process requires the pressure level equal to or slightly higher than atmospheric pressure with no need for increased strength characteristics of the tanks. However, the energy costs for liquefaction and losses due to the Roth-para conversion [58] and heat influx to the cryogenic vessels make the application of this technology economically viable for the large volumes only, for example, in the space industry.

1.7.2 Adsorption methods of hydrogen storage

Adsorption methods of hydrogen storage are associated with the interaction of hydrogen with the surface of the adsorbent [61]-[63],[64] using van der Waals forces. This interaction is considered to be weak. It extends to one monolayer depth for the temperatures above critical (32.98 K at 1.31 MPa). Therefore, hydrogen storage materials must have a high specific surface (Table 4).

Table 4. Adsorption of hydrogen by carbon nanomaterials and zeolites [65].

Material	**Formal surface, m2 / g**	**Absorption H2,%wt**	**Adsorption conditions**
Carbon nanofibers	-	0,7	20^{o}C, 10 MPa
Carbon nanofibers + liquid crystals	1758	3,5	77,3 K, 0,8 MPa
Single-walled nanotubes	2560	4,5	77 K, 0,1 MPa
	-	0,5	25^{o}C, 0,1 MPa
Multi-walled nanotubes	-	2,27	77 K, 10,3 MPa
	-	0,3	25^{o}C, 10,61 MPa
ZSM-5	-	0,7	77 K, 0,1 MPa
NaY	725	1,8	77 K, 1,5 MPa
CaX	-	2,19	77 K

Zeolites are characterized by the low values of hydrogen storage capacity, particularly at the room temperatures. It explains their inability to compete on the market of hydrogen storage systems.

In [66]-[70], high hydrogen sorption capacity of activated carbons was reported to reach up to 10 ÷ 13%wt at 77 K and 5.5 MPa. The higher capacity of carbon nanotubes and nanofibers was noted in [71],[72]. However, these studies were not sufficiently reliable and did not proceed beyond experimental results. In [73],[74], well-qualified carbon nanomaterials suggest that the initial optimism regarding their use for hydrogen storage systems is unjustified. Figure 9 presents the results of electrochemical measurements [63],[64] of the reversible hydrogen content versus the specific surface

area of several samples of carbon nanotubes and graphite with a high specific surface. Figure 9 also presents theoretical limits for the mass content of hydrogen in carbon nanotubes (3% mass content at a specific surface of 1315 m2 / g and a temperature of 77 K).

Recently, high-porosity organometallic frameworks (MOFs) with a high specific surface area (up to 3000 m2 / g) became interesting for the researchers [65],[75],[77]. MOFs represent a new class of polymeric materials, the structure-forming elements of which are mononuclear or polynuclear coordination centers in the form of ions of metals, bound by organic fragments.

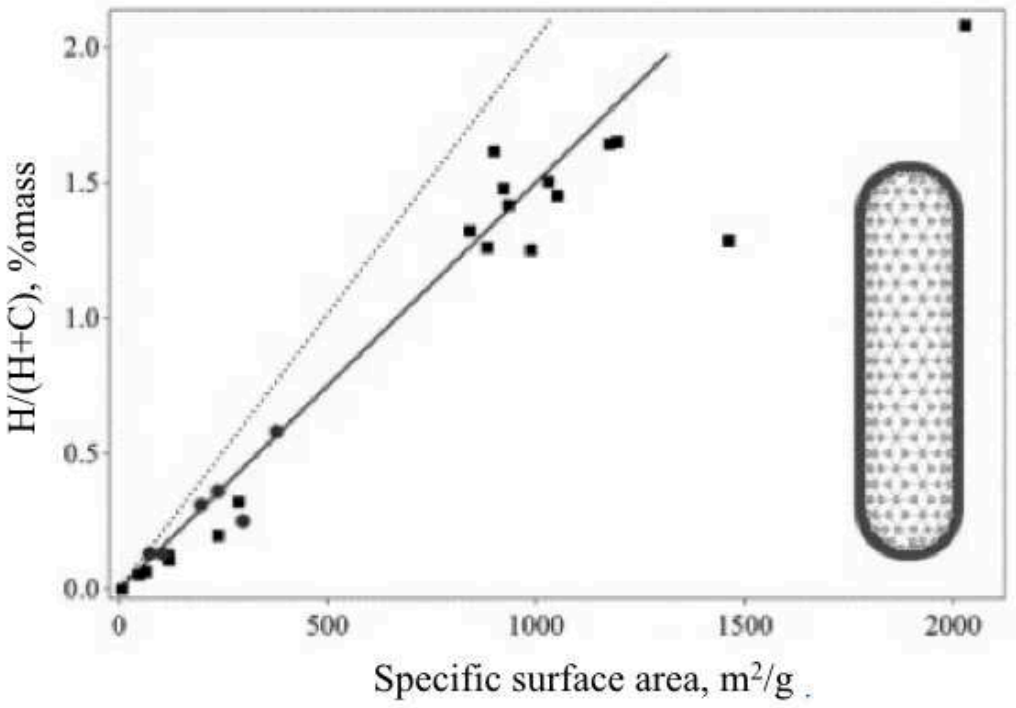

Figure 9. Reversible hydrogen content depending on the specific surface of several samples of carbon nanotubes (circles) and graphite (squares) with a high specific surface (measured at 77 K [64]), line - approximation for graphite, points - calculation of the amount of hydrogen in a monolayer on the surface of the substrate.

An important difference between organometallic scaffolds and other porous carbon materials and zeolites is the absence of a linear relationship between the hydrogen storage capacity and the specific surface area. The real contribution to adsorption is not made by the formal specific surface but by the total volume of micropores [78],[79]. The main advantage of such systems is the variety of possibilities for synthesis with

predefined parameters by varying the properties: volume and pore diameter, the polarizability of the organic fragment, the selection of inorganic secondary structural units, changes in topology, etc., This proves that MOFs can be a promising technology for hydrogen storage systems.

1.7.3 Chemical methods of hydrogen storage

All materials for chemical storage using chemical bound of hydrogen can be divided into two groups. The first group includes the substances containing hydrogen in their composition and capable of releasing it at the certain conditions (an increase of temperature, an action of the catalyst) [55],[58], for example, ammonia and unsaturated hydrocarbons. The second group includes energy-storage substances that do not always contain chemically bound hydrogen in their composition. But these materials are capable of generating it during the oxidation process with water, for example, a spongy iron, interacting with water vapor at 550-600 °C.

The main advantage of storage and transportation of hydrogen in a chemically bound state, for example, in the form of ammonia, methanol, ethanol, is the high density of hydrogen content (~ 100 kg / m3). The mass content is also high: for example, 5.65 kg of ammonia (17.7% by weight) is consumed to produce 1 kg of hydrogen. The use of methanol as a raw material for the production of hydrogen and reducing gases present a possibility to reduce the costs of transportation and storage of hydrogen. The cost of obtaining hydrogen from methanol is 20% lower than from the natural gas. Generation of hydrogen from methanol at elevated temperatures (~ 400 ° C) in the presence of a catalyst is similar to the use of materials from the first group. The main disadvantage of storing hydrogen in a chemically bound state is the difficulty of reusing the material. Exceptions include unsaturated systems for which reversible catalytic hydrogenation/dehydrogenation processes can be achieved. Amorphous, film and nanocrystalline materials are of particular interest. In recent years, carbon nanostructures have been used as hydride-forming materials. Among the carbon materials, fullerenes have also been tested [71],[80],[87]. For example, catalytic hydrogenation/dehydrogenation of double bonds in fullerenes allows reversible binding up to 6.3% (by mass) of hydrogen. Hydrogenation / dehydrogenation catalysts of fullerenes are the hydrides of intermetallic compounds. However, the hydrogenation/dehydrogenation processes can be achieved at the elevated temperatures of ~ 400 ° C only, with hydrogen pressure of 10 MPa. And high temperatures are

associated with high energy costs. In the case of fullerenes, an indirect process of polymerization of double bonds presents a disadvantage, because it reduces the reversible hydrogen capacity of the system during cyclic operation.

Liquid organic hydrogen carriers (LOHCs) are liquids or low-melting solids that can be hydrogenated and dehydrogenated in the presence of catalysts and at the specific temperatures and the process can be reversed. There is also no need to produce a new material for each cycle as the structure stays in the initial form after dehydrogenation [82], which constitutes as one of the advantages of the technology. Also, LOHCs perform pong-term storage without losses, provide high purity of hydrogen, transport hydrogen under standard requirements; the technology is compatible with an existing infrastructure. However, the technology needs further development as for the small-scale applications no set catalysts or processes exist. These types of applications also possess basic requirements such as safety, fast kinetics, and other.

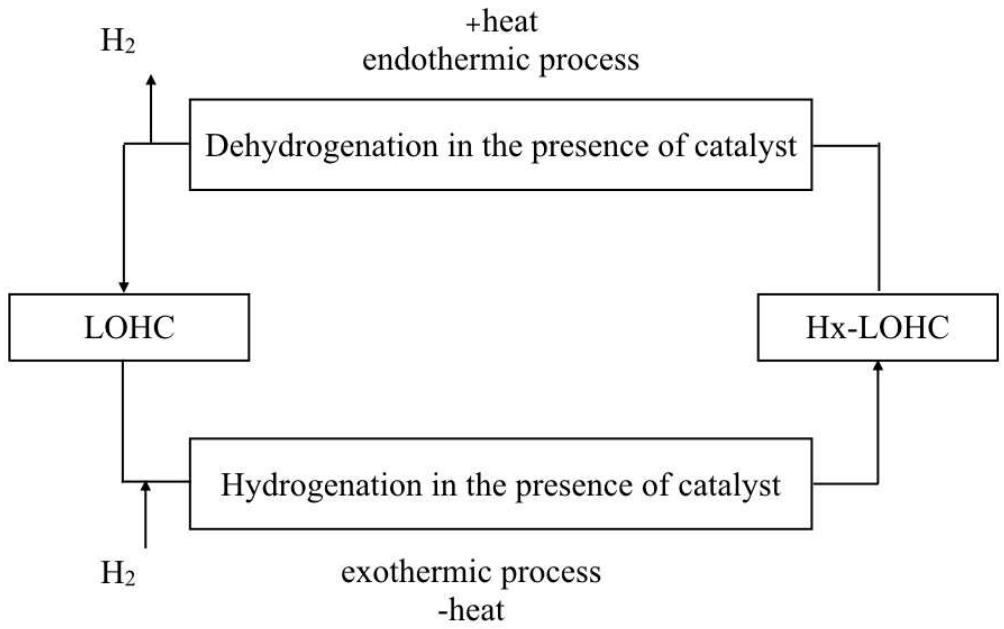

Figure 10. The scheme of the LOHC hydrogenation and dehydrogenation

In Figure 10, the processes of hydrogenation and dehydrogenation are shown. First, the LOHC is hydrogenated in the presence of catalyst with removed heat from the system. Then a catalytic dehydrogenation is performed with the presence of catalyst and supplied heat. LOHC with no hydrogen present is transported back to the initial system.

The process of accepting and releasing hydrogen from LOHC is done with the support

of metal catalysts in a heterogeneous form [83]. Some examples include Ni and Ru catalysts, which support hydrogenation process at 100–250 °C and 10–50 bar. The dehydrogenation process catalysts examples include Pt and Pd that support this process at 150–400 °C below 10 bar. The process of accepting hydrogen by the LOHCs is carried out with an excessive heat that needs to be removed from the system or recovered in the system.

Some cyclic compounds can be also used as LOHCs, some of these compounds include (i) hydrocarbons with storage capacity 6.2-7.3 wt%, (ii) carbazoles with storage capacity 5.1-6.7 wt%, (iii) pyridines and quinolones with 4.8-7.2 wt%, (iv) pyrroles and indoles with 3.2-7.1wt% [84].

An example of the possible application for a family house is shown in [85]. 5 MWh annual consumption rate requires 3400 kg of LOHC to supply 187 kg of hydrogen. Of course, the overall efficiency can be improved by utilizing excessive heat from hydrogenation process and from the FC (the latter is investigated in the current thesis).

The advantages of LOHCs include the absence of limitation for storage size and time. For example, Hydrogenious GmbH showed different size classes from 30 kW to 1 MW power with capacity from 10 MWh to 1 GWh [86]. LOHCs also show satisfactory energy density (6.2wt%). Also, LOHCs keep hydrogen even at the long-term period and transportation at the ambient conditions.

However, LOHCs are still relatively out of commercial market for hydrogen storage and need further research to bring the technology to the developed stage. Especially uncommon area for the research was a small-scale storage. For example, aromatics were hydrogenated in oil refineries but on a big scale. Still, optimized processes and catalysts are needed for small-scale application discussed in current thesis.

1.7.4 Metal hydride technologies for hydrogen storage and purification

Reversible hydrides of intermetallic compounds have a high potential for future hydrogen storage and purification. The general formula for the representation of hydrides is $A_mB_mH_x$, where A is a metal forming a stable binary hydride, B is a metal that does not interact with hydrogen under normal conditions (usually a transition metal, for example, Fe, Co, Ni, V, Mn, Cr, etc.) [56],[61],[63],[88]-[104]. The greatest importance for the application of the material is represented by hydrides of the AB_5

type (A - rare earth metals, Ca), AB_2 and AB (A - elements of the titanium subgroup), A_2B (A is usually Mg). Among the advantages of storing hydrogen in metal hydrides is high safety, because hydrogen is stored in a solid-phase bound state. The advantages also include high storage density (higher than that of liquid hydrogen) and the possibility of selecting equilibrium temperatures and pressures of the hydrogen uptake/release reaction from a wide range. The main disadvantage is a low mass storage density, which does not exceed 1 to 2%wt. However, there is the number of applications that do not consider low mass storage density as a significant limitation, for example, stationary applications.

The reaction of formation and dissociation of hydrides in the generalized form is written as follows:

$$\frac{2}{x}Me + H_2 \leftrightarrow \frac{2}{x}\left(MeH_x\right) \tag{1.1}$$

where *Me* is a metal (an alloy, an intermetallic compound or an element), MeH_x is its hydride.

The interaction of hydrogen with intermetallic compounds (IMC) and alloys can be represented using isotherms of equilibrium pressures, a schematic representation of which is shown in Figure 11. The first zone corresponds to the dissolution of hydrogen in the metal (α-phase), the second zone is a saturated solution of hydrogen in the metal and hydride (β-phase). With a further increase in pressure, the composition of the hydride phase changes as well. In the two-phase region, the pressure does not change or changes insignificantly; the position and size of this section of the "plateau" vary with temperature. At the temperatures above critical, the "plateau" is absent, and a continuous transition from the solution to hydride phase of the variable composition is happening, thus at $T > T_k$, these phases are indistinguishable. The accumulation of hydrogen occurs precisely in the "plateau" section with a change in the relative amount of hydride and metallic phases. The maximum amount of reversibly absorbed and liberated hydrogen is determined by the size of the "plateau" along the X-axis. For many systems, the hysteresis of sorption-desorption processes is observed. The temperature dependence of the hysteresis is different for different systems. The desorption pressure is considered to be the closest to the equilibrium pressure on the "plateau." For engineering applications, the slope of the "plateau" in the PH_2- (H/Me) coordinates is equally important as hysteresis. Thus sorption/desorption processes are

happening at the variable hydrogen pressure level. It is generally believed that the slope of the "plateau" is associated with various kinds of inhomogeneities, such as the inhomogeneity of the microstructure, the segregation of impurities, the presence of temperature gradients, and many others.

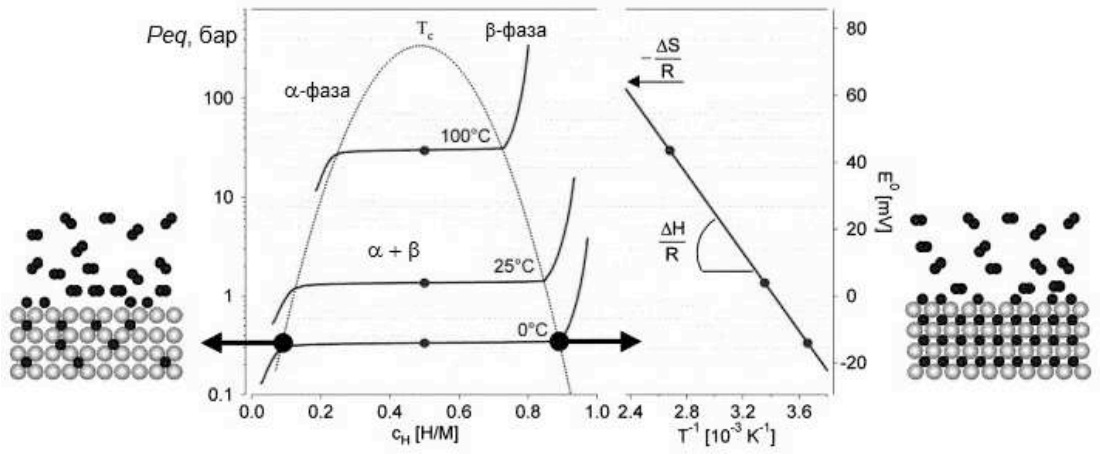

Figure 11. Isotherms of the reaction of an interaction of metals (intermetallic compounds) with hydrogen (H/M - the number of hydrogen atoms per atom of metal)

The temperature dependence of the "plateau" for most alloys corresponds to the Van't Hoff equation:

$$\ln p_{H_2} = \frac{\Delta H}{RT} - \frac{\Delta S}{R} \tag{1.2}$$

where ΔH (thermal reaction effect) and ΔS (entropy change) are assigned to one mole of molecular hydrogen H2.

The energy of the hydride formation ΔH depends on the physical properties of the hydride and can be determined by the calorimetric method. Its value varies significantly for well-known hydrides. The interaction of IMC with hydrogen includes the following stages [56],[61],[63],[88]-[104].:

- physical adsorption on the surface of the IMC;

- chemisorption of hydrogen on active surface centers, resulting in the dissociation of the hydrogen molecule by atoms;

- diffusion of hydrogen atoms from the near-surface layer into the volume of the compound forming a solid solution (α-phase);

- ordering of hydrogen atoms by the formation of hydride (β-phase).

From the analysis of the experimental data, some general aspects of hydrogen - IMC

interaction are obtained:

- the presence of voids in the IMC for the hydrogen atoms placement,

- 10-20% increase in the volume of IMC while interacting with hydrogen;

- formation of hydride in the vicinity of structural imperfections with the subsequent growth of a new phase by the ordered arrangement of hydrogen atoms with a sufficiently strong interaction between them.

The basic alloy with rare metals is the intermetallic compound LaNi5 (AB5 type). Since lanthanum is rather expensive, it can be replaced by mischmetal (Mm), which contains 25...35% La, 40...50% Se, 4...15% Pr, 4...15% Nd, 1...7% Sm + Gd and unavoidable impurities (Fe, Si, Mg, Al). $LaNi_5$ ($MmNi_5$) alloys are doped with various elements (B, Al, Si, Ti, V, Cr, Mn, Fe, Co, Cu, Zn) in order to tune thermodynamic properties of the AB5-H2 system, for example, Ce reduces stability of the MH (increase of plateau pressure / decrease of temperature); Al, Mn – increase the stability). As the result, doping can increase the ability to absorb hydrogen, decrease the number of activation cycles, enhance the stability of characteristics during operation and reduce the cost. Sorption capacity of hydride-forming materials of the RNi5 type was noticeably increased by replacing the part of the rare metals with Ca (for example, $Ca_{1-x}Ce_xNi_5$) and by replacing the nickel atoms with other elements (Mg, Al, Ti, Zr, Mn, Mo, Cr, V, Fe, Co, Si, Zn and Sn) [56],[61],[63],[88]-[104].

Hydrides based on the titanium alloys have a considerably low cost and can serve as an alternative to alloys based on lanthanum. Investigations in the field of these materials are mainly related to Ti-type alloys based on TiFe, TiMn, TiV and aimed for improving the reversibility of hydrogen absorption-excretion processes, improving the thermodynamic characteristics of alloys, and increasing their hydrogen capacity.

Magnesium can bind a substantial amount of hydrogen (per unit mass), has low density and a low cost. However, magnesium reacts with hydrogen at rather high temperatures (250...400 °C), and it is difficult to activate. Magnesium is transformed into a powder with particle sizes less than 50...75 μm and doped with Ni, La, Ce, Cd, Fe, Lu, Sn, Er, Ti, Mn (A2B alloys Mg_2Ni, Mg_2Cu, etc.) in order to increase the absorption/desorption rate. The main task of studying alloys based on magnesium is to find alloying elements that reduce the absorption and desorption temperatures of hydrogen.

The typical representatives of the AB_2 alloy are the so-called Laves phases: $ZrFe_2$,

$TiCr_2$, $ZrFe_{1.5}Cr_{0.5}$. Better illustration of the Laves phases which form MH and have practical importance is TiMn (2±x). The alloys of this type are relatively inexpensive, have sufficiently high dissociation pressure at the near ambient temperatures. The mass content of hydrogen reaches 2%.

One of the promising directions for the development of hydrides with given properties is the method of different metals combination. Thus, to obtain an alloy with the lowest possible formation energy, the combination of exothermic and endothermic metals is used. Hydrides with substantially lower formation energy than those of the parent metals can be obtained. The creation of composite materials from intermetallic particles encased in matrices of Al, Cu, Ni is used to increase the effective thermal conductivity of the powdered IMC [88], which can reach 1-12 W /(mK). However, the mass content of the accumulated hydrogen in such system can slightly decrease. Additionally, composite materials are still significantly more expensive than alloys of intermetallic compounds. Table 5 lists some hydrides and their main characteristics.

IMC can also be classified according to the dissociation temperatures at the normal pressure levels: 0-150°C - low-temperature alloys, 150-300°C - medium temperature, higher than 300°C - high-temperature alloys.

Table 5. The main characteristics of metal hydrides [104]

Alloy composition	Hydrogen content, %mass	Hydride dissociation temperature, ºC	ΔH^{o}_{rev}, kJ/g H_2	Equilibrium pressure at 25 ºC (sorption), MPa	Equilibrium pressure at 25 ºC (desorption), MPa
$LaNi_5$	1,43	13	–30,98	0,2	0,165
$CaNi_5$	1,39	43	–31,82	0,055	0,047
TiFe	1,75	-5	–28,05	1,0	0,53
Mg_2Cu	2,04	273	–72,85	-	-
Mg_2Ni	3,84	253	–64,48	-	-

The presence of impurities has a significant effect on the hydrogen absorption kinetics of intermetallic alloys [61],[63],[105]-[110]. Even the presence of gases that have no interaction with the surface of the particles of the absorbing material leads to a decrease in the hydrogen absorption rate. Thus, the absorption of hydrogen from its mixtures with Ar, N2, CH4, and CO2 does not reach the theoretically possible value during static exposure for several hours; it can only be achieved in a circulatory mode. This phenomenon happens due to the accumulation of nonabsorbable impurities in the free volume of the reactor. These impurities in the reactor block the access to the

surface of the absorbing material. Argon, nitrogen, and methane do not interact with the surface of the hydride phases at the temperatures below 100 °C.

When metal hydride decomposes, high-purity hydrogen is released, and carbon dioxide chemisorbs on the surface of the powder. CO2 does not have a substantial interference with hydrogen, and the hydrogen released during decomposition can contain impurities CO2 [107]. In the presence of oxygen impurities, three reactions occur: (1) the formation of hydride, (2) the oxidation of hydrogen and water formation, (3) the oxidation of the surface and hydroxide or rare earth metal oxide formation. The speed and other characteristics of these processes are determined by the temperature, pressure, chemical composition of the intermetallic compound, and oxygen concentration. Thus, with an oxygen content less than 0.01% of volume, the hydrogen sorption characteristics of the intermetallic compound deteriorate insignificantly. However, in the presence of oxygen 0.1% of the volume, the absorption capacity of these compounds falls two times lower after 100-150 sorption/desorption cycles [109]. The presence of insignificant amounts of CO, SO2, and H2S in hydrogen suppresses the hydrogenation process and has a "poisoning" effect on the IMC [109].

The data shows that the purification and separation method of hydrogen from gas mixtures with the help of intermetallic compounds can be used for the applications in combination with preliminary "poisoning" impurities removal only. The most common hydrogen-absorbing material for hydrogen purification systems is the AB5 alloy (based on LaNi5). These alloys show greater resistance to oxygen and water poisoning compared to FeTi-type alloys. The tendency of these alloys to degrade can be reduced by additional doping, for example, with aluminum [110]. In the case of the surface poisoning, the absorbing properties can be sufficiently restored through a reactivation procedure by cyclic hydrogenation with pure hydrogen [111].

1.7.5 Intermetallic alloy (IMC) practical implication

Production characteristics of metal hydride systems must meet the requirements of the consumers of hydrogen, for example, low-temperature fuel cells that need high purity hydrogen (over 99.95% volumetric). Selective absorption of hydrogen by intermetallic compounds supply high-purity hydrogen to low-temperature FC in stationary autonomous power generation systems. The technology is also highly reliable, efficient and safe in operation.

Hydrogen sorption by IMC is performed with heat removal from the system; the reverse reaction requires heat supplied to the system. The pressure in the MH storage and purification systems can vary from relatively small pressure to 10 atm, and the temperature varies from 20 °C to 80-90 °C. These characteristics enable the use of cold and hot water resources already available to the consumer on site with low energy costs, ensuring safety requirements of the technology. Additionally, a concept of exhaust heat utilization from PEM FC is investigated in this dissertation. The state-of-the art in MH storage and purification system is described below.

1.8 State of the art in MH reactors

Unlike conventional hydrogen storage systems, keeping the gas under extremely high pressures of several hundreds of bars, the metal hydride (MH) storage has an ability to keep hydrogen in a bounded form at the pressure levels significantly lower [112],[113]. MH hydrogen storage uses a reversible chemical reaction forming MH during the process of hydrogen sorption and coming back to alloy or intermetallic compound when hydrogen is released. There is a number of challenges both on the fundamental level and on the level of system design.

An isotherm of a reaction between metal and hydrogen has a clear "plateau," where a pressure change can be neglected creating an approximation that absorption and desorption processes take place at a constant pressure and temperature [113]. This is one of the major factors affecting MH material efficiency and it is originated from the presence of impurities that create compositional fluctuations [114] and interfere with the components of intermetallic compound [115]. This phenomenon was first quantified by Larsen and Livesay [116] and then by Fujitano et al. [117], Lototsky, Yartys et al. [118],[119], Park et al. [120]. Thus, to create a system with high compression productivity it is necessary to take into consideration temperature dependencies of the components of an intermetallic compound. In 1937, Lacher [121] suggested using PCT diagrams with statistical and thermodynamic features for this purpose. This approach was further developed by the number of research institutes [119],[122],[124]. This method helps to identify pressure ranges for an MH material, as inlet pressures in MH reactor higher that equilibrium ensures hydrogen absorption with heat release and the pressures lower than equilibrium create desorption process with a heat consumption [113].

Also, the direct and reverse processes of metal - hydrogen reaction affects the duration of the hydrogen sorption/desorption cycle that varies significantly for each MH material and affects MH reactor dynamic performance. Since many MH materials experience fast reaction with hydrogen the process itself from the viewpoint of the system in general often limited by a heat transfer [125],[126]. The number of challenges here includes, for example, operation at low temperatures or presence of impurities in hydrogen [127]. These challenges highly affect kinetic factors that can only be controlled on the systematic level, which means that the modeling of heat and mass transfer to and from an MH material is crucial for the rates of hydrogen uptake and release [128],[129]. Besides that, degradation effects [130],[131], tolerance to impurities in hydrogen and specifics of structure and morphology are widely known in the literature. However, they stand out from the scope of this research.

Summing up, on the fundamental level of MH material, it is important to ensure hydrogen absorption and desorption at the near to equilibrium conditions [128], it is also important to control heat and mass transfer that affects kinetic factors of the reaction.

On the level of system design and engineering, there are two main goals: it is important to ensure fast hydrogen charge/discharge rates and high-efficiency level. These goals are associated with some challenges, including general layout of the system, design of the reactor elements, heat transfer method, and devices, optimization of MH material using parts of the system, gas connections, and system control. Overview of the general layouts of MH reactors was presented in the patent description by Lototsky, Yartys et al. [132],[133]. Recent concepts operating at a medium level of temperatures and generating high pressures include multi-stage reactors created by Ergenics Inc. [134]. Most of the systems use water as a heating/cooling agent [135]. However, intensification of heat supply/removal is still the main problem of the MH system that is highly connected to the low thermal conductivity of a solid state MH in the form of powder [136]. Thus, the challenges of design, such as packing density, heat transfer resistance, a geometry of the system elements [137], require modeling approach with further experimental verification, examples can be found in Refs. [138]-[143]. Intensification of the heat transfer can be achieved by an increase of the surface area of an exchanger, which is done by using long MH reactors with small wall thickness, "shell-and-tube" solution [144], fins [145], metal blocks [146] or/and with a parallel

connection of the tubes [147]. Studying these aspects [148], issues of modeling and optimization [149] and typical MH reactor systems are presented in a patent [150]. One of the important factors of the heat exchange in the described system is a type of heating/cooling process: fluid [123],[151], electric heating [152],[153], convective air cooling [154], gas-gap thermal switch [155],[156], Peltier devices [157],[158], heat pipes with catalytic combustors [159],[160]. Heat transfer was studied in all forms of placement, such as external, internal, and combined. It was also tried in different arrangements, sizes, and transfer matrixes.

Due to the limited amount of recent research on economic aspects of MH reactors, an estimated cost of the prototypes from Brazil [161], Ukraine [162], and LNA [163] remain at the levels of $23,000, $32,500, and $66,000 respectively.

Every system is highly individual and made with respect to specific situation and requirements. No overall method of creating an optimal sized system with short cycles, increased productivity, low weight, and lowered amount of MH material is present in the literature as most of the publications introduce case-based approach. Thus, the creation of an overall approach and method of MH reactor design is one of the aims of this thesis.

1.8.1 Metal Hydride (MH) and PEM Fuel Cell (FC) Integration

Another important aspect of MH storage technology utilization is its integration with FC. Current subsection presents few examples of the integration on different scale as well as discusses some of the aspects of the latter with advantages and disadvantages of the technology. Main advantages of the MH are a high volumetric density of stored hydrogen (100 gH L^{-1} and higher) and relatively small pressures comparing to traditional hydrogen cylinders [164]. For estimated optimum MH tank system hydrogen release needs to occur at temperatures of 333-353 K, which are close to the operating conditions of PEM FC [165]. One of the core benefits of the integration is the utilization of waste heat produced by an FC [164], [165]. It allows to use 40-45% of heat and thus boosts the efficiency and performance of the overall system [164].

Metal hydrides are usually considered as an alternative to the high-pressure Gas Cylinders (tanks). These tanks can provide fast charge and discharge rates and are more simple from the system point of view. At the same time, several features of these tanks such as costs, a low density of hydrogen gas as well as the low gravimetric

content of hydrogen drive the research towards metal hydrides as a hydrogen storage technology [165]. Traditional fuel cell systems with compressed gas (CG) tanks as hydrogen storage might be improved by integration of MH as well [166]. That brings advantages of both types of hydrogen storages to the hydrogen energy system. The system of low-temperature FC supplied by hydrogen from both CG and MH connected with FC by a common manifold and provided with thermal control and management system shows the better performance in operating regimes. Thus, the shorter charge times might be obtained together with a slower pressure drop. The peak of consumption of H2 becomes smoother in the process of FC supply compared to the systems where MH is a single type of storages. The charge pressure of H2 in the MH-CG systems becomes smaller while a volumetric capacity of the storage increase. Moreover, proper temperature management increases the efficiency of the system and reduces the costs [166].

Energy storage systems which don't use high-pressure gas cylinders and have only MH as hydrogen storage might be a good alternative to the conventional hydrogen storage systems. MH storage is usually used in such systems because of the low operating pressures, decreased costs, maintenance and losses. One of the studies of MH-FC energy storage system demonstrated the overall efficiency of around 11% [167]. The system included PEM fuel cell H-3000, an electrolyzer with 6,67 NL/min hydrogen production rate, and (LaCe)Ni metal hydride (7140 L storage capacity). The research showed that MH tank is a safe and compact alternative of high-pressure cylinders. This solution helped to avoid the need of compressor and provided the reduction of costs affiliated with a compressor. The efficiency of the system was considered low due to the losses in fuel cell stack and electrolyzer control system. The use of modern electrolyzers might increase the efficiency of the system.

Besides standard fuel cell - metal hydride combination both could be integrated into larger systems and become components of isolated micro-grids. In the scope of micro-grid metal hydride and batteries could be considered not as a competitive technology but as two parts of storage complex. The optimal design of the system which includes renewable sources of energy (PVs and wind turbines) as well as a combination of energy storages (battery bank and metal hydride tank) might become economically efficient with the low risk for investors and payback period within the mid-term. The study which evaluates the creation of such a system on an island in Greece shows that

it's feasible to build it technically and economically in the conditions of the present day [168]. The advantage of the system is its modularity which allows one to pick optimal size and combination of its components. This system could be upgraded and scaled in the future by adding more power sources and storage capacity. According to the present system, the optimal MH capacity is equal to 12 Nm3 is sufficient to store hydrogen for 1 kW fuel cell (and be supplied from 1,2 kW electrolyzer) [168].

Metal hydride has a potential to be implemented in micro-scale hydrogen energy systems. Micro-scale metal hydride storages can provide hydrogen supply for a portable power generation units based on micro-scale PEM FC. These metal hydride cartridges (i.e., Horizon, 1 g H2) can supply micro FC of 50-90 Wh kg^{-1} [169]. These systems are already comparable with Li-ion batteries.

Current thesis designs and develops the system where MH and FC integration is part of a small-scale stand-alone system providing power to a small settlement in an off-grid environment. Additionally, an idea of utilizing heat from a FC is realized in a hardware kW scale system.

1.9 Goal of the research

The goal of the research is to demonstrate the technology from technical and economical point of view and to create an experimental cogeneration energy system with MH hydrogen energy storage H2Smart having a power of 1 kW. The system should be designed to be an experimental energy storage system in Smart Grids and to be an essential part of the educational process in Energy Systems programs at Skoltech. The technology ensures quality of electrical energy in micro energy systems that have a load and distributed energy sources through the use of hydrogen energy storage. Hydrogen is produced by electrolysis utilizing waste energy from the renewable sources. Electricity is generated by PEM fuel cell.

The tasks of the research include

- The design and development of the schemes for low power (H2Bio) and 1 kW power (H2Smart) systems, where H2Bio is capable of both storing and cleaning input gas and H2Smart utilizes excessive heat from the FC making the system more autonomous
- Selection and verification of the main components, including the backup supplies.

- Preliminary experimental investigations and simulation of the proposed concept, formulating design requirements for the 1kW system.
- IMC selection and creation depending on preliminary investigations, design requirements, technical requirements.
- System integration of the components FC, MH reactor, back up supply for the H2Bio; electrolyzer, MH reactor, FC, back up supply, radiator for the H2Smart.
- Economical estimation and comparison for the stated case.

Chapter 2 Experimental investigations of low-power PEM FC and MH storage system integration - H2Bio system

In order to experimentally investigate the possibility of integrating low-power PEM FC and MH storage, the H2Bio experimental energy system was designed and developed. It has also formed the base to study heat and mass processes in such systems of hydrogen storage and purification and became an essential part of the educational process in Energy Systems programs at Skoltech. The proposed technology provided PEM fuel cell with high-quality hydrogen even when the initial source was (or was emulated to be) a biohydrogen.

H2Bio has the variety of functions, including the process of storing hydrogen and cleaning biohydrogen that can be a mixture of gases with carbon dioxide and hydrogen or a model of the mixture of gases close to real biohydrogen. The cleaning and storing process uses the properties of intermetallic alloys that selectively absorb hydrogen from the mixture of gases forming metal hydrides. Purified hydrogen is stored in a solid-phase bound. The fuel cell energy system with hydrogen meets all required characteristics. The possibility of measurements and control of the main parameters is ensured in order to perform experimental investigations.

2.1 Experimental set-up

The scheme of the experimental setup is shown in Figure 12. The system includes the source of biohydrogen, the MH block based on two reactors that clean and store hydrogen, PEM FC Hoppecke E-200 with 175W power, and an automatic control system for scientific research.

In this set-up, MH storage is chosen to be a low pressure storage that can take hydrogen both from pure H_2 and from the mixture of gases [170],[172], providing additional practical implication. Hydrogen from the tank enters MH storage reactors or can be supplied to the FC directly. After the storage in MH reactor, hydrogen is supplied to PEM FC, which supplies the load. Additionally, a small capacity battery back-up supply is introduced to the system to supply the load during FC shut downs and start-up procedures. All the measurements are taken by NI-PXI control system and displayed using LabView interface in a computer integrated to the H2Bio system.

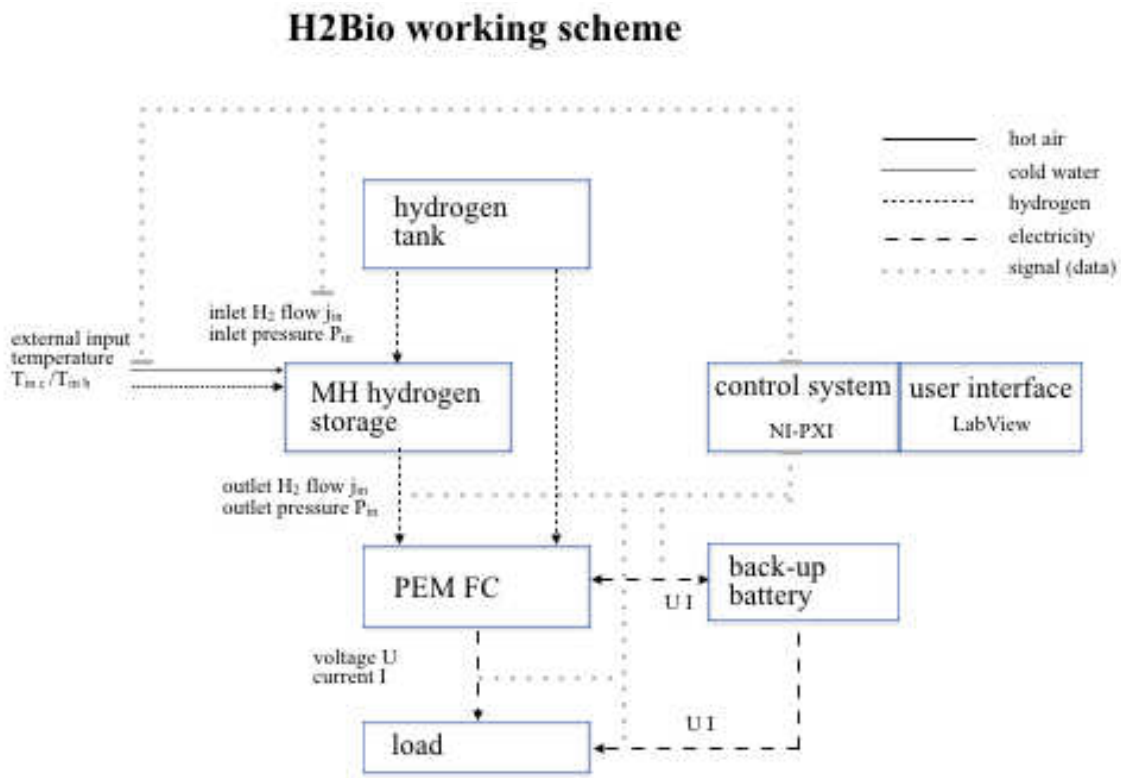

Figure 12. Scheme of the H2Bio set-up

Hydrogen sorption process in MH reactor requires heat dissipated from the reactor, thus cold water is supplied to the system. Hydrogen desorption process requires heat supplied to the reactor, the system uses external heat carrier in the form of hot water supplied to the system. Depending on the need of experiment or availability of hydrogen, it could be supplied into the FC from a storage tank or MH-reactor.

Table 6. Technical characteristics of H2Bio

Maximum working pressure	no more than 1 MPa
Fuel cell power level	175W
Hydrogen production rate	3 norm l/h
Metal hydride reactor metallic alloy	$LaNi_5$
The amount of hydrogen stored	200 l
Nominal pressure of MH reactor charging	no more than 0.5 MPa
Nominal hydrogen consumption rate	no more than 3 norm l/h
Cooling type	water 0...95°C
Connection	public electricity network 50 Hz, 220 V public water network

Gas and hydraulic schemes of the set-up are shown in Figure 13 and Figure 14. The description of the symbols is listed in Table 7.

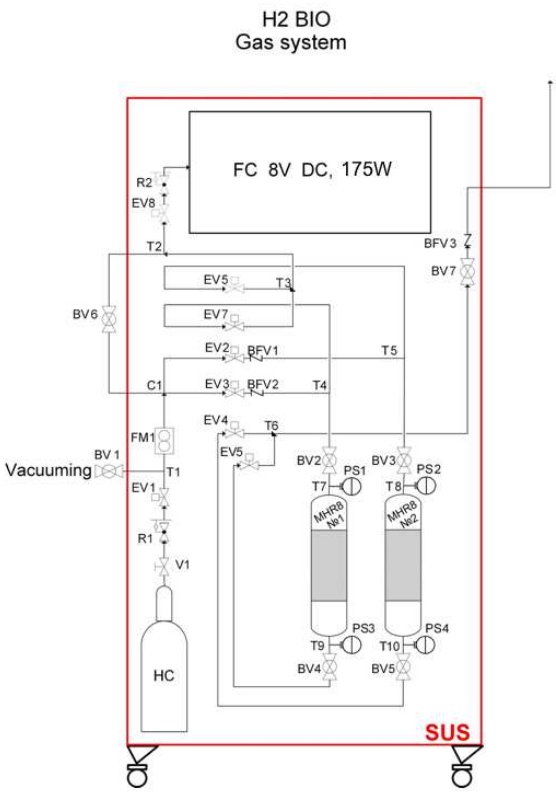

Figure 13. Gas scheme of the H2Bio set-up

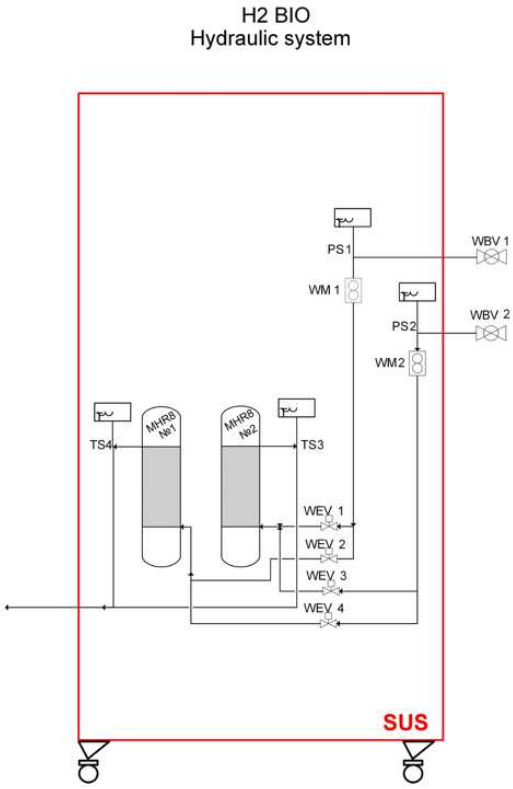

Figure 14. Hydraulic scheme of the H2Bio set-up

Table 7. Components of the H2Bio set-up

Symbol	Component
HC	Hydrogen cylinder
V1	Valve
PS1 – PS4	Absolute pressure sensor
FM1	Flow rate meter
C1	Cross
BFV1-BFV3	Back-flow prevention valve
SUS	Set-up structure
R1	Reducer
R2	Reducer
MHR 8 №1,2	MH reactor for storage and cleaning
T1-T10	T-tube
FC	Fuel cell

BV1-BV7	Ball valve
EV1 – EV8	Electric valve
TS1 – TS4	Temperature sensor
WM1, WM2	Water meter
WBV1, WBV2	Ball valve (water)
WEV1 – WEV4	Electric valve (water)

Figure 15. General view of the H2Bio set-up

2.1.1 Working principle and characteristics of MH reactor

General view of the reactor is shown in Figure 16 and Figure 17. The reactor has a modular design with the main element – MH cylinder with a separate connection to hydrogen and cooling/heating agent. The presence of both internal and external heat exchangers provides efficient heating/cooling process, using the "tube-in-tube" concept. Two nozzles ensure continuous performance.

Table 8. Technical characteristics of MH storage reactor in H2Bio

MH reactor metallic alloy type	AB_5 type ($LaNi_5$)
Alloy composition	$La_{0.9}Ce_{0.1}Ni_5$
The amount of the alloy	1 kg
The amount of hydrogen stored	100 norm l
Cooling type	water 0...95°C
Maximum pressure	1.5 MPa

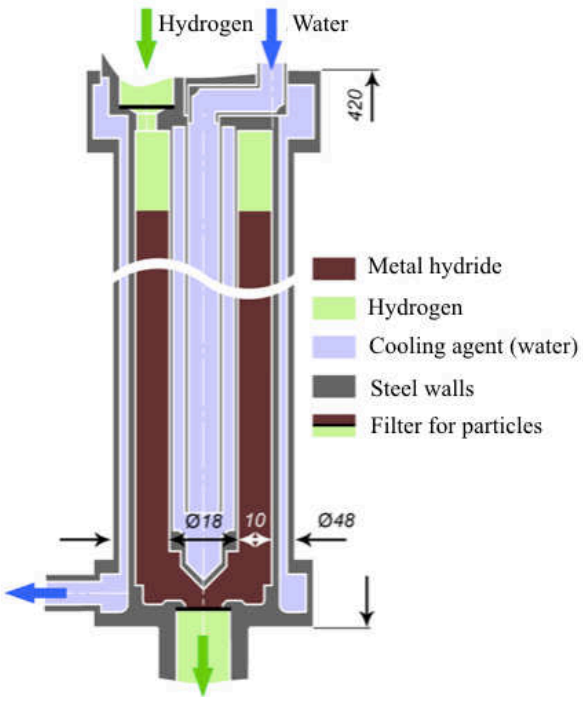

Figure 16. Scheme of the MH reactor

Figure 17. View of the reactor

In order to charge the reactor, hydrogen (or a mixture of gases) is supplied to the top intake nozzle under the pressure that does not exceed 0.5 MPa. Cooling water removes the heat of the reaction and supports a charging process inside the reactor. The maximum water temperature should be lower than equilibrium temperature for charging pressure; this measurement can be obtained from the PCT diagram of the metallic alloy. The end of the charging process can be noted by the absence of cooling water change on the control interface in LabView. Output nozzle releases gas impurities from the reactor.

In order to discharge the reactor, output nozzle is connected to hydrogen receiver

(PEM FC in H2Bio system), and nominal discharge pressure should not be lower than 0.05 MPa gage pressure. As the hydride decompounding requires additional heat, hot water is supplied to the system through the external and internal heat exchanger. Minimal water temperature should be higher than the equilibrium temperature for the discharge pressure, that can be obtained from the PCT diagram of $La_{0.9}Ce_{0.1}Ni_5$, maximum temperature should not exceed 95°C. The discharge can also happen through the top nozzle, the end of the process is controlled through the absence of water temperature change.

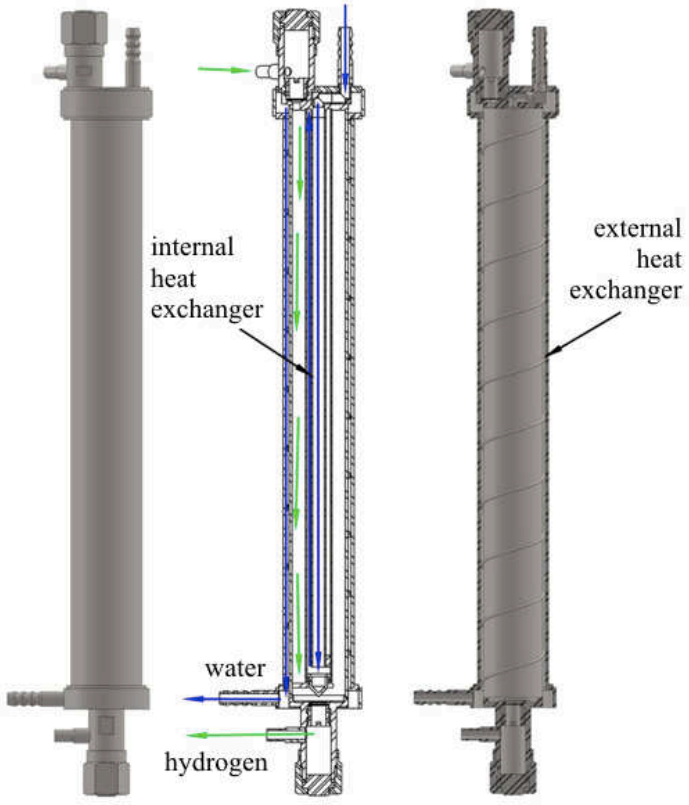

Figure 18. General view of the reactor

2.2 Results of the experiments

The goal of the experiment was to investigate the joint functioning of low-pressure MH reactor, PEM FC, the battery, and the load. Thermal and electrical parameters of the setup were measured, including current on the load and the battery, power of the load and the FC. The current was controlled externally to simulate volatile load, and the power of the load was calculated. The FC reacted to the load current and covered the need, the crisis shutdowns of the FC were also noted, measured, and explained. Additionally, the effect of external conditions was studied.

Different working regimes were tested throughout the experiments. First, regular performance of hydrogen desorption from the first reactor directly to the FC was studied with an almost constant load change. It can be noted that water supply was kept from 45 to 55°C and the temperature was rapidly decreasing each 5-7 min (Fig. 18c).

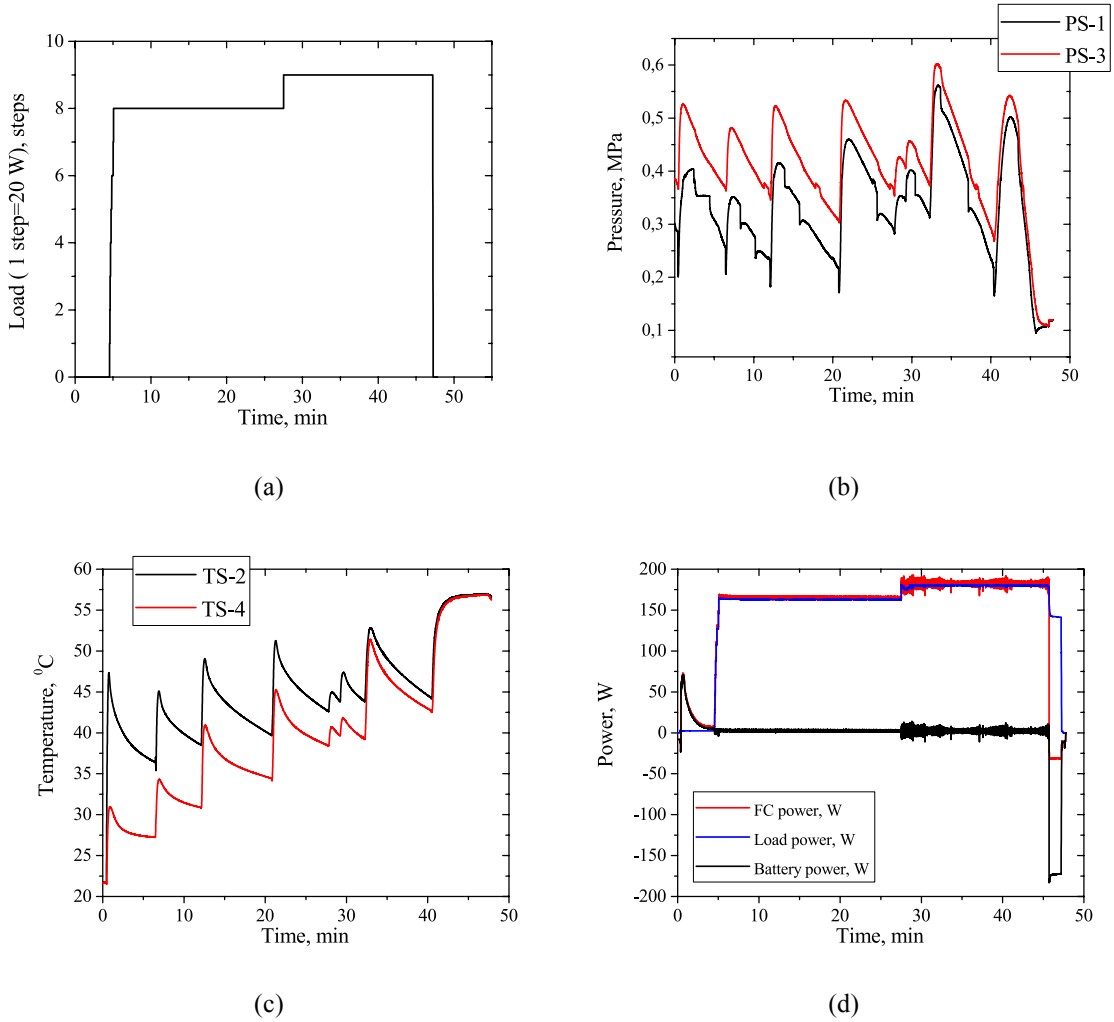

Figure 19. Results of the experiment one: (a) – load power, (b) – pressure after the reactor, (c) – temperature of the water (black) and of the reactor (red), (d) – power of the load, FC, and a battery

The process can be explained by the external conditions of the experiment, which forced the water temperature in the system to decrease. In Figure 19d, power levels on the FC (red line), battery (black line), and a load (blue line) are shown. It can be noted, that the FC was charging the battery until the load was introduced to the system on the 5th minute. The FC met the need of the load throughout the experiment except for the 46th minute, where a low H2 pressure was supplied to the FC from MH reactor due to the discharge of the reactor. During the FC low pressure shut down, the battery met the demand of the load automatically.

During the second experiment, a steady increase of the load was introduced (Figure 20a). Again, an additional hot water supply was needed to steadily increase the temperature in the reactor as the reactor discharged more and more until the low pressure occurred on the 70th minute when the reactor was close to being fully discharged.

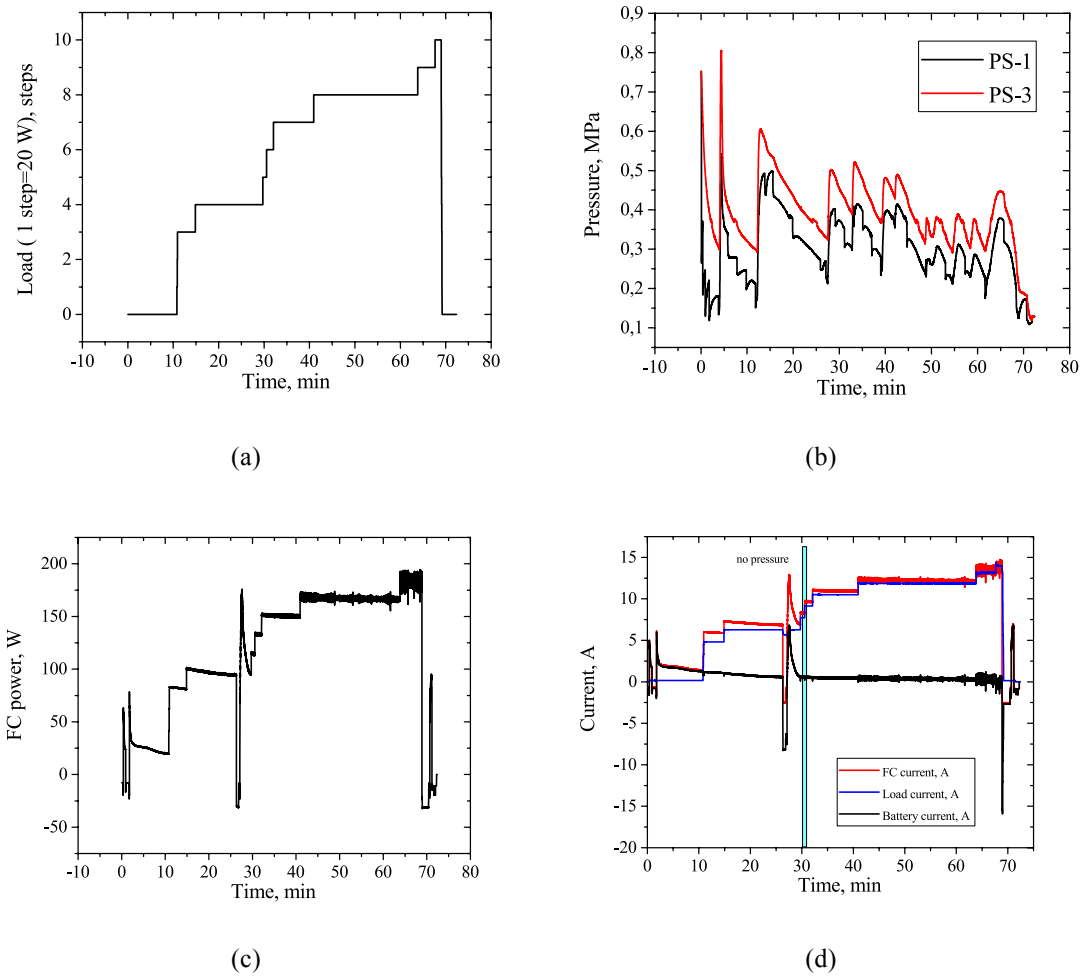

Figure 20. Results of the experiment two: (a) – load power, (b) – pressure after the reactor, (c) – power on the FC, (d) – current of the load, FC, and a battery

H2Bio system has two MH reactors. During the third experiment, the reactor one was charging when the reactor two was discharging to the fuel cell. The load was introduced decreasing and increasing, simulating volatile nature of the real load. The temperature was kept around 45^{o}C. However, the discharge process in the reactor two forced the rise of the temperature of the heating agent for the FC to meet the load demand as long as possible. In the Figure 21d, the power of the FC, load, and a battery are shown. The FC fully met the load demand.

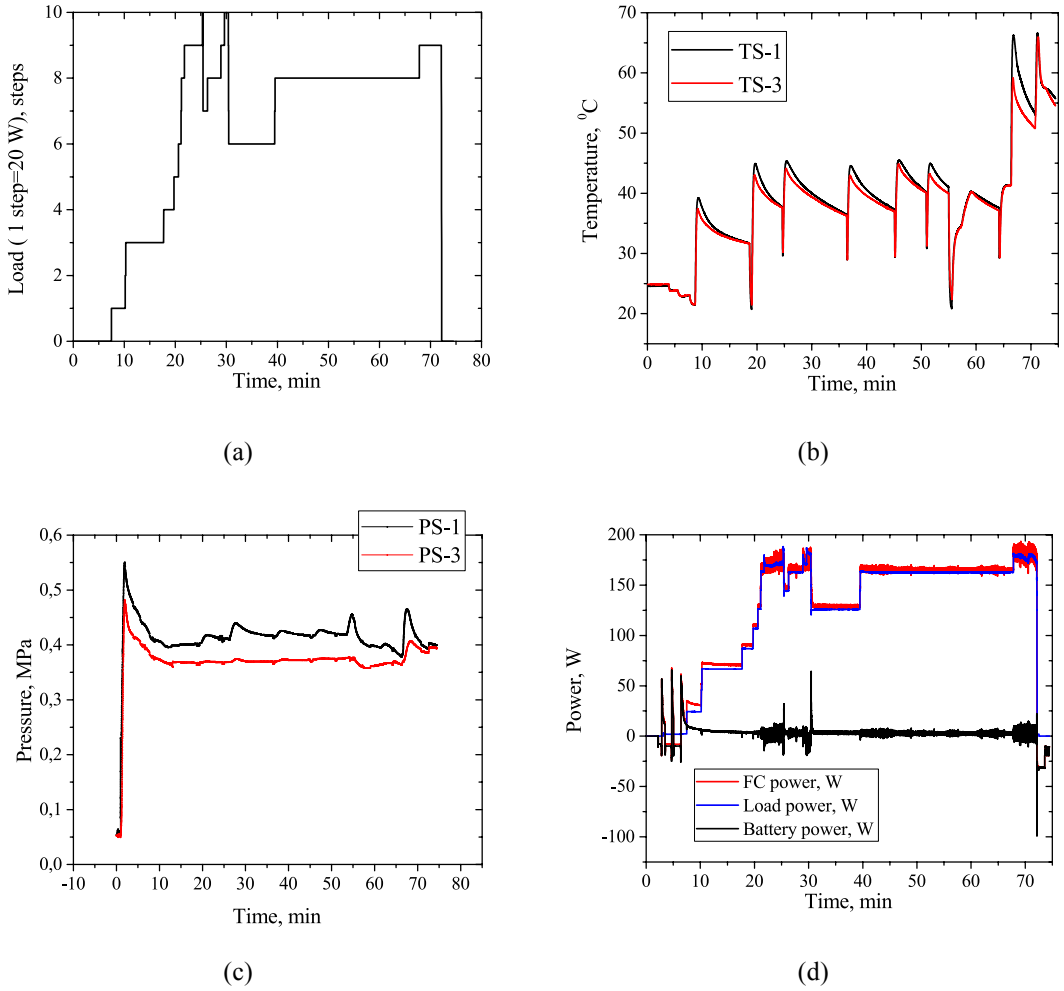

Figure 21. Results of the experiment three: (a) – load power, (b) – temperature in the reactor, (c) – pressure after the reactor, (d) – power on the FC, load, and on the battery.

Finally, performance of hydrogen desorption from the first reactor directly to the FC was studied with a changing load. The load power graph in Figure 22a shows that the load had changed rapidly on the 10th and the 95th minutes and grew steadily from the 20th to the 90th minute. The hydrogen flow rate (Figure 22b) was represented by the graph with impulses when FC intake was active. It was noted that the FC does not require hydrogen in a steady manner and require high volumes of hydrogen each period of time. During the first experiments, MH reactor could not provide such an impulsive output thus a buffer between the FC and the MH reactor was added to enable MH reactor to collect hydrogen prior to entering the FC.

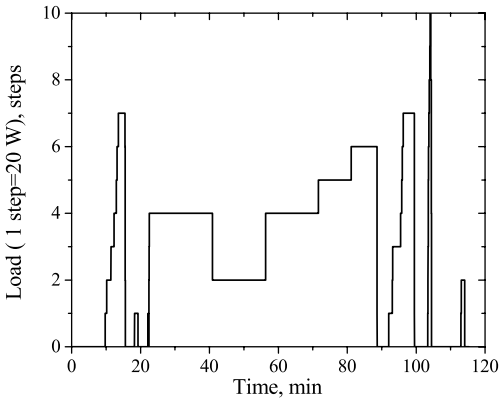

(a)

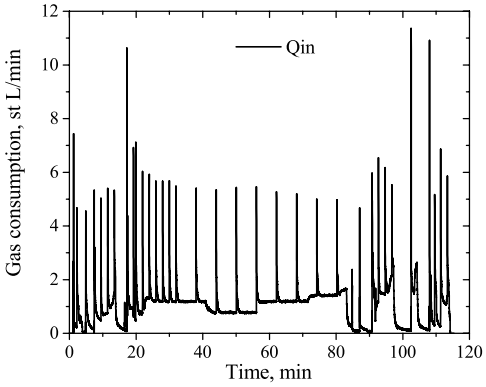

(b)

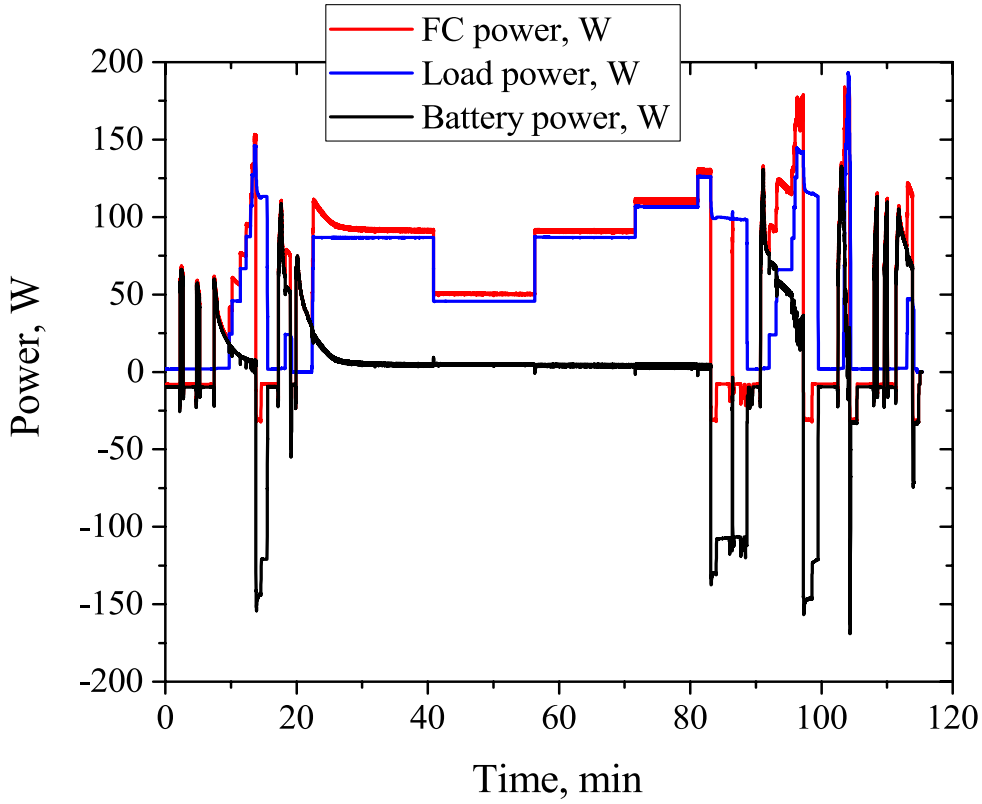

(c)

Figure 22. Results of the experiment four (a) Load power, (b) hydrogen flow rate, (c) power of the FC, load, and a battery.

Concluding the experiments in this section, few compelling outcomes were received. The FC impulsively requires hydrogen, thus a buffer or an additional free volume in the reactor should be added in the next set up. General working regimes of the system can be analytically concluded (in the next subsection). The system performs as expected. However, high-level heating agent temperature was required closer to the end of the experiment.

2.3 Working regimes and system integration outcomes

Figure 23 shows frequently obtained profiles of the current on the battery, observed in the previous experiments.

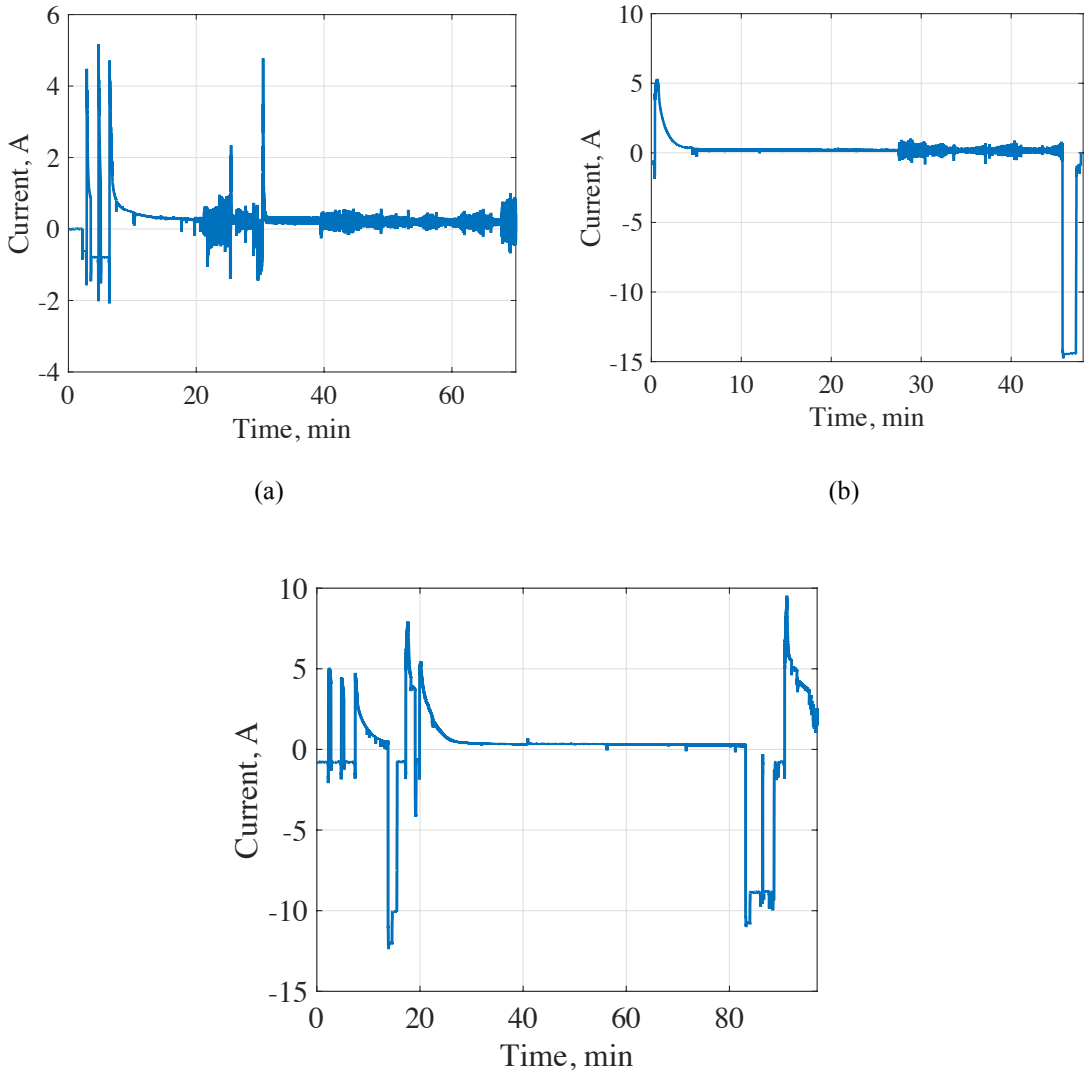

Figure 23. Working regimes of the H2Bio system battery: (a) – typical, (b) – optimal, (c) - critical

It was experimentally found that most of the outcomes of the experiments could be formulated and generalized into four working modes of the system. These four working modes of the system repeat one after another: the start of the system, optimal performance, and different shutdowns. Three current curves above represent the most common working regimes of the backup battery that supplies the FC. It is important to investigate in order to formulate a technical need for the backup supply and possible ways to limit or even eliminate its usage.

Mode 1 - fuel cell system start – one of the biggest issues with the FC system is the need of additional power to start it, it was experimentally found that the normal FC start-up procedure usually takes three initial starts of the FC. It can be explained by the FC trying to heat up the system inside the fuel cell. It is, however, unclear why the number of the peaks in the Figure 23a and Figure 23c equal to three approximately from -2 to 5 A each. It can be connected to the automated system inside the commercial FC.

Mode 2 – regular working mode of the fuel cell is the working regime we are aiming for while designing the systems. During this working regime, the FC meets the load demand and charges the battery whenever the load demand does not exceed or equal to the maximum power level of the FC. The Figure 23b experience this regime throughout most of the experiment, while Figure 23a and Figure 23c only show this regime stable starting from the 30th minute of the experiment.

Mode 3 - unexpected **fuel cell shut down** due to the **low hydrogen pressure intake** – as it was discussed in the previous subsection, the FC requires hydrogen intake in an impulsive manner. In order to solve this issue, the buffer was installed to the system. The rest of this regime examples happened closer to the end of the experiment when the reactor has already been discharged. However, the battery should have enough capacity to meet this rapid demand peaks that can be best observed in Figure 23c. The performance of the battery in these peaks meeting the maximum demand of the load presents a higher requirement for the backup system installed together with the FC.

Mode 4 - immediate **high power demand** that is not met by the FC – it often happens that the FC needs additional time to adjust to a rapid increase of the load. During the experiments in the previous subsection, additional time was given to the FC to adjust, however, in a real situation the system needs to be ready to meet the rapid increase, which again presents a requirement for the backup power supply.

2.4 Effect of ambient air conditions on system performance

Throughout the experiments of H2Bio, a loss of power was detected. The FC was no longer capable of producing 175W; instead, it could only meet 90W of load demand. The change of the output power had happened when the centralized heating was turned on in the lab. We assumed that humidity level in the room has decreased leading to the loss of necessary humidity level on the FC membrane.

Since the FC produces water particles as the result of chemical reaction, we run the system with no to minimal load for about three months every day. Unfortunately, the power output did not get back to normal. In order to study the ambient conditions on the FC to avoid further loss of output power, the series of experiments were designed to investigate the effect of different humidity levels and temperature levels on the FC. The influence of inlet air temperature was studied, because the designed system is usually placed in a special container outdoors.

2.4.1 State of the art

Theoretically, FC efficiency is much higher than the efficiency of combustion based power generation systems. However, given all the uncertainties regarding chemical reactions and FC membranes, a theoretical efficiency remains higher than the practically achieved. The heat generated inside the FC performs another negative effect as it causes the degradation of a membrane, diffusion layers, and a catalyst. Normally, FC systems have cooling agents in the form of water or air running through the system or the heat exchangers removing heat and keeping the cell operation temperatures around 60-80^{o}C. MH system can utilize this heat and the next kW level system called H2Smart proves this concept (in the following chapters).

Many scientific contributions discuss the problem of water management [173],[180]. In the works of Kim and Hong [173], a substantial impact on a cell voltage by the temperature and relative humidity is shown on the example of PEM FC with a total 100 cm^2 area of activity. The humidity level from 40% to 100% was sent to cathode and anode from two external humidifiers. In [174], a 2D simulation of a single channel with no external humidification was created to investigate a temperature profile along the channel. The profile was changed by the heat removal only. Independent from air temperature, the cell of 300 cm^2 was studied in [175] with no information about the amount of water entering the cell and a cathode and anode temperatures influence on the cell performance were studied in [176].

The performance of the cell in a climatic chamber was investigated by Hottinen et al. [177] in the range of external temperatures from 10^{o}C to 40^{o}C with an outcome that the fuel cell performs better at the lower temperatures and the change of relative humidity from 25% to 90% has a positive effect on the cell at all of the temperature levels. In [178], a mathematical simulation model of PEM FC showed that increasing current

density and lower temperature lead to an increase in cell sensibility to temperature changes overall. In can be concluded that conventional polarization curves do not show temperature and humidity uncertainty, the authors, instead, suggest using an area of polarization where a current and voltage density consider temperature changes along the cell.

As the next step, a 3D model of an FC with microchannels located in parallel has suggested that higher performance is achieved at 100% relative humidity on the anode side and 60% on the cathode side [179] in case of a relatively constant operational temperature. On the contrary, [180] discovers that a relative humidity on a cathode has a higher impact on the cell performance rather than an anode relative humidity. Also, Hottinen et al. in experiments [177] discovered that increasing gas temperatures have a positive affect on an output cell voltage.

The goal of these experiments is to study an influence of temperature and relative humidity using experimental approach. The objectives of these experiments include the comparison of FC efficiency in the fixed levels of RH (25%-35% and 95%-100%) with the changing inlet air temperature and the comparison of FC efficiency under fixed air temperatures and changing air relative humidity.

2.4.2 Theoretical investigation

A theoretical approach to determine the efficiency of any FC uses the formula

$$\eta = \frac{\Delta G}{\Delta H} \tag{2.1}$$

where ΔG is a Gibbs free energy and ΔH is a fixed value that can be equal to a lower heating value of H_2 in the case of the water reaction product or a higher heating value of H_2 in the case of vapor reaction product. Gibbs free energy depends on the temperature and pressure. With an increase of the temperature Gibbs energy decreases and FC efficiency reduces. With an increase of pressure, Gibbs energy increases and positively affects the efficiency.

The connection between voltage and temperature is derived by linearizing the free energy about the standard condition of 25^{o}C, assuming that the change in enthalpy does not change with temperature [181]. Due to the negative change in entropy, the voltage output decreases with temperature. The FC has theoretically higher efficiency at low temperatures [181]. On the contrary, higher temperatures grow the kinetics of

the reaction, [181] where mass transport, ionic conduction, and other processes become faster at higher temperatures. Only balancing between these two effects and choosing the right temperature range can result in achieving maximum efficiency. For PEM FC this temperature is considered to be around 60^{o}C to 80^{o}C [181].

The influence of air relative humidity can both prevent the interaction between reactants if it is too high and result in low permeability of the membrane if it is too low [181]. Also, the relative humidity in the air helps to remove heat from inside the system preventing the temperature to grow above 90^{o}C as this accelerates water evaporation and results in a membrane drought. To contrtol the temperature inside the FC, the automatic cooling fans are installed in the system. An additional cooling system that can also emulate different external conditions regarding different relative humidity levels was added to H2Bio.

2.4.3 Added cooling system to the experimental set-up

A cooling system was designed for H2Bio and integrated to the previous system; it can change the characteristics of inlet air. The scheme and the elements of the system are shown in Figure 24.

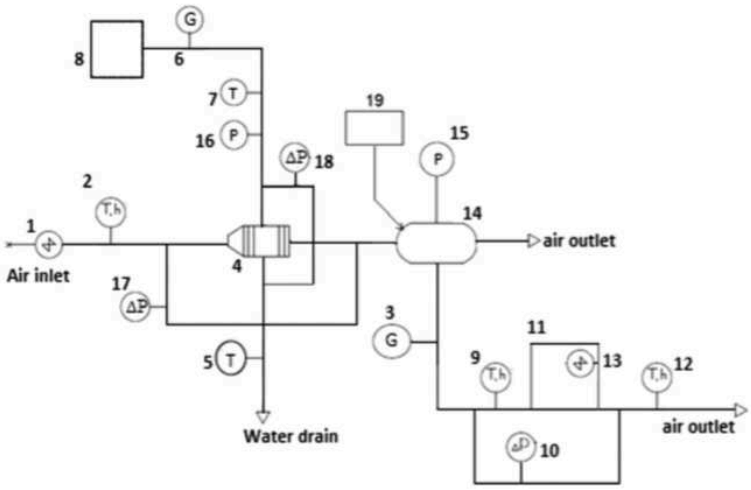

Figure 24. Cooling system scheme. 1 - fan; 2, 9, 12 - temperature and humidity sensors (air); 3, 6 - flow rate sensors (air); 4 - heat exchanger; 5, 7 - temperature sensors (water); 8 - thermostat; 10, 17, 18 - pressure drop sensors (air); 11 - FC; 13 - FC fan; 14 - air reservoir; 15, 16 - pressure sensors (air)

A fan 1 blows the air through a heat exchanger 4 to the air reservoir 14, which has an open outlet. This set up enables to create an air flow with constant properties and low overpressure and velocity. The automatic system of cooling was not changed inside the FC; current can emulate constant exterior conditions for the experiments. Additionally,

the flow meters and sensors take different measurements throughout the experiment.

Since the temperature can be changed in different blocks of the heat exchanger and the FC, the temperature was measured before and after these blocks from 7 to 5, from 2 to 9, from 9 to 12. An absolute pressure of the water line was measured before the heat exchanger at 16; the pressure difference was measured before and after (at 18) the heat exchanger. The sensor 15 measured the absolute pressure in the line with air and the sensor 14 - in the air reservoir; 10 and 17 measured the pressure difference. A room humidifier with piezo element was used to create different ambient humidity levels.

The flow rate of hydrogen and inlet air temperature measurements had 0.8% and 0.5% relative accuracy. Power measurements were taken using voltmeter and ampere meter results with an inaccuracy of 0.15%. The air humidifier had a relatively low accuracy of 3%.

2.4.4 Experimental results and discussions

H2Bio writes values every 0.3s into a file. The power output is shown in Figure 25. Previously, the maximum output power was equal to 90W, but the recovery experiments, as well as first experiments with the change of ambient conditions, led to an increase to 120W output power. The installed heat exchanger created a temperature range from 15^{o}C to 25^{o}C. In this experiment, only a temperature effect on the FC performance was studied.

The influence of inlet air temperature on the efficiency of the FC was calculated using the integration method [182]. It was chosen due to the uneven behavior of the experimental curves. The relation between the efficiency and inlet air temperature is shown in Figure 26. It is clear that efficiency grows when inlet air temperature is lower.

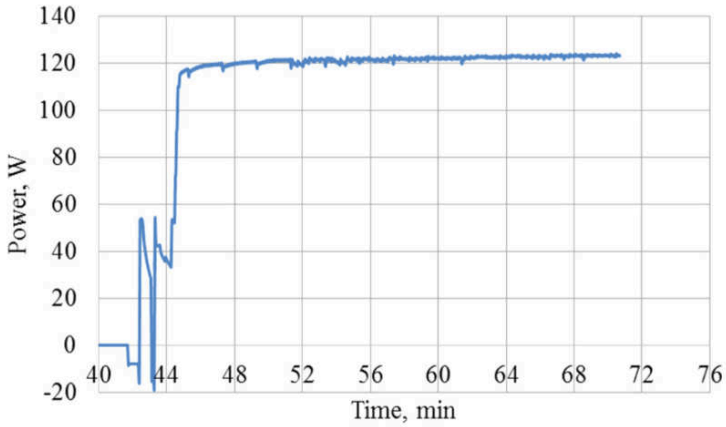

Figure 25. Typical behavior of the FC power curve.

To investigate the effect of the level of humidity on FC performance, a humidity controller was added to the system. The cross effect of humidity and inlet air temperature was obtained. There were three humidity levels: 20%–25%, 60%–65%, and 95%–100%. All three humidity levels were tested at three temperature levels: 19°C, 22°C, and 24°C.

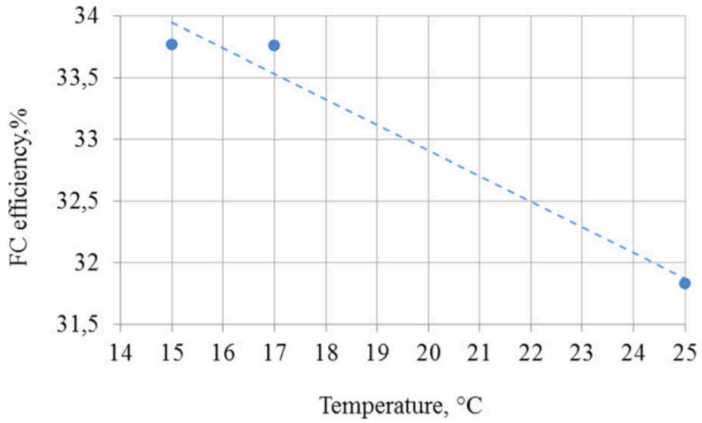

Figure 26. Effect of inlet air temperature of FC efficiency.

In Figure 27, the efficiency of the system increased with increasing relative humidity. The decrease in temperature again positively affected the efficiency with no connection to the level of relative humidity.

Figure 27. Effect of inlet air temperature and relative humidity on FC efficiency.

However, this dependence is quite weak as the efficiency changed only by 0.22% between 19°C and 24°C. The change in relative humidity from 25% to 100% during 18°C -19°C temperature level only resulted in an increase of efficiency by 1.14% and by 0.81% at 23°C - 24°C.

As a result, the dependence of FC efficiency on the relative humidity and inlet air temperature was studied. It was experimentally found that the lower air temperature results in better FC performance and this dependence is in the range of 15-25oC does not have a linear dependence. In order to achieve this, an experimental setup H2Bio was upgraded with a system that controls inlet air temperature and humidity. Experiments led to a conclusion that an increase in relative humidity has a positive effect on FC efficiency, but it is rather small.

2.5 Chapter 2 conclusions

The novel H2Bio 175W power system was designed and developed. The outcomes of this chapter include system integration of the new reactor with commercially available PEM FC and a battery backup supply, study of working regimes of the system, MH reactor output pressures, system integration difficulties, backup power supply working modes, ambient conditions. All the outcomes of this study prove the possibility of creating an energy storage system capable of utilizing "MH storage – FC – load" concept, adding important scientific progress for the lab level technology. Additionally, all the outcomes are essential for the creation of the next level kW scale energy storage system.

Experimental investigations of the H2Bio can be concluded as follows:

- Two MH reactors 140l each with proposed novel design can both store and clean hydrogen due to the metallic alloy selectively absorbing hydrogen

- System integration of novel reactors suggests using free space in the next design of the reactor or installing a buffer before the FC to provide the necessary volume of hydrogen for the impulsive manner of FC intake
- Commercial FCs have different working regimes and require an energy source for start-up procedures and as a backup supply. Different energy sources were tested in the simulation test bed and described in Chapter 3 of this thesis.
- An air cooling system carries out from an FC stack an excessive heat that can be used and utilized in the design of the next kW scale energy storage system for MH desorption process. The possibility of this concept is experimentally investigated in the Chapter 4. The kW scale energy storage system was designed, developed, and tested in Chapter 5.
- The power output of the FC rapidly decreases with increased ambient temperature and limited relative humidity
- The efficiency of an FC increases with increased relative humidity and decreased outlet temperature. However, the effect is somewhat small: for the range from 18^{o}C to 24^{o}C, the FC efficiency difference is 0.6%, when the relative humidity in the same range reaches the increase in 3.4% in the relative humidity change from 25% to 100%.

Chapter 3 Novel energy storage simulation methodology and hardware-in-the-loop tests

During the experiments on H2Bio system described in the previous chapter, a need for additional energy source for the FC operation was formulated. Power supply from the battery is normally needed for the periods of the fuel cell start-up and for the compensation of the power consumption peaks exceeding the maximum FC power. Additionally, FC may experience unexpected shut downs that also need a compensation from the back-up supply. In this chapter, a simulation testing facility was designed and developed with the purpose of experimentally comparing different types of batteries working in tandem with the FC used in the systems of this thesis. The creation of energy storage simulation methodology in the form of hardware-in-the-loop tests described in this chapter helps to avoid expensive physical experiments that require the purchase of different battery components.

3.1 Battery system design state-of-the-art and problem statement

Current technologies do not present sufficient capacity for the grid scale tests and the system integration purposes. A battery emulation system integrated to a physical AC/DC converter can be programmed to provide a physical model of novel technologies in the form of an output voltage. Running novel simulation methodology and allowing physical experiments for the grid requirements response and the system integration tests allows informing the technology development ahead of availability at scale.

Battery system design includes six steps. First, the battery parameters form the basis for the design. Then the discharging current, short circuit current, and conductor size are calculated. And finally, after the protection devices are selected, the whole battery system assembly is implemented [183]. The first step introduces a high level of uncertainty when battery size and type are being defined as both depend on the hybrid system components, system requirements, weather conditions, etc. For the case introduced in this thesis, Bateman village, a lead acid battery was chosen for the H2Bio system; however, a similar case from [184] argued a different choice of battery for the case with similar weather conditions and performance criteria.

Narrowing down by the development level of the technology, there are four types of batteries described also in the Chapter 1 (Table 1,2) quite mature and reliable with

many examples on the market [185]: Lead Acid with low specific energy and limited number of cycles but economically viable, Nickel-cadmium functioning in extreme temperatures with environmental concerns, medium level toxic Nickel-metal-hydride with high energy density but fast self-discharge rate and expensive Lithium-ion with high number of cycle and low maintenance. All four types of batteries have numerous examples of usage in FC systems [186], in power generation systems [187], but a strong methodology of choosing the type of battery suitable for each case is still not defined.

The high cost of physical equipment for experimental tests provides modeling approach with an additional advantage. In the literature, there are economic and "cost of use" models [187] that make a comparison based on one criterion. Tremblay et al. [188] uses three types of battery models: electrical, electrochemical, and experimental [189],[190] and states explicitly that electrical characteristics of the battery are reliable enough to use for the system design. The modeling has also been improved by introducing mathematical models with probability [191] and Thevenin models [192].

Tremblay-Dessaint model [188] was integrated into a physical battery emulator Regatron that produces an output voltage of different battery types. It is a regular AC/DC converter with an output voltage calculated from the initial parameters of a battery type. Theoretically, any energy storage can be programmed into this emulator. In this thesis, an experimental set-up was created to test different types of batteries to work in tandem with PEM FC thus a controllable load has been added to the system through a Triphase inverter controller and connected to the battery emulator Regatron. It created a model based physical battery-testing set-up for a specific case of H2Bio PEM FC. In general, any current profile can be integrated to the model in order to test different types of batteries in a pseudo-physical test environment.

3.2 A mathematical model of simulation

Tremblay/Dessaint model uses the state of charge only as a state variable and accurately reproduces the curves from the manufacturer for the four types of battery chemistries: Lead-Acid, Lithium-Ion (Li-Ion), Nickel-Cadmium (NiCd) and Nickel-Metal-Hydride (NiMH). The battery model supplies an output voltage to the voltage source and uses a non-linear equation based on the actual state of charge of the battery [188].

The five mathematical curves build the dis/charge curve (Figure 28):

Part 1: Nominal voltage (battery constant voltage) [V]

Part 2: Internal resistance loss [Ω]

Part 3: Polarization Voltage [V]

Part 4: Polarization resistance [1/AH]

Part 5: Exponential Zone voltage [V]

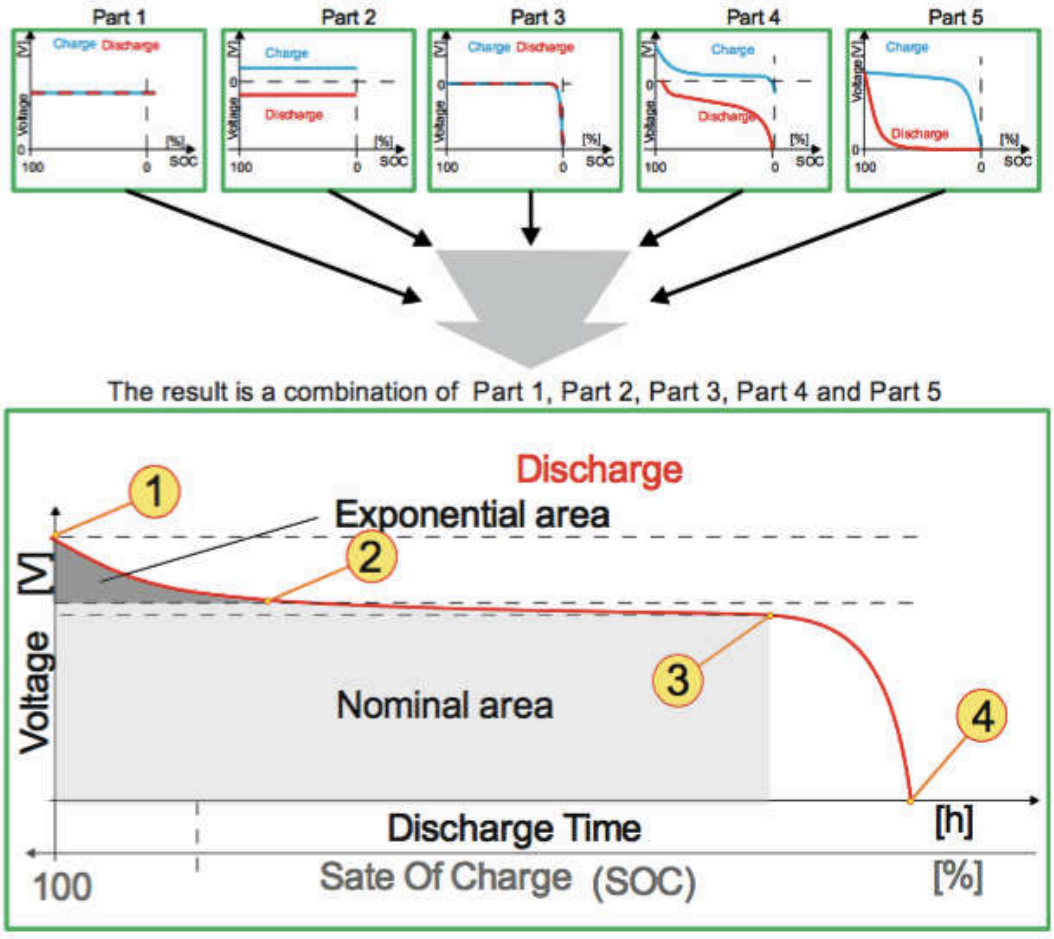

Figure 28. A mathematical model based on Tremblay/ Dessaint, 2009. 1 – fully charged battery, 2 – the start of the exponential zone, 3 – end of the nominal area, 4 – end of the discharging/start of charging

The most significant advantage of the model is the simplicity of the extraction of the parameters, as no experimental measures need to be taken. The requirement is in three points from the typical discharge curve of the manufacturer: fully charged voltage, the end of the exponential zone, the end of the nominal zone and the maximum capacity, usually, also the internal resistance (R) can be found.

The model has few assumptions. The internal resistance is assumed constant during the cycles and does not change. The characteristics of the model are taken from the discharge characteristics and used for the charging as well. There is no change in capacity of the battery with the amplitude of the current. There is no temperature dependence, self-discharge, and memory effect. The model has few limitations. The minimum load on the battery is 0V, the minimum capacity of the battery is 0 Ah. The maximum state of charge cannot overcome 100% even if the battery is overcharged [188].

The proposed model and approach can be used to model other types of batteries as well. The model itself can be upgraded to increase the level of accuracy, which is currently depends on the points extracted from the discharge curves.

The described model for four types of batteries has been used programmed into a Regatron GSS battery emulator and used in this experimental setup.

3.3 Methodology

Battery emulator Regatron GSS receives power from an AC university grid. DC side of the emulator is connected to the Triphase DC/AC converter. Energy flow is then sent to an AC side of the Triphase converting battery voltage (ranging from 10 to 70V) to send back to the University grid. The flow of the current is simulated using Triphase model in Matlab, where current curves are programmed from real profile data obtained in Chapter 2 of this thesis. The goal of these experiments is to test different types of batteries working in tandem with PEM FC for the design of the kW scale system.

3.4 Experimental set-up scheme and components

The experimental set-up (Figure 29) consists of a battery emulator and controller. It can generally be characterized as a bidirectional AC/DC/AC converter. The Regatron GSS control system is based on a mathematical model of Tremblay and Dessaint [188], where different models of different batteries are programmed. The BatSim controller receives few input parameters, including a battery type, the state of charge, battery model data. These parameters are used to calculate desired output voltage reference to be introduced at the DC-link and set that voltage by feed-forward decoupling control. The three components: rectifier, controller, and a math model combined to simulate the performance of any battery as seen from the DC-link.

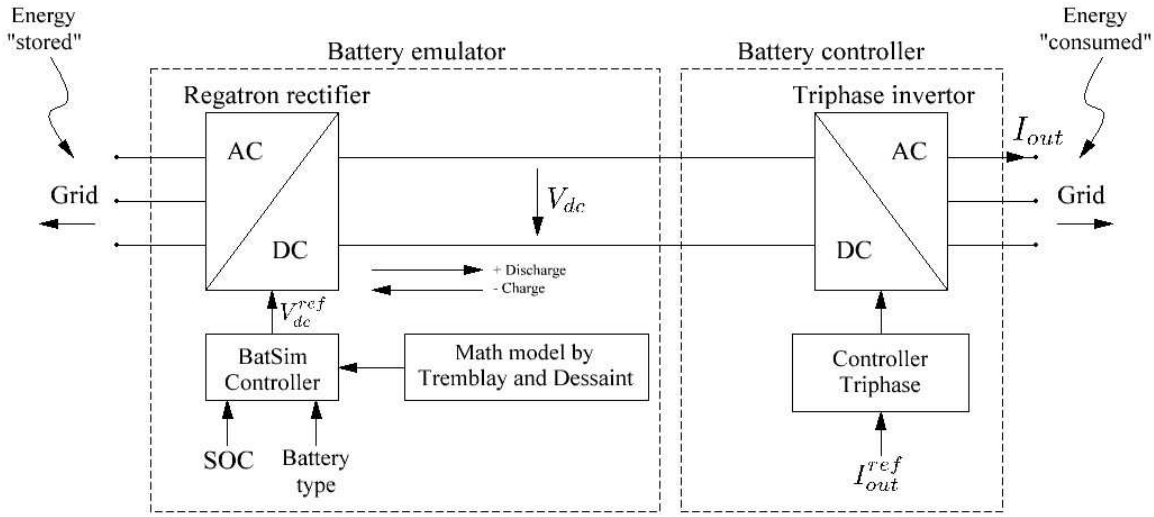

Figure 29. Set-up scheme

The Triphase inverter and controller perform as a battery current control system. The system accepts current output reference as an input parameter and introduces the desired value. The created scheme is capable of emulating any battery in case of the presence of a proper mathematical model. Also, the system models not only charge or discharge currents but also the terminal voltage change according to the state of charge of the battery. The set-up components are present in Figure 30.

Figure 30. View of the simulation experimental set-up

1). Battery emulator. Regatron TC.GSS hardware emulates four types of batteries

(NiMH, NiCd, Li-ion, Lead acid). It is physically an AC/DC converter with a script based performance currently running on the Olivier Tremblay and Louis-A. Dessaint [188] mathematical model.

2). Bottom-layer control. The current flow is controlled to or from the simulated battery using Triphase model in Matlab. AC/DC power converter has two functions. First, it controls DC bus voltage and forms 3-phase AC voltage vectors to correspond to required currents. The model uses 3-phase to d-q coordinates transformation. While I_q represents reactive current component and can be controlled directly, I_d component is calculated in order to maintain DC bus voltage. Second, DC/DC converter aims to control DC charging/discharging the battery connected to DC side. The model allows setting this current value in Amperes and current flow direction (to or from the battery). Flowing from battery DC formed by DC part of converter model charges the DC bus. The AC part of the model calculates I_d component for the AC and forms the corresponding AC voltage in order to create AC currents that will discharge DC bus capacitor and maintain it on required level.

Integrated current control model has been added to the Triphase control scheme (Figure 31).

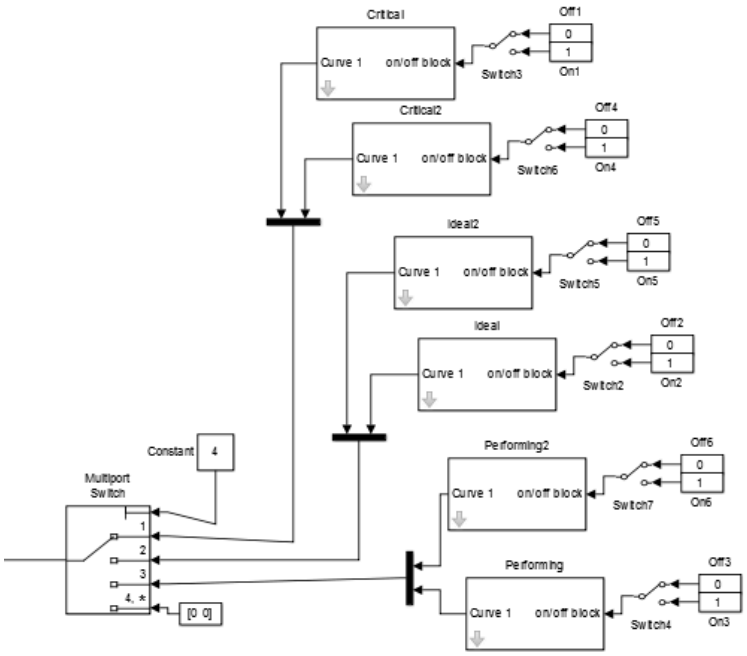

Figure 31. The proposed current curve that represents three working modes of the battery

3.5 Characteristics of the tested batteries

In the first experiment, Li-ion battery was charged to 80% state of charge; it had 15 cells in series and 15 cells in parallel. In the second experiment, NiMH battery was initially charged to 80%. The model had 30 cells in series and 5 cells in parallel. The third model of NiCd battery was initially charged to 80% state of charge. The model had 30 cells in series and 15 cells in parallel. Finally, the Lead-acid battery was initially charged to 80% state of charge. The model had 30 cells in series and 4 cells in parallel.

3.6 Results

After obtaining charge and discharge curves, it was clear that a separate case based criteria need to be formulated prior to the analysis. First, the battery serves as a backup supply in the system thus it meets the load demand when the FC is out of operation. Also, the battery is needed to compensate peaks of the power consumption, which exceed the maximum fuel cell power. In this case, battery suffers a rapid discharge regime with a loss of energy, which needs to recover as soon as possible before the next FC shut down. The depth of discharge can be obtained from the state of charge graph. Since almost all the batteries had a very close level of capacity and the same initial state of charge percentage, the change of the graph can determine the highest rated power among all four. It is essential for the proposed system in this dissertation to have high power performance for the battery to make sure that the fuel cell shutdowns will not affect the load.

Second important criterion comes from the rapid charge regime as the FC starts to charge the battery after normalizing operating condition, as the battery needs to recover the energy spent. But it also important to take into consideration the smoothness of the graph as rapid changes lead to the shortened life cycle. The velocity of the recovery can also be obtained from the state of charge graph. The slope of a tangent line to the SOC graph during the battery charging regime was used.

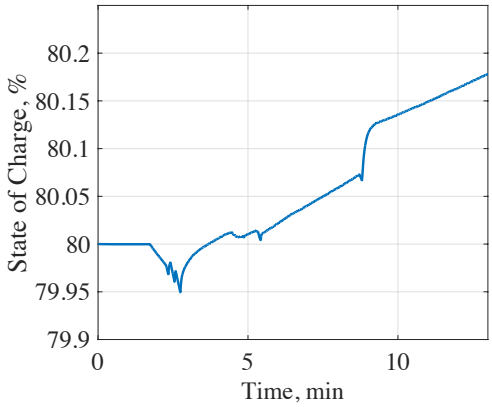

Figure 32. SOC of the Li-ion battery model

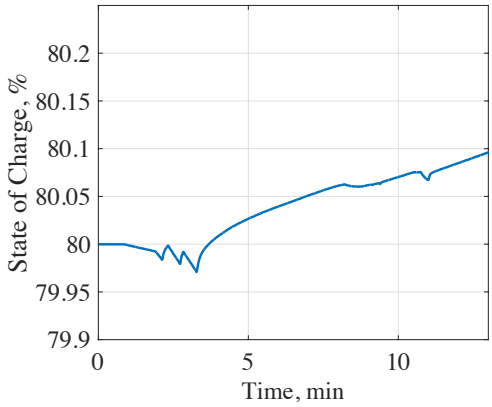

Figure 33. SOC of the NiMH battery model

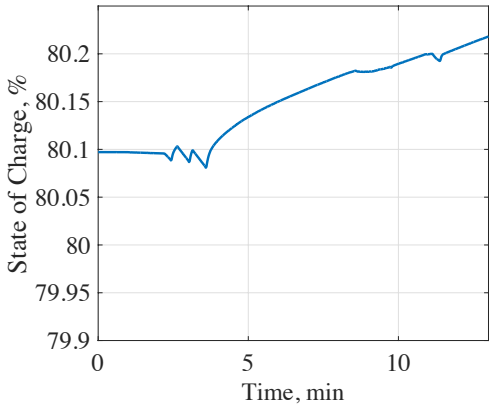

Figure 34. SOC of the NiCD battery model

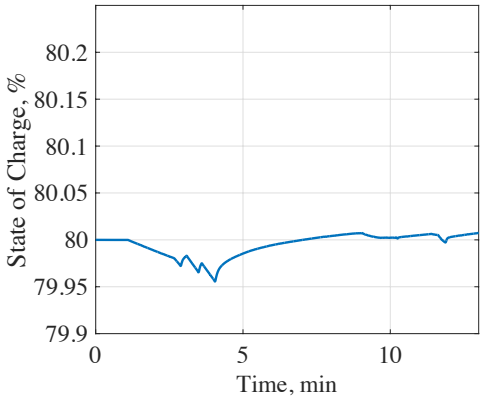

Figure 35. SOC of the Lead Acid battery model

When we obtained the graphs, it became evident that the capacity of the batteries need to receive closer attention, as the depth of discharge is almost identical and highly depends on the capacity.

Regarding the slope of the tangent line, Li-ion battery has the sharpest graph during the charge, NiMH and NiCD are close in the growth rates, Lead Acid has the smoothest graph of all. After the additional analysis on the economics, environmental friendliness, and other criteria, a Lead Acid battery was chosen for the use in the system.

The methodology and an experimental set up itself created the test bed for future energy storage systems design and development that was previously limited by the theoretical investigations and very specific cases from the literature. With the methodology described in this thesis, any system requiring an energy from the battery can be simulated if the needed current profiles are known (experimentally obtained).

3.7 Fitted Efficiency and Degradation Models

The model was improved by adding fitted efficiency and degradation models. Parameterized efficiency and degradation models have been created by conducting a parameter sweep using the physics-based battery model developed in [193]. The result is a function for capacity loss as a function of the state of charge and state of health and a function for efficiency regarding state and charge and power. These simplified (Figure 36) functions were embedded as scripts within the Regatron battery emulation system.

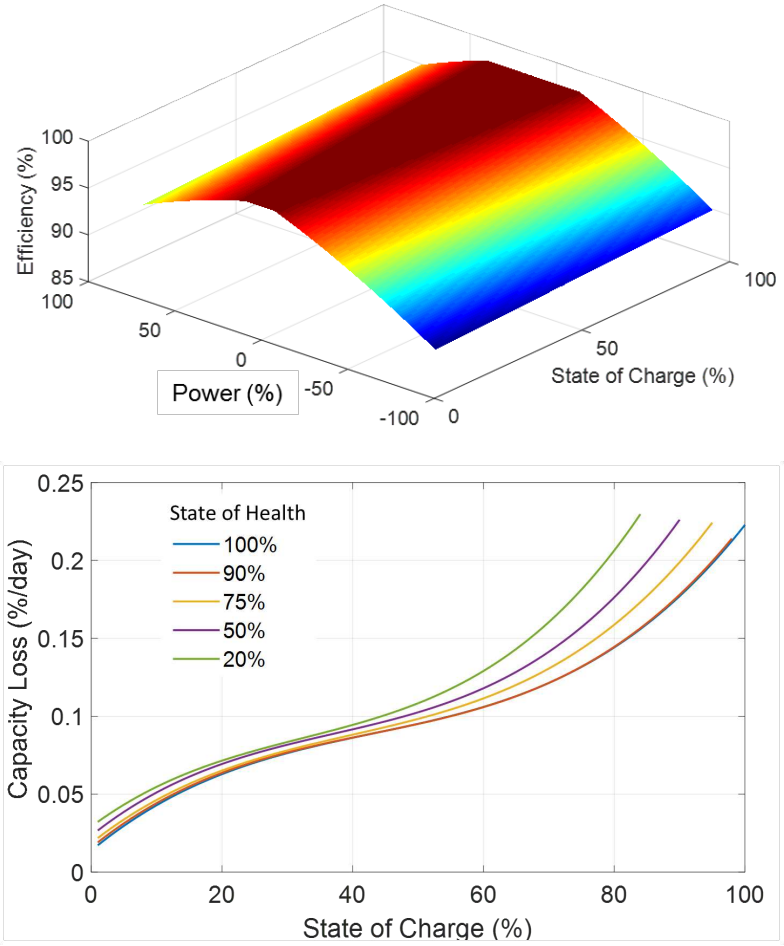

Figure 36. Fitted degradation and efficiency models, using the results from a parameter sweep of simulations of a physics-based model

3.8 Results

The results are presenting the capacity and energy losses from the Li-Ion battery for the typical, optimal, and critical working regimes of the H2BIO, with the battery starting at a state of charge of 20%, 50%, and 80%, are shown in Figure 37. Operating the battery at a higher state of charge leads to a greater loss of capacity and lower

energy losses while operating at a low state of charge leads to lower loss of capacity but higher energy losses. Operating cost will be a function of the operating point, but will also depend on the cost of degradation vs. the cost of energy losses.

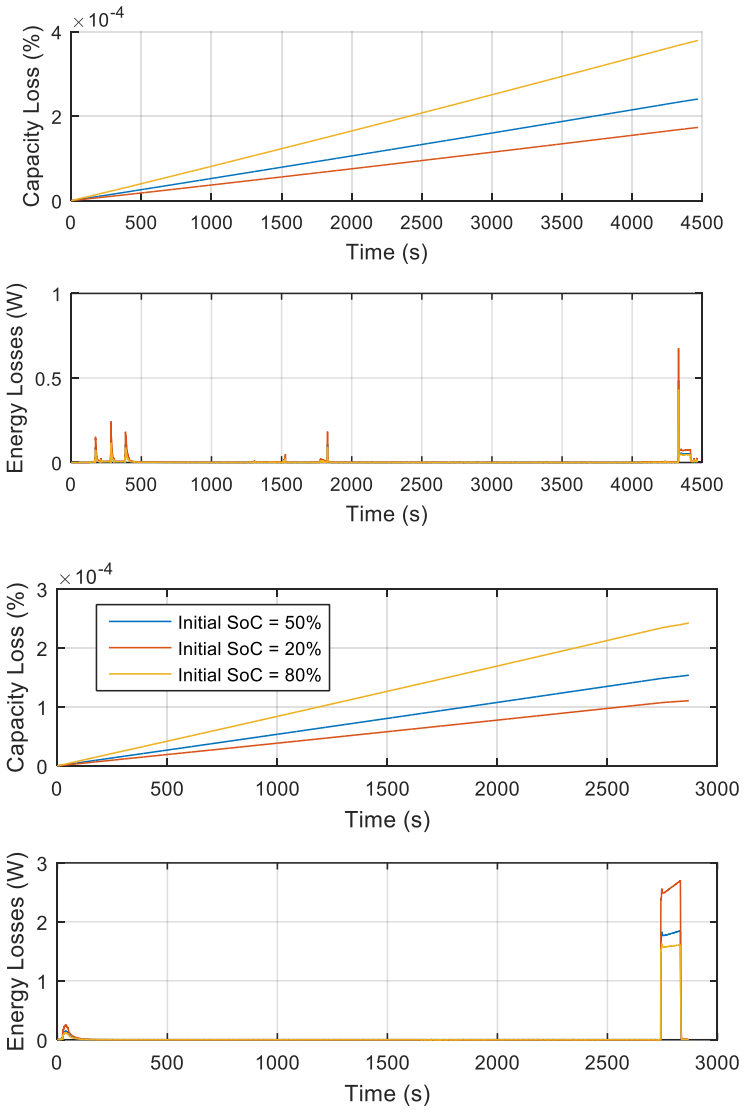

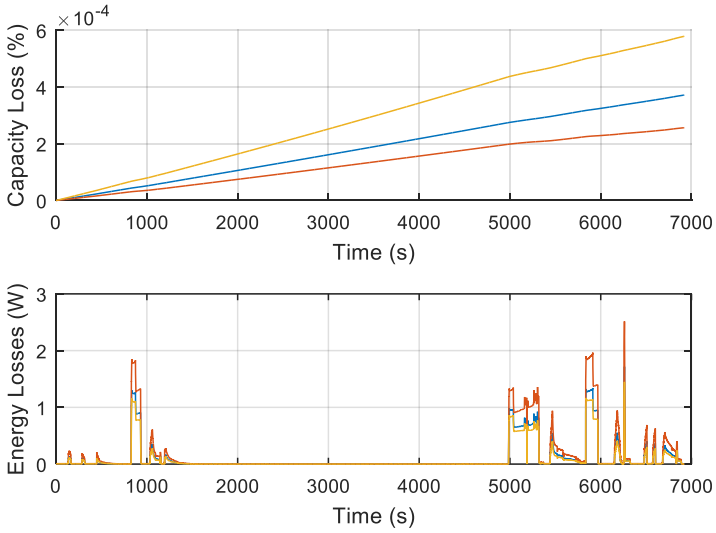

Figure 37. Results showing the capacity and energy losses from the Li-Ion battery for the typical, optimal, and critical working regimes of the H2Bio, with the battery starting at a state of charge of 20%, 50%, and 80%

3.9 Chapter 3 conclusions

Proposed energy storage simulation set up is capable of modeling different types of batteries and testing them in a physical situation with current profiles obtained from real experimental set ups. This approach enables mathematical models examining in an actual physical condition as a tool for energy storage system design. For the case investigated in this thesis, a current profile of the energy demand from the FC was obtained and integrated into the setup. The current profile was tested on four different types of batteries that were described and compared theoretically among other energy storage technologies in the Chapter 1 and the obtained SOC graphs were compared.

The Lead Acid battery showed a smooth operating regime as well as fast recover to the initial SOC, thus was chosen as a backup supply for the FC in the next experimental setup design.

The mathematical model of the methodology has also been improved with additional degradation and efficiency models and helped to maintain cost analysis for the capacity level of the battery. The results showed that higher SOC battery operation leads to a greater loss of capacity and lower energy losses. Lower SOC battery operation leads to lower loss of capacity but higher energy losses. Based on the case requirement, the system must supply electricity to the small town for as long as the solar energy is not functioning, thus the battery needs to maintain as high SOC as possible and the system needs to automatically charge the battery whenever it is possible. This concept has

been developed in Chapter 5.

Even though the difference in the outcomes cannot be considered as significant for the purpose of tandem operation with the FC for the specific case described in this thesis, the smoothness of the response to the operating regimes, the recover dynamics of these batteries and other experimentally obtained results make a sufficient contribution to the current theoretical basis of the battery technical characteristics comparison (Table 1, 2). The simulation test bed and methodology described in this thesis provide a valuable contribution to the process of energy storage system design that was previously limited by theoretical comparison.

Chapter 4 Preliminary experimental investigations of excessive heat output

Research objectives of the preliminary experimental investigations include internal and external FC exhaust heat temperature measurements and qualitative assessment of the desorption process inside a MH reactor. The goal is to experimentally investigate the possibility of external heat carrier replacement noted in Chapter two for the future kW scale autonomous H2Smart prototype and form technical requirements for the intermetallic compound for the MH reactor.

Throughout the experiments, the internal temperature of 1 kW power PEM FC was tested in different working modes from zero load to 800W. The measurements were taken by a temperature sensor inside the stack. Also, the temperature and velocity of airflow from the cooling fans of the same FC were measured. For this, the load was steadily increasing, and the measurements were taken by the anemometry method. For the qualitative assessment, a hot airflow was simulated and the desorption process was measured inside a MH reactor.

4.1 FC internal temperature measurement

1 kW PEM FC was connected to a load that could perform from 0 to 800W. Different sets of load were introduced throughout the experiment. In the Figure 38a, zero load was introduced until the 50th minute. However, the battery inside the system was charging, which kept the overall output power from the FC around 200W decreasing to 100W as the battery was getting charged. After the 50th minute, an additional load of 500W was introduced, making the total load of 600W for the FC, decreasing to 550W till the end of the experiment.

In the Figure 38a, the temperature increased to 26^{o}C and slowly decreased as the load was decreasing. On the 50th minute, after an additional load was introduced, the temperature grew significantly to 38^{o}C and stayed around this measurement. After the load was switched off, the temperature slowly decreased to 25^{o}C.

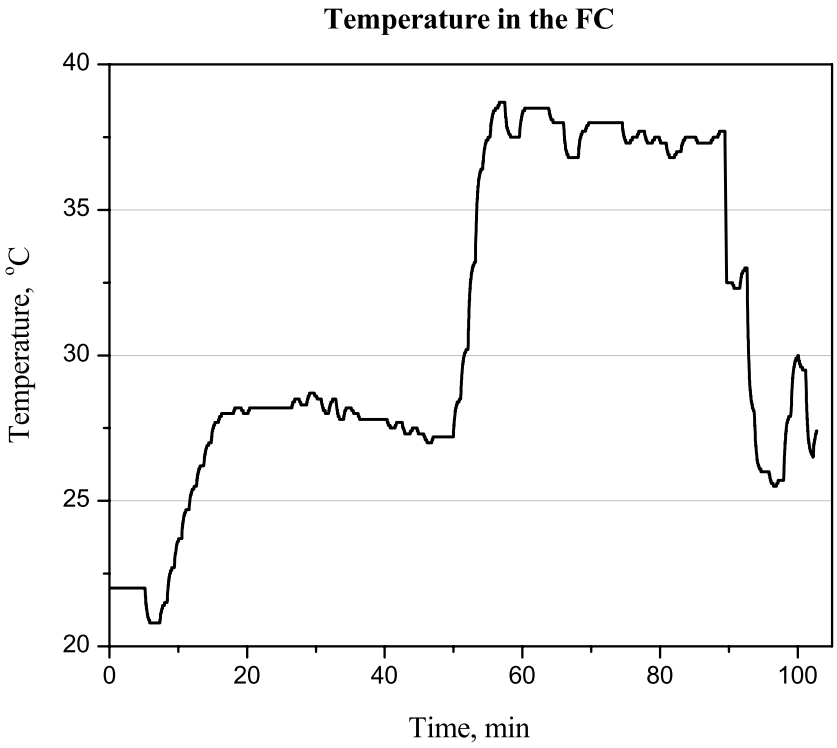

(a)

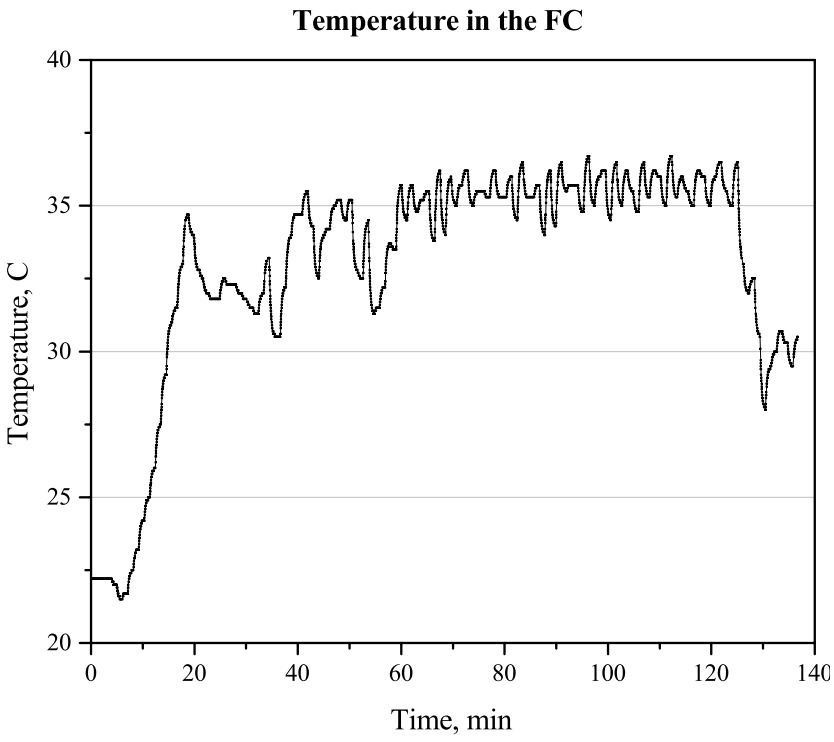

(b)

Figure 38. Temperature inside the 1 kW Hoppecke 1100 PEM FC during different working regimes

(a) – zero load, constant load (400W-500W); (b) – volatile load, maximum load (800W)

For the second test (Figure 37b), on the 10th minute, a load started to steadily increase from 300 to 700W until the immediate shut down was introduced in the 20th minute. When the FC does not receive enough pressure of hydrogen, the automatic shut down stops the electricity generation process. The FC made a few attempts to restart until we supplied enough pressure for it to restart in the 38th minute.

It is interesting to note that regardless the numerous shut down and crisis working regimes, the temperature in the Figure 37b never goes lower than 25^{o}C. We assume that this happens due to a previously collected heat after 20 minutes of stable operation. Another crisis was introduced in the 55th minute. The reaction of the system was similar to the described above. For the rest of the experiment, the load changed from 500W to 800W, introducing volatile load regime. And, in the 130th minute, the load was switched off, and the temperature slowly decreased to 28^{o}C. After the 130th minute, the system turned off an automatic battery charging process where the temperature started to grow again, showing similar results as on the previous experiment.

To conclude inlet temperature measurement experiment, a variety of load scenarios were tested, and the internal temperature of the FC was measured throughout these scenarios. The findings of these tests are the following:

- The FC heats up to 25-30^{o}C even in the absence of load
- Crisis shutdowns do not bring a rapid decrease in the FC, on the contrary, the temperature stays on the levels higher than the zero load temperature
- It can be estimated that 30^{o}C is a lower average FC internal temperature with lower temperatures during the start-up procedures

4.2 FC exhaust heat output measurement

The output heat flow of the exhaust air from the commercial 1 kW Hoppecke E-1100 PEM FC with five cooling fans on the back (Figure 39) was experimentally measured. A temperature of the flow and a velocity were measured on each cooling fan separately. While measuring these two parameters, the change of power was in the range from 75 to 835 W, steadily increasing, the last measurement was taken when the load decreased from 835W to 640W. The thermal anemometry Testo 450 was used for the measurements, the output heat was measured in a dynamic airflow state. Output temperature measurement of the FC exhaust heat can be found in the Figure 40, the

output velocity from five cooling fans is shown in the Figure 41.

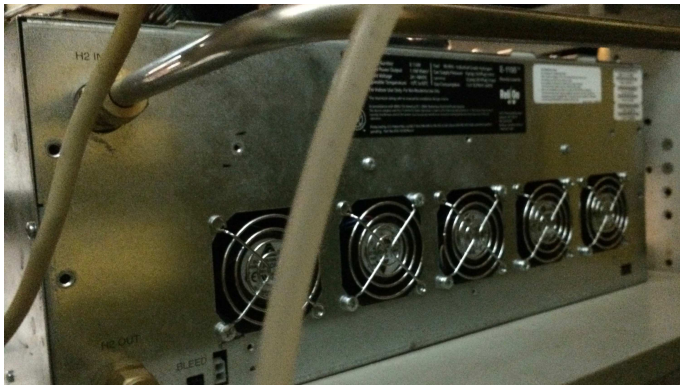

Figure 39. The view of 1 kW Hoppecke 1100 PEM FC with five cooling fans on the back

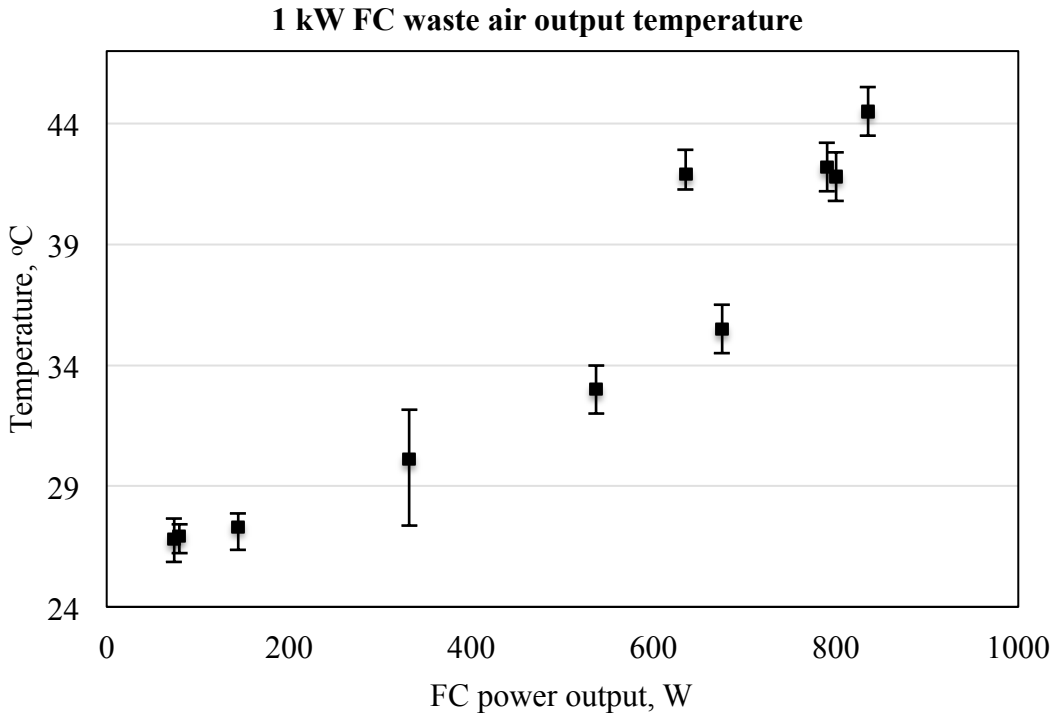

Figure 40. 1 kW Hoppecke E-1100 PEM FC exhaust air temperature (averaged for five cooling fans and scatter)

In the Figure 40 all the measurements for each power level were averaged for five cooling fans and scattered. Most of the points show low to no difference between the cooling fans along the backside of the FC for each power level. Also, the temperature of the exhaust air steadily increases as the power level increases. Since FC is reactively

answering to the load, the more demand is introduced, the larger amount of reactions take place inside the reactor, inside the cell. Thus, the more heat is produced. The point that is outside the overall shape (640; 42) was obtained closer to the end of the experiment after the maximum load for this experiment was introduced. The assumption here, again, is that the FC accumulates heat inside the system and the temperature measurements will be higher closer to the end of the working session.

The comparison of the change of power with the change of temperature leads to poor results. The change of power was from 75W to 835W, while the temperature changed from 26.5°C to 44.5°C only. The overall external temperature went above 25°C right after the start of the experiment but did not increase higher than 45°C (318K). This outcome significantly limits the variety of possible metallic alloy compositions that could be used in such systems.

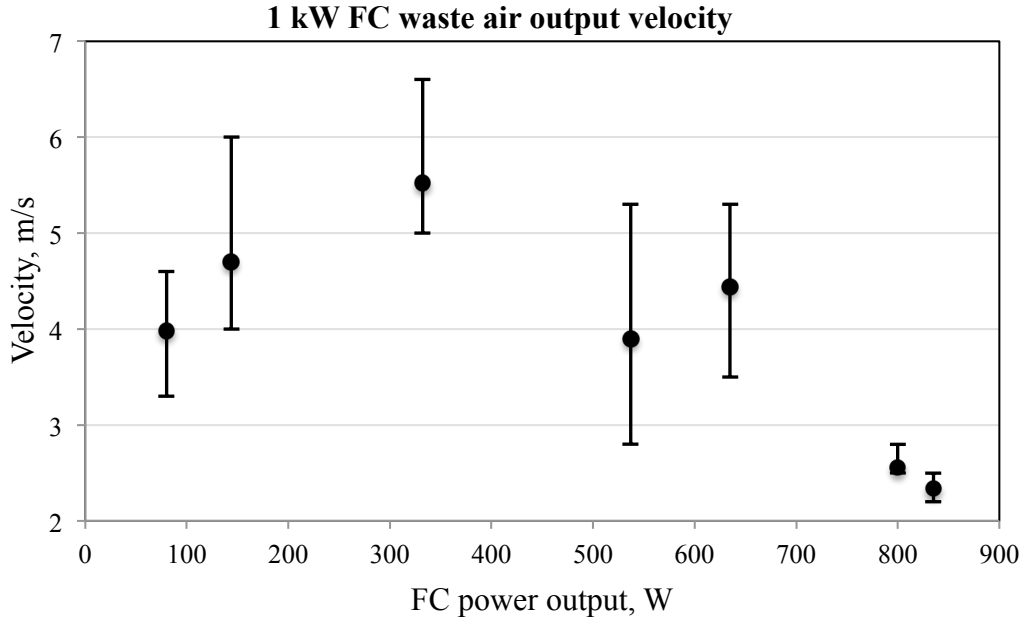

Figure 41. 1 kW Hoppecke E-1100 PEM FC exhaust air velocity (averaged for five cooling fans and scatter)

The results of velocity measurement along the backside of the FC are shown in the Figure 41. On the contrast with the temperature measurement, the velocity of the cooling fans is not equal among the five fans for one specific power level. Also, no correlation was found with the increase of power. Since the cooling system of an FC is automatic, the assumption regarding these outcomes is that the change of velocity serves as the variable for the amount of the heat released from the FC.

The velocity of the fans decreases when the load is close to its maximum levels to save the power. With the decrease of load, a more intensive cooling period starts with the increase of cooling fans' velocity until the collected amount of internal heat is released completely.

Summing up, the lower average temperature level of output air of the FC is 30^{o}C, and the chosen alloy should ensure required pressure levels with the heating agent temperatures around 20^{o}C. The difference in 10^{o}C was kept for the losses in the system and possible unstable output air levels.

After the internal and external temperature measurements with the FC, the backside of the FC was equipped with a radiator, shown in the Figure 42, Figure 43.

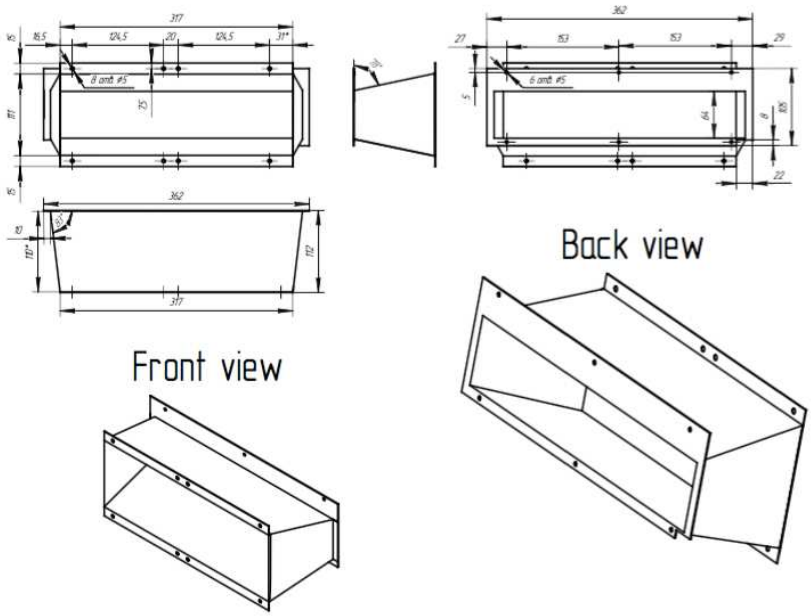

Figure 42. The design of the radiator

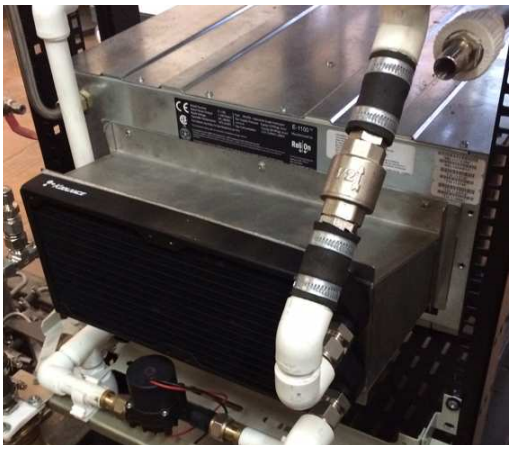

Figure 43. The view of the radiator that utilizes waste heat of the FC in H2Smart

The radiator collects exhaust heat from the fuel cell and warms up the water inside the system. The water then is sent to the MH storage system, ensuring the necessary level of heat for hydrogen desorption process. The experiments to prove it are described in the following chapter.

4.3 Qualitative investigations of air-heated MH reactor concept

For this experiment, a MH storage reactor of a bigger volume made in JIHT RAS was chosen to test the possibility of using air as a heating agent for the desorption process of the MH reactor. Of course, air is not considered as the best heat carrier for this system. It is only considered as a heating agent due to the availability of excessive air in the system already. The next step of the development of the concept described in this Thesis includes the change of the heat carrier and realization of the concept in a thermosyphon system. However, at this stage of development it was important to qualitatively test the desorption process using a heat carrier in the form of air for the purpose of the development of a kW scale system described in Chapter 5.

In this section, the qualitative experiment demonstrates the possibility of heating up of the 13 st.m^3 maximal hydrogen storage capacity [207] reactor made in JIHT RAS initially designed for liquid cooling/heating by the air, having parameters similar to the outlet air of commercial air-cooled PEMFC system with capacity in the range of 1 –2.5 kW (e). The data on Hoppecke H2.power product, provided by the manufacturer, is provided in Table 9. The primary goal of the experimental investigations is to obtain the data on the volumetric hydrogen flow at discharge and how it corresponds with the demanded refueling flow of the PEM FC stack.

Another important issue is the maintaining of the pressure at the reactor outlet to fit the requirements of the PEM FC stack. Since the equilibrium parameters (*P*-*C*-*T*) of the hydrogen absorbing materials are mainly defined by the composition of the alloy [208]-[212] and $LaNi_5$ family gives wide opportunities to achieve the demanded parameters by the modification of the initial composition, here the question of the outlet pressure is recognized as secondary.

Table 9. The parameters of Hoppecke H2.power PEM FC power generation units

Installed H2 power (kW)	Air volume flow (m^3/h)	Air temperature at maximal load (^oC)	Proposed area for in- and out air flow (cm^2)	Hydrogen consumption at maximal load (st. l/min)	Minimal stack inlet pressure (MPa)
1.1	391	50 - 55	289	13	0.0551 – 0.0830
2.5	883	50 - 55	660	30	0.0551 – 0.0830

4.3.1 Experimental setup

The reactor RS-1 detailed design and experimental tests are presented in [213]. The reactor consists of stainless tubes with inner channels for liquid heating and cooling. MH placed in the gap between the inner channels and the external wall of each tube.

The reactor has 49 tubes, 65 cm in length each, with common hydrogen collector. Each tube holds MH inside due to a stainless mesh filter. The intermetallic alloy used in the system is $La_{0.5}Nd_{0.5}Al_{0.1}Fe_{0.4}Co_{0.2}Ni_{4.3}$, and it fills around 70% of each tube, the total weight of the alloy is 81 kg, the properties are presented in Table 10 [194].

Table 10. The properties of $La_{0.5}Nd_{0.5}Al_{0.1}Fe_{0.4}Co_{0.2}Ni_{4.3}$ [194]

Temperature (^oC)	Equilibrium desorption pressure (MPa)	Hydrogen mass content, max (%)	Desorption heat (kJ/mole H_2)	Heat capacity (kJ/(kg ^oC)
25	0.11	1.1	35.3	0.42
80	1.16			

The reactor combines liquid cooling inside and natural convection on the outside of the reactor. For the intensification of the latter, the cover has rectangular ducts (200*600 mm) on the top and the bottom of the cover. For this experiment, the cover has been flipped horizontally to provide horizontal airflow to simulate the geometry of the flow from the PEM FC. The scheme of the set up is shown in Figure 44. Three 1kW power electric heaters provided airflow to the inlet of the duct, were connected in parallel and

had a manual control by variation of voltage from 0 to 220V (AC). The use of curve duct prevented direct thermal radiation from the heaters to the first MH tubes in order to maintain the convection nature of the external heat transfer in the experiment. The total simulated thermal power Q is equal to the heat output by the 2.5 kW PEM FC cooling system:

$$Q > W_e(1-\eta)/\eta, \tag{4.1}$$

where W_e and η represent electric capacity and efficiency of PEM FC. The efficiency of the commercial systems is taken η = 0.46, taking into consideration hydrogen lower heating value. The outlet of the cover was equipped with five PY-1238H240S axial exhaust fans with the capacity of 190 m^3/h in a row. The temperature measurements were taken through the drilled hole in the inlet duct.

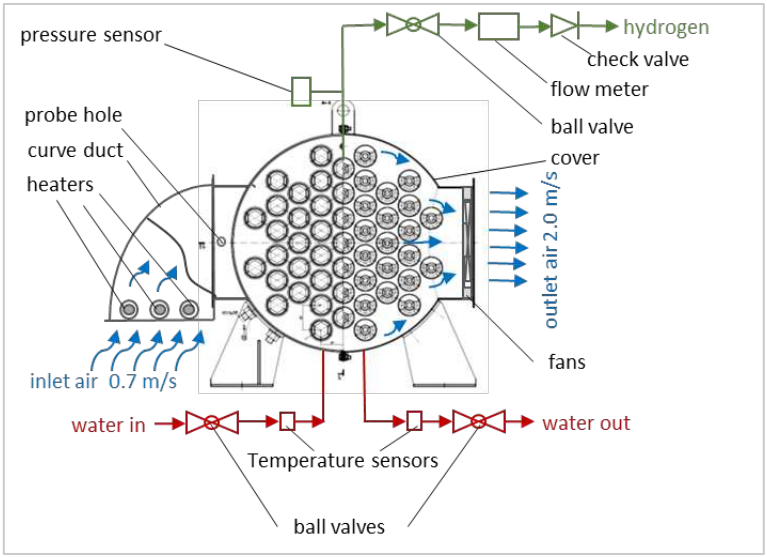

Figure 44. Experimental installation scheme.

Prior the experiments, electric heating parameters were tested; the target 50°C inlet temperature was obtained at 1.7 kW electric power on the heaters. The velocity measurements at the inlet of the duct were taken by thermal anemometer Testo 415, giving the average of 0.7 ± 0.1 m/s. The measurements of the air temperature at the inlet of the reactor were measured by the flexible type-K thermocouple probe in several points.

The outcomes of the preliminary tests are the following:

1). MH cartridges inside the reactor create hydraulic resistance thus the obtained volumetric flow was below the characteristics of the H2power 1.1 kW (Table 9), which means that the 50^{o}C air heating can be considered as the “lower” estimate character.

2). An excessive thermal power of 1.7 kW has also covered all the heat losses in the system, thus the 50^{o}C air flow in the experimental setup models real system integration of MH energy storage with 1 kW PEM FC.

Additionally, the reactor had the residual water inside the system (12 l), was charged to 50% of the capacity, did not have the alloy composition optimized to the given temperatures and pressures, and did not have thermal insulation on any of the outer surfaces. All of these components contribute to the statement that current experimental set up corresponds to the “lower” estimate.

The measurements during the experiment include pressure (absolute) in the reactor, water temperature inside the reactor, hydrogen flow at the outlet of the reactor. The methodology of the experiments is the following:

1). The reactor was closed with steady-state values of hydrogen pressure and stable water temperature inside the reactor.

2). The fans were switched on; the heaters received 1.7 kW electric power (175V AC). The hot air was supplied to the system resulting in the pressure grow inside the reactor.

3). The ball valve was opened creating no limitations for the hydrogen flow except the hydraulic resistance of the piping between the reactor and an atmosphere.

4). Hydrogen pressure and flow data were taken for the time period of 75 minutes.

5). Two initial thermal states were introduced in different experiments. During the “hot” start the reactor was initially warmed up to 30^{o}C. “Cold” start had the ambient temperature of the reactor.

The parameters of the experimental investigations are presented in Table 11.

Table 11. The parameters of experimental investigations

	Inlet air velocity (m/s)	Inlet air flow (m^3/h))	Air temperature after heaters (^oC)	Initial temperature of reactor	Initial hydrogen abs. pressure (MPa)	Initial SOC (%)
"Cold" start	0.7 ± 0.1	300±43	50 ± 2	17	0.14	50
"Hot" start	0.7 ± 0.1	300±43	50 ± 2	30	0.15	41

4.3.2 Results of experimental investigations

The change of hydrogen flow from the reactor and the change of pressure for the cases of "hot" and "cold" start are shown in Figure 45. Red lines in Figure 45 and Figure 47 represent the required refueling rate for H2.power 1.1 and H2.power 2.5 kW PEM FC systems for the reference.

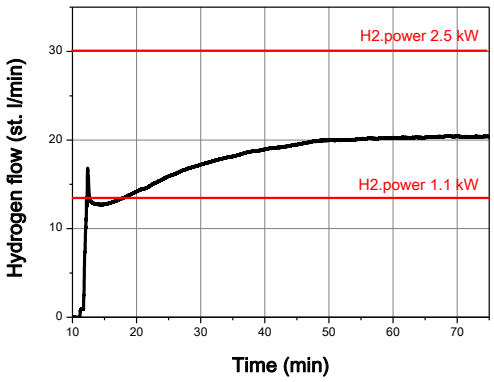

Figure 45. Hydrogen flow at air heating of RS-1 reactor (cold start). Red lines – the required refueling for the H2.power 1.1 and H2.power 2.5 kW PEM FC systems.

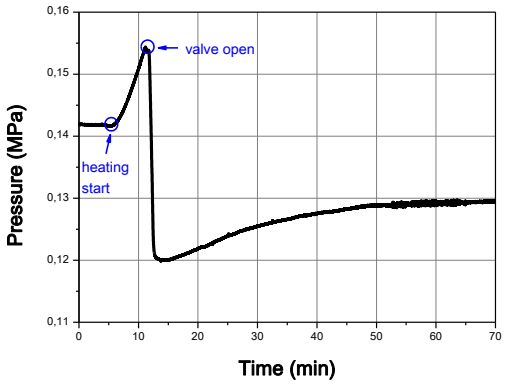

Figure 46. Absolute pressure in RS-1 reactor at air heating (cold start).

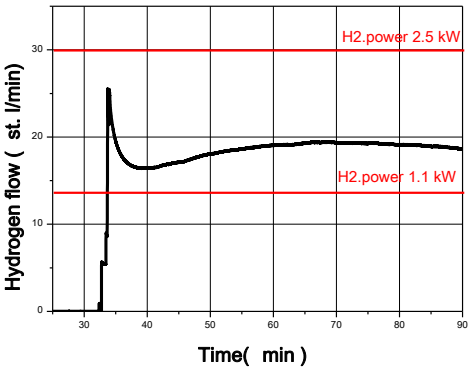

Figure 47. Hydrogen flow at air heating of RS-1 reactor (hot start). Red lines – the required refueling for the H2.power 1.1 and H2.power 2.5 kW PEMFC systems.

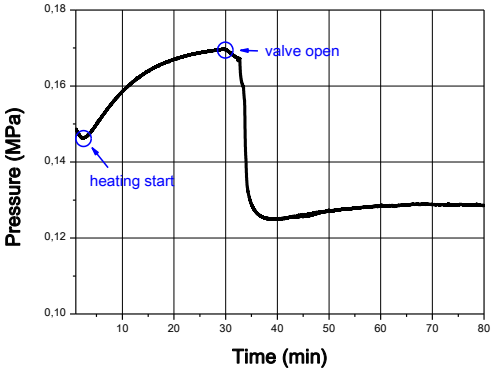

Figure 48. Absolute pressure in RS-1 reactor at air heating (hot start).

The temperature of the water inside the hydrogen storage system has reached 30°C during the "cold" start and 34 °C for the "hot" start. The tendency to the water temperature grow was noted in both cases.

The reactor provided a steady flow of hydrogen for more than 75 min higher than the refueling rate need of 1.1 kW (e) power. In this experiment, the reactor was taken with water and natural convection heating and cooling processes with no major upgrade made for this experiment. The level of hydrogen flow did not reach the required refueling rates for the 2.5 kW (e) power. The proposed method demonstrated a sufficient reserve for receiving higher results as no thermal insulation was present. The reactor could be emptied from the water inside the system. The AB_5 alloy with higher saturation pressure at 30°C and the same level of reaction heat could be chosen. The passive heat transfer intensification could also be used.

One of the important outcomes is that the use of PEM FC exhaust air as the heating agent has the risk of condensation with manufacturer's declared relative humidity of the air exceeds 90%. This creates a need for water evacuation from the heat exchange surfaces.

4.4 Chapter 4 conclusions

Preliminary investigations and experimental results show the possibility of using the exhaust air flow from a commercial kW scale PEM FC for the needs of desorption processes in the MH storage system that previously needed a liquid external heating agent and limited the use in the autonomous systems. The proposed novel method of

both utilizing waste heat and replacing heating agent in the MH show satisfying results for further development of the system that is carries out all the processes at the safe operation regimes. The desorption process might be also supported by the pressure instead of the temperature of the heat carrier, however, in this case an electrolyzer would have to perform higher pressure levels too, which brings an overall pressure level of the system higher, affecting safety requirements of the system. In this thesis, a safe operation was at the cornerstone of the proposed concept thus the next chapter investigates possible IMC and system design for the obtained temperatures of the heat carrier rather than bringing the pressure level up.

Possible next steps may include the introduction of thermal insulation, further investigation in metallic alloys with the search for higher pressure rates at the low temperatures 20-40 ^{o}C, heat transfer intensification, radiator replacement by the design of the reactor itself. However, the design of the reactor should take into consideration high humidity level of the outlet FC hot air and eliminate condensation issues. The possibility of using the proposed concept with the high-temperature FCs shows interesting scope of research that lies outside of the purpose of current thesis.

Chapter 5 Design and development of a 1 kW hydrogen energy storage system prototype based on PEM fuel cell and MH

For the case of Northern region of Russia with high solar potential, described in Chapter 1, an energy storage system concept was introduced to work coupled with solar panels. The proof-of-concept of such systems was designed and developed in the form of H2Bio experimental set up. However, the need for additional back-up power supply, external heat carrier and hydrogen supply has been noted as a major point for improvement in the next power level systems of such concept. In the Chapter 3, possible back-up systems were tested. In the Chapter 4, the possibility of utilizing internal excessive heat from the FC was experimentally proven. As the result of the investigations in Chapters 2-4, current Chapter 5 presents the design and development of a 1 kW scale hydrogen energy storage system with no need for additional heat carriers supplied. Additionally, the system is equipped with an electrolyzer for hydrogen production on the spot of system integration and with a lead-acid back-up battery supplies system. The developed system is designed to function at the safe operation regimes and low pressure levels.

5.1 Technical and design requirements for the system

A novel energy generation system was designed to store excessive energy from renewable sources of energy or the simulation of renewable sources of energy. The technology ensures the quality of electrical energy in micro energy systems that have a load and distributed energy sources through the use of hydrogen energy storage. Hydrogen storage component uses a solid intermetallic alloy that forms metal hydride as the result of a chemical reaction with hydrogen. Electricity generation is performed by 1kW PEM FC. Exhaust heat from 1kW PEM FC is utilized for desorption process in MH reactor, sorption and desorption processes in H2Smart use hybrid heating and cooling techniques to perform comparative analysis on the same system. The main parameters of the system are measured and controlled through NI-PXI and LabView interface.

Table 12. Technical characteristics of H2Smart MH storage system

Fuel cell power level	1000W
Maximum working pressure	no more than 1MPa
Metal hydride metallic alloy	$LaNi_5$

The amount of hydrogen stored in MH reactor	1000 l
The nominal pressure of MH reactor charging	no more than 0.5 MPa
The nominal excessive pressure of MH storage discharge	no less than 0.055 MPa
The maximum excessive pressure of discharge	no more than 0.083 MPa
The nominal hydrogen consumption rate	no less than 13 norm l/h and no more than 15 norm l/h
Type of cooling/heating	hybrid: air and water
Heat agent 1	air, 50…55°C, consumption rate 391 m^3/h, inlet velocity 0,7 m/s
Heat agent 2	water, 0…95°C

System components of H2Smart include water preparation, electrolyzer, low-pressure hydrogen storage, PEM FC, control. The system is designed in a separate module and located in a 19-inch stand. The weight and the dimensions of the system require the doorway width to be at least 800 mm. One person can transport the module horizontally.

Table 13. The technology used in the system components of H2Smart

System component	Technology	Development level
Water preparation	Deionization using ion-exchange filters and subsequent filtration.	The technology is developed; numerous solutions are available on the market.
Electrolyzer	Electrolysis of water with solid polymer	The technology is developed; numerous solutions are available on the market.
Low-pressure hydrogen storage	Reversible solid-state storage of hydrogen in metal hydrides	Pilot samples, separate examples of integration to storage and compression systems
Fuel cell	Electrochemical generation from the reaction of hydrogen with air oxygen in the cells with electrolyte	The technology is developed; the work is done towards reducing the cost of installed capacity, increasing the efficiency. A steady growth of commercial sales

		around the world
Control system	Control technology based on NI-PXI with the user interface in LabView	The technology is on the market

Technical characteristics of the H2Smart system components:

1. Electrolysis subsystem consists of H2box-100 electrolyzer with 100 norm l/h (standard) and with hydrogen pressure 1.5 – 3 atm;
2. Hydrogen storage subsystem consists of specifically designed MH reactor with nominal charging pressure up to 0.5 MPa, nominal excessive discharging pressure no less than 0.05 MPa, nominal hydrogen consumption rate no less than 15 norm l/h (standard), cooling type: liquid (technical water 0…95^{o}C), 5 kg of intermetallic compound $La_{0.9}Ce_{0.1}Ni_5$, hydrogen capacity 1.35% mass., 67,5 kg (750 norm l). Maximum capacity of 1000 norm l can be reached by 6.7 kg of the intermetallic compound.
3. The exhaust heat storage system is the radiator, a heat exchanger with water as a heating agent.
4. PEM FC is an air-cooled E-1100 with nominal power 1100 W, 24/48 V (DC), hydrogen consumption rate 14 norm l/min (during the nominal power 1100 W).
5. Automated system of control and measurement works on the NI PXI (National Instruments, USA).

5.2 Scheme of the system, working principle

The system (Figure 49) uses excessive electrical energy as an input (regular 220V in this set up). The electricity is supplied to the electrolyzer and releases hydrogen, which is being processed through a hydrogen dehumidifier that is integrated to the electrolyzer due to high-level requirements for the absence of humidity in hydrogen that is sent to the metallic alloy.

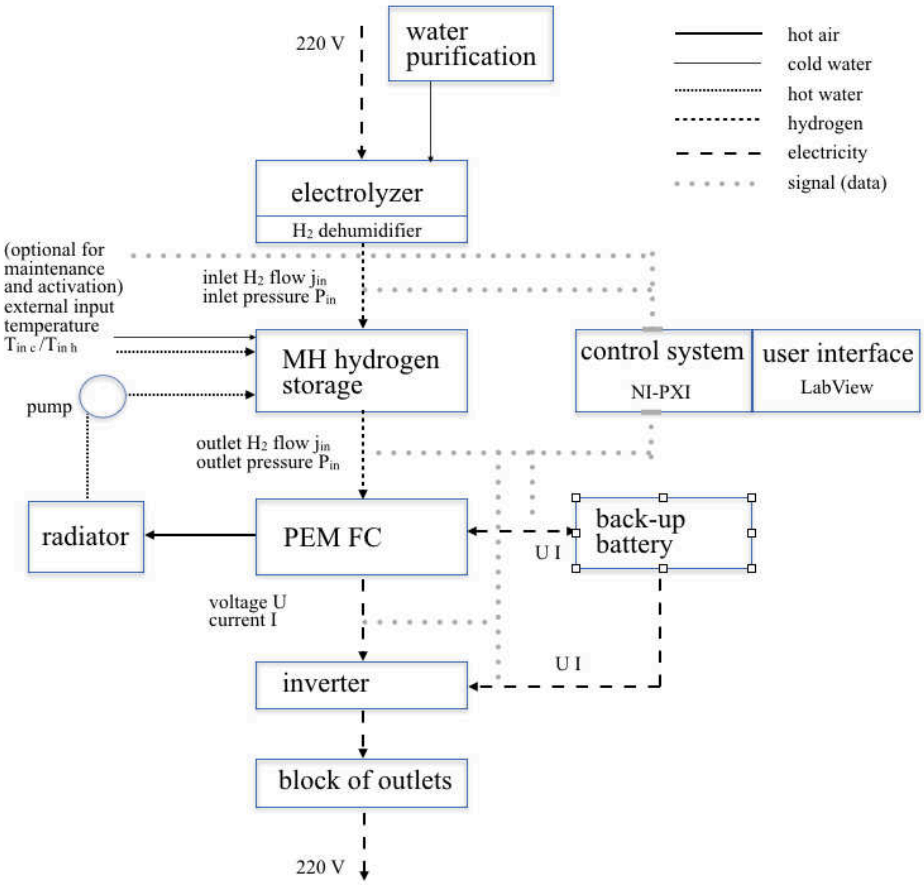

Figure 49. The scheme of the H_2Smart experimental setup

Dehumidified hydrogen enters the sorption process inside the reactor. The chemical reaction of the formation of MH requires heat removal thus cold water supplied to the reactor either through an external input or from the radiator. Hydrogen is stored in the reactor until the demand load exceeds the electricity production rate from the renewable sources of energy or the simulation of such production. When this happens, the FC is started by a small capacity backup battery supply and hydrogen is released from the reactor by desorption process with additional heat supplied. After the FC has reached nominal working conditions (60°C – 80°C inside the stack), the radiator starts to collect waste heat from the cooling fans of the FC and sends warmed water to the reactor for further desorption process of hydrogen.

The H2Smart output is a 220V outlet through an inverter. An automated system collects different sets of data and responds to the user changes made in LabView interface using NI-PXI integrated to a personal computer.

Gas scheme of H2Smart is shown in Figure 50, the hydraulic scheme in Figure 51, an outline dimensions in Figure 52.

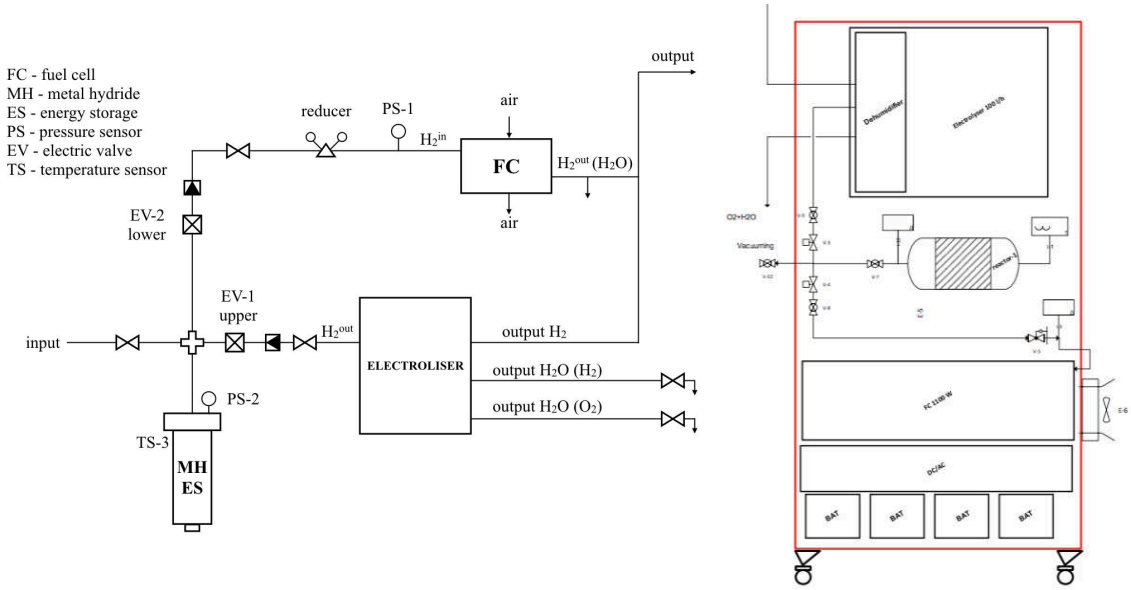

Figure 50. Gas scheme H2Smart

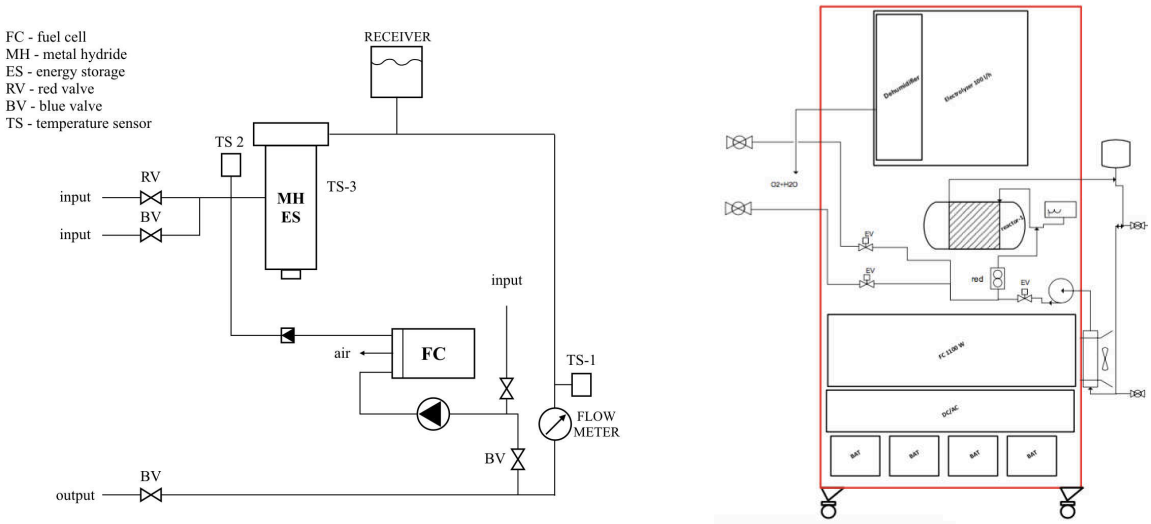

Figure 51. Hydraulic scheme H2Smart

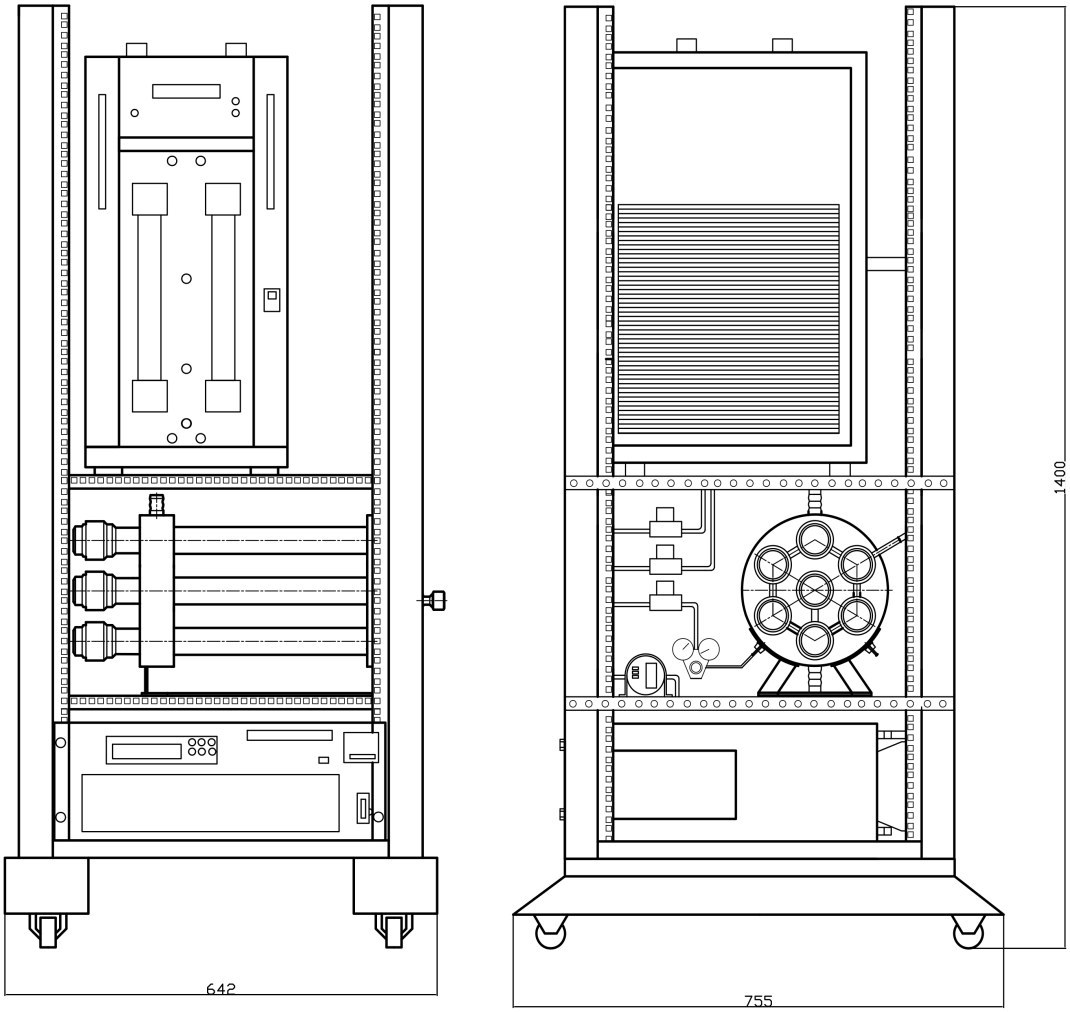

Figure 52. Outline dimesions of H2Smart

Table 14. The list of measuring and testing equipment

Name, type	N	Designation	Main characteristics
Absolute pressure sensors CORUND –DA-001M	2	КТЖЛ. 406233.001	max. pressure 2.5 MPa
Manometer DMME	2	GOST 2405	accuracy class 1.5
Thin-film platinum temperature sensors	4	DIN EN 60751	Temp. range: -70 to +500 °C
CZ-08491-12 Digi-Sense	2	ISO 9001(certified in RF)	Temp. range: -70 to +500 °C

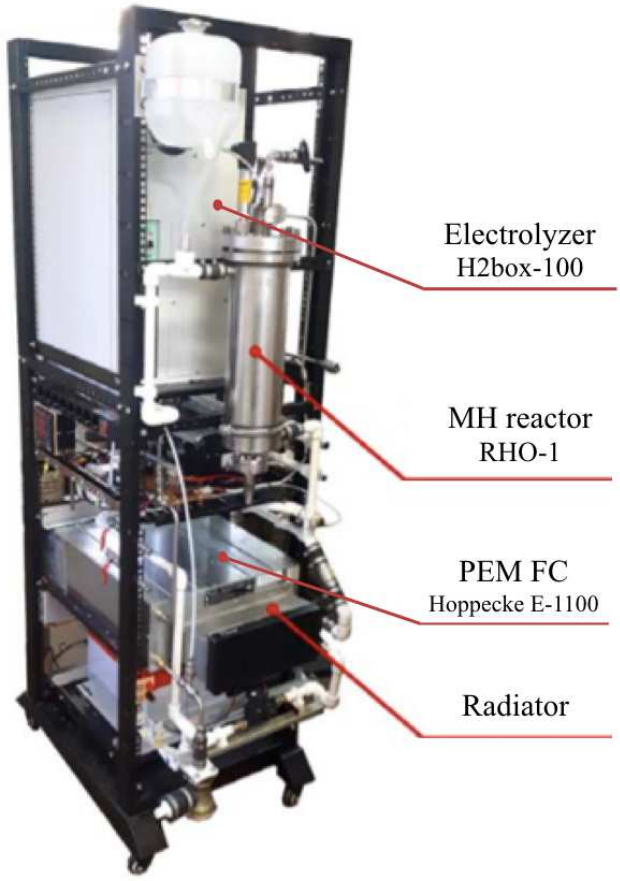

Figure 53. Final view of H2Smart

5.3 System components

5.3.1 «H2box-100» hydrogen electrolyser

Electrolyzer H2Box-100 produces electrolytic hydrogen for industrial and research laboratories to supply chromatographs and gas analyzers with plasma-ionic detectors and other technological processes that require pure hydrogen. The main component of H2Box-100 is an electrolyzer with solid polymer electrolyte with a high proven resource (more than 20000h). Uses standard 220 V input, has fully electronic control, ensures electricity conversion no less than 96.5%.

The high level of automatization of the generator provides a safe utilization of the device and allows to control the technological characteristics of the electrolysis:

- a current flow rate of hydrogen
- conditions of a hydrogen dryer system
- conditions of a water filtering system

- cumulative operational time

- other vital characteristics of the generator

The H2box-100 generator is easy to transport, install and use because of the technological solutions implemented in the generator. It is equipped with replaceable cartridges with ion-exchange resin and silica gel.

Table 15. Technical characteristics of H2box-100

SPECIFICATION OF «H_2BOX 100»	
Hydrogen quality	GOST 3022-80-A
Hydrogen quality (in the percentage equivalent to dry gas)	99,99%
Nominal capacity	100 l/h
Output pressure (set-point range)	1,5 – 3 atmg
Time to reach the operating parameters	15 min
A volume of distilled water	4 l
Power consumption (nominal working parameters)	< 450 VA
Maximum power consumption	< 600 VA
Distilled water flow-rate	< 0,1 l/h
Overall dimensions	300x450x600 mm
Weight	38 kg
Operating conditions	
Ambient air temperature	+5 ºC ÷ +35 ºC
Relative humidity at +35 ºC	Up to 80%

Figure 54. View of the electrolyser H2Box-100

5.3.2 PEM FC

Table 16. Technical characteristics of PEM FC E-1100

Type	FC with a solid polymer electrolyte
Cooling type	Air
Nominal power	1100 W
Nominal voltage	24/48 V (DC)
Height	7 inch
Hydrogen consumption	14 norm l/min (at the nominal power 1100 W)
Hydrogen purity	99.95%

Figure 55. View of PEM FC

5.3.3 MH reactor

MH system is the subsystem in H2Smart that is being studied with respect to heat and mass transfer processes thus an ability to measure temperature inside the reactor, input and output pressure, input and output heating agent parameters is needed. The reactor should be easy to assemble and disassemble as also the characteristics of different metallic alloys are being studied as well.

The module cartridge type reactor is shown in Figure 56.

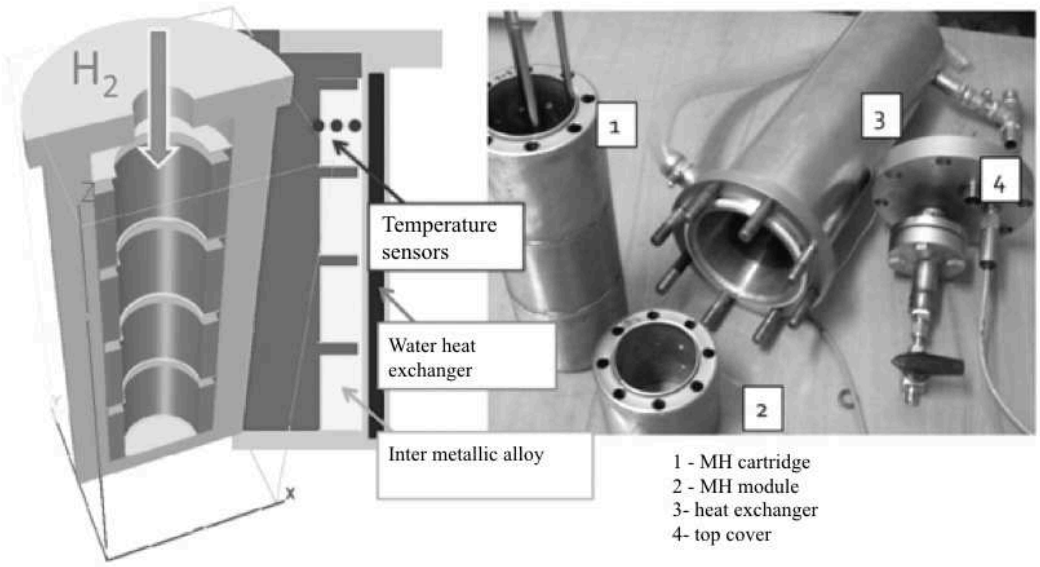

Figure 56. Module MH reactor for hydrogen storage and purification

The reactor has two inlet nozzles, four MH cartridges, water heat exchanger and the flange with a hermetic high-pressure connector for the output of temperature sensors' signal cables. The heat exchanger is also an outer shell of the reactor ensuring strength, rigidity, and tightness of the structure. At the same time, inside the durable casing, there is a tube for cooling and heating agent.

The cartridge holds intermetallic alloy and stores hydrogen when the MH is formed. Due to a significant change in volume of an intermetallic alloy, the design of the cartridge must withstand significant mechanical stress. At the same time, the inner walls of the block must contain porous material that lets the gas in restraining from letting in the metal dust to the free volume of the module and then into the pipeline system. Thus a cartridge cannot be a rigid structure.

The reactor is filled with 5 kg of $La_{0.9}Ce_{0.1}Ni_5$, maximum H_2 capacity is 1000 norm l (st.L), and nominal operating capacity is 720 norm l (st.L).

For the purpose of sustainable and accurate design and implementation of the MH reactors of this type, the additional tests and experiments were needed [195] . Below there are experimental verification tests for two kinetics models presented in [196]-[199]. Several boundary conditions were used in the calculations:

- The third level boundary conditions were set on the inner and outer walls of the

cylinder.; the temperature of the cooling liquid, as well as the heat-transfer coefficient, were taken from the experimental data.

- The variable pressure was set on the input cross-section of the reactor; the dependence of pressure variations over time was taken from the experimental data.

Figure 57 represents the results of calculation of an integral concentration of consumed hydrogen [200]-[204] in the solid state in comparison with experimental results. The calculations were provided with the use of two kinematic models. The data provided by the alloy manufacturer was used for the equilibrium pressure calculations.

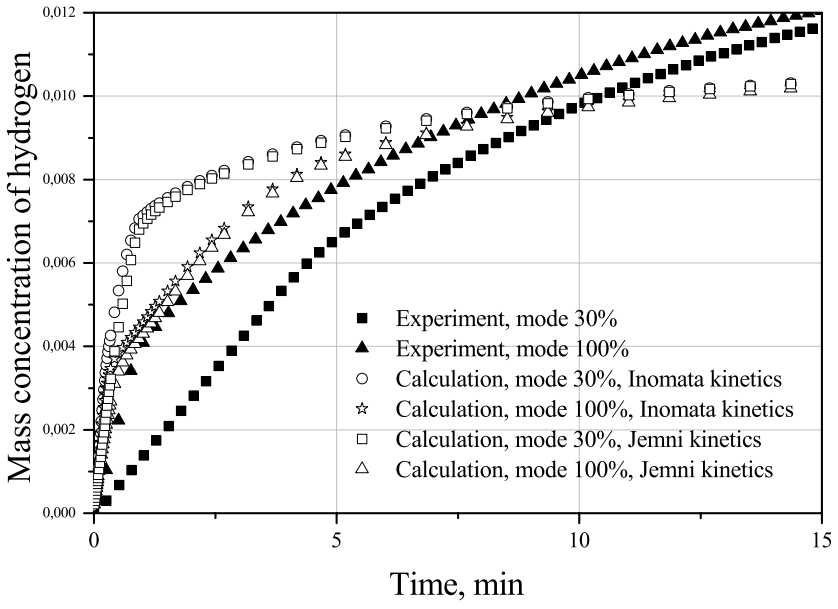

Figure 57. The change in the average integral hydrogen concentration in the solid phase in the process of sorption

It might be seen that calculation results have a significant deviation from the experimental data. Moreover, the calculations which were provided with several different kinetic ratios give the same result.

Based on the comparison of the calculated model with the experimental data, a correction curve was established for the equilibrium pressure of the hydrogen-accumulating alloy as a function of the stored hydrogen concentration, taking into account the actual data on the effective capacity of metal hydride accumulators obtained in the course of experiments on reactor charging.

Figure 58 shows the change in the average integral concentration of bound hydrogen in the reactor during the charging process, calculated using the selected equilibrium

pressure dependence. The selection was made for the maximum mode, that is why in this mode there is the best correspondence between the results of calculation and the experimental data. In the other modes, a deviation is observed at the initial moments of time, which may be due to the dependence of the plateau width of the equilibrium isotherm on temperature, which was not taken into account in this calculation.

Figure 59 represents the temperature change in the bed during the sorption process, calculated using the selected equilibrium pressure dependence. As can be seen from the figure, some correspondence (according to the maximum temperature) is observed in all modes; however, obviously, the conditions for cooling of the reactor and the thermal conditions of its operation require further clarification.

Thus, because of the mathematical modeling, it was possible to achieve a good quantitative correspondence with experimental data on the average integral characteristics of the MH operation and qualitative correspondence in local characteristics.

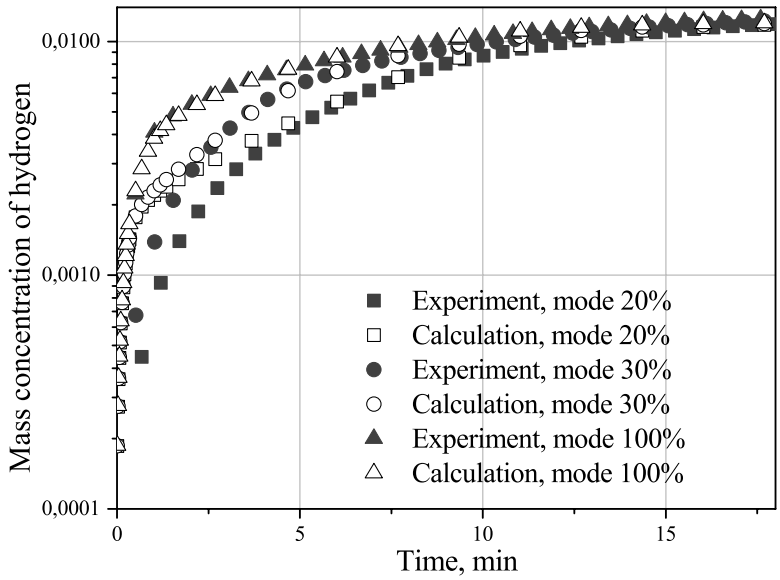

Figure 58. The change in the average integral concentration of bound hydrogen in the process of sorption (calculations using a modified model)

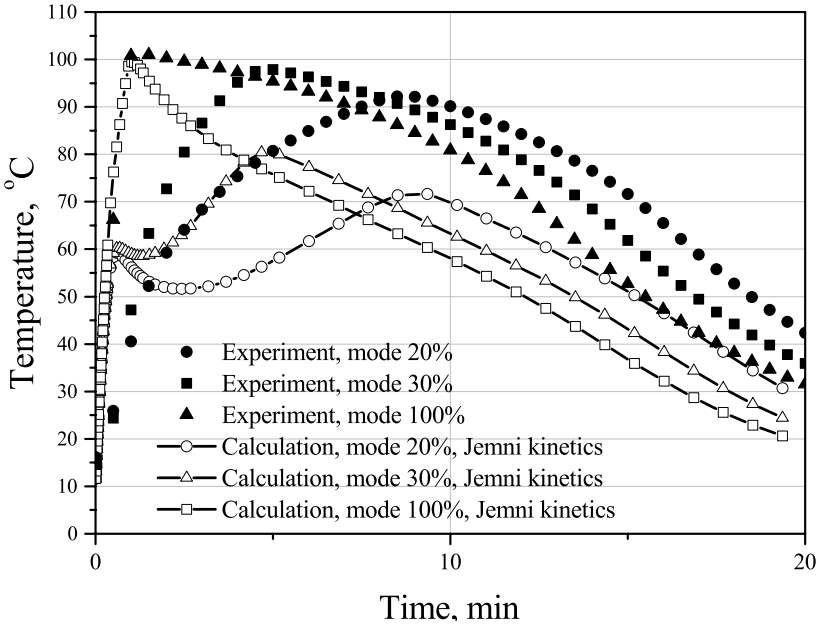

Figure 59. Temperature change in backfill during sorption

5.4 Alloy material composition and preparation

In the works of JIHT RAS [205] -[207], a variety of $LaNi_5$ family alloys were studied. For the creation of MH energy storage reactor, it is necessary to obtain physicochemical characteristics of the intermetallic compounds. The measurement of these parameters has been performed in the experimental investigation of a PCT diagram (pressure, concentration, temperature) using the Sievert method [214]. PCT diagrams were generally described in the subsection 1.7.4 in Chapter 1. They provide enough information to choose a proper alloy that will release satisfactory output pressure of hydrogen experiencing relatively low 30°C - 40°C temperatures of heating agent. As an outcome of this study, a $La_{0.9}Ce_{0.1}Ni_5$ was chosen for the designed system.

5.4.1 Experimental setup description

The method was modified for the bigger scale samples measurement. The laboratory unit YS150 was used, the installation scheme is shown in Figure 60. The installation enables the measurement of sorption and desorption isotherms for material samples from 10 to 800 g at the temperatures from 243 to 673 K and at the hydrogen overpressure up to 15 MPa.

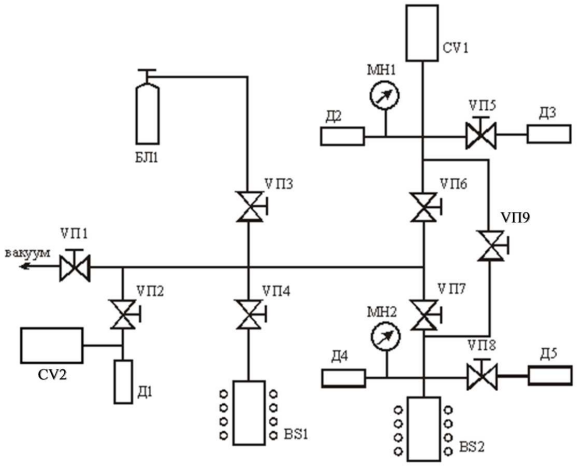

Figure 60. Laboratory unit for measuring the desorption isotherms. БЛ1 – compressed tank with hydrogen; ВП1-9 - valves; BS1 – hydrogen accumulator filled with $LaNi_5$; BS2 – working autoclave; CV1 – buffer autoclave CV2 – vacuum capacity; Д1 – absolute pressure sensor (0-1 atm); Д2, Д4 – excessive pressure gauges (1-150 atm); Д3, Д5 – excessive pressure gauges (1-10 atm)

The activated material sample is placed to BS2 and carefully vacuumed by the turbomolecular vacuum pump “Drytel 1025” until the residual pressure reaches 0.1 Pa. The temperature is kept in the range from 243 to 373 K during the isotherm measurement by the low-temperature thermostat “KRIO-VT-01”, for the measurements in the range from 373 to 673 K the heater of the working autoclave is used.

In the buffer tank CV1, through valves ВП 3,4 and 6, from the hydrogen accumulator BS1 hydrogen is supplied under pressure up to 15 MPa. The pressure and temperature of the buffer tank are fixed by a platinum resistance thermometer Pt and a pressure sensor D2. Then, the amount of hydrogen gas in the buffer tank and the adjacent pipeline section is equal to the amount of hydrogen in all of the the individual sections of the plant. The buffer tank is then connected to the working autoclave BS2 using the valve VP 8. After equilibrium is established (the sorption process is considered complete if the temperature and pressure in the working autoclave remain constant for 30 minutes), the equilibrium amount of hydrogen remaining in the system in gaseous form is calculated as the sum of the quantities in the buffer tank, the working autoclave and the connecting pipelines. The amount of hydrogen absorbed by the sample is calculated as the difference between the initial and equilibrium amount of hydrogen.

The measurement of isotherms of hydrogen desorption is carried out by selecting

calibrated portions of hydrogen from a working autoclave into a buffer or vacuum vessel. After equilibrium is reached, the pressure in all parts of the installation becomes equal. For the desorption process to begin, some amount of hydrogen is taken from the buffer autoclave with a closed valve VP 8. And then the amount of hydrogen in the system is calculated as the sum of the quantities in all tanks. By connecting the working autoclave with the buffer autoclave by the valve VP 8, the desorption process begins. After the equilibrium is reached, the amount of hydrogen in the system is calculated.

The sensors D2 and D4 are used to measure the pressure in the range from 1 to 15 MPa. To improve the accuracy of measurements in the pressure range from 0.1 to 1 MPa, the sensors D3 and D5 are used. The error in measuring pressure by the sensors D2-D5 is 0.05%. When measuring the pressure levels below 1 bar, the sensor D1 is used. The error of the sensor D1 is 0.5%. The temperatures of the working autoclave, vacuum tank, and the pipelines are measured by the chrome-alumel thermocouples with compensation for the cold junction temperature TP5-10. The temperature of the buffer tank is measured with a platinum resistance thermometer Pt. The error in measuring the temperature is ± 0.05 K. The design of the installation also allows changing the volume of the working autoclave.

Calculation of the molar volume of the liberated hydrogen is carried out using the modified Van der Waals equation proposed by Hemmes and co-authors [215]. Comparison of calculation results and literature data [216],[217] shows that in the temperature range from 250 to 500 K and pressure up to 15 MPa, the value of molar volumes obtained using the equation differ from the literature data by less than 0.1%.

5.4.2 Experimentally obtained PCT diagram

The hydrogen-absorbing alloy $La_{0.9}Ce_{0.1}Ni_5$ [218] was mechanically shredded to a particle size less than 5 mm and inserted into metal hydride hydrogen storage units. 100 g of the selected alloy were used to study the absorbing properties. The desorption isotherms of $La_{0.9}Ce_{0.1}Ni_5$ are shown in Figure 61.

The heat of reaction determined by the Van't Hoff equation is ΔH = 30.7 ± 0.5 kJ / mol H_2, the entropy change ΔS = 110 ± 1 J / K mol H_2, the linear approximation of the plateau isotherms in the form φ (X) = φ_0 (X - 0.5) gives the following value for the slope coefficient of the plateau: φ_0 = 0.29 ± 0.06. The value of the hysteresis

coefficient is φ_h = 0,4 ± 0,05. The maximum hydrogen capacity of the alloy is 1.34 ± 0.005% of the mass. The reversible capacity of the alloy is 1.10 ... 1.15% of the mass or 120.. 130 norm l / kg (stL/kg) of the alloy.

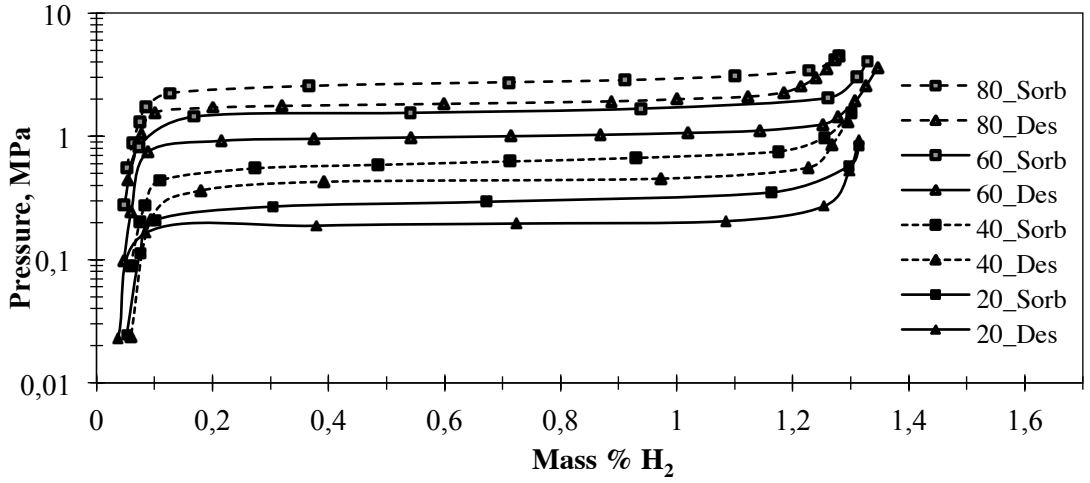

Figure 61. P-C-T (pressure, concentration, temperature) diagram of $La_{0.9}Ce_{0.1}Ni_5$ [218]

According to the 1 kW Hoppecke E-1100 PEM FC specification, operating gage pressure of hydrogen should be in the range between 0.55 and 0.83 bar, which is 0.055 to 0.083 MPa respectfully. Experimentally, we marked the low level of hydrogen gage pressure to be around 0.13 MPa for the safe operation. On the PCT diagram, the 20°C desorption plateau is situated on the level of 0.2 MPa, and the 40°C desorption plateau is situated on the level of around 0.45 MPa.

It can be concluded, that the needed pressure of hydrogen from the MH reactor with this alloy can be reached at the temperatures below 20°C. Thus, the proposed alloy is suitable for the use in this MH system.

5.5 Experimental results, working regimes

The goal of these tests was to experimentally prove the possibility of integration of the proposed MH reactor with a commercial 1kW PEM FC, explore working regimes of the system, run the system coupled with a backup battery power supply.

MH hydrogen storage reactor uses a cartridge approach with free space inside the cylinder. In the previous MH storage system design a practical problem with PEM FC performance has occurred. PEM FC hydrogen intake level is not constant with high peaks of hydrogen demand throughout the operation. An additional free space cylinder was introduced to the system meeting simultaneous FC demands. In the current design, free space was integrated into the reactor with no need for additional free space

cylinder in the system. Heating and cooling processes are performed by water supplied to the gaps between the housing and the camera. A detailed description of the reactor design and development is presented in Chapter 6. The MH was fully charged before the start of the experiment and was discharged by the desorption process for about 100 min. The pressure in the MH reactor is shown in Figure 62, power distribution – in Figure 63.

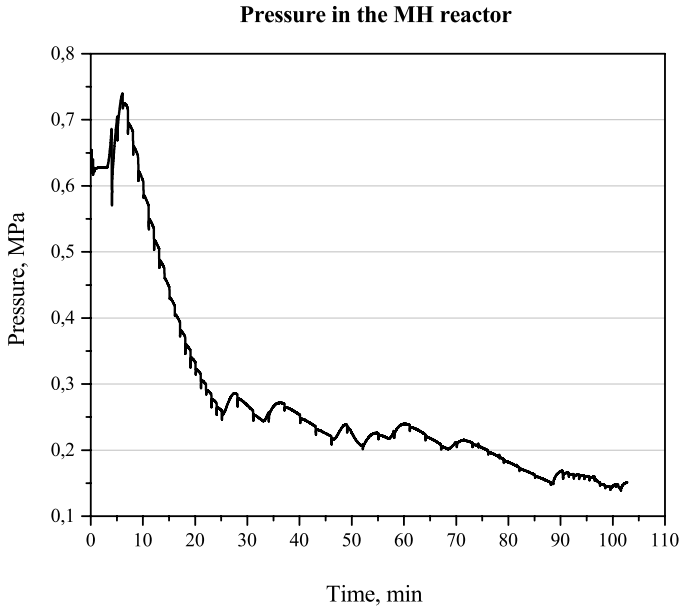

Figure 62. Pressure in the MH reactor

Previously, the pressure level of an FC hydrogen inlet pressure was found experimentally to be around 0.13MPa [194], [205]-[206]. In this experiment, the MH reactor was able to maintain needed pressure level for the entire duration of the experiment. The graph shows that the pressure rose to 0.7MPa before the valve was open, then it decreased to 0.25MPa and started to decrease with the decrease of the amount of hydrogen left in the system. Peaks on the graph are the periodic pressure drops (figure 43), H2 purging impulses which are necessary to remove excessive water from the fuel cell. Their appearance is typical for the operation of fuel cells at temperatures below 100°C.

During the first 4 minutes the battery was supplying the FC start-up procedures, then the load on the FC was zero. Thus the FC was recharging the backup battery. On the 50^{th} minute, a 450W load was introduced. It was kept for 40 minutes, and then went back to zero. During these 40 minutes, the FC both met the load and powered up the battery. It was noted that in the case of load level being equal to the power FC could

provide, charging of the battery stops automatically. In the cases of the load being higher than the FC, the battery performs backup supply for the load. It was investigated more in the 6.2 of the current paper.

In Figure 63, the results of the experiments are shown in the two working regimes of the system:

1). zero demand load when all the energy from the FC charges the backup battery

2). increased demand load to 450W when the FC supplies both the battery and the demand

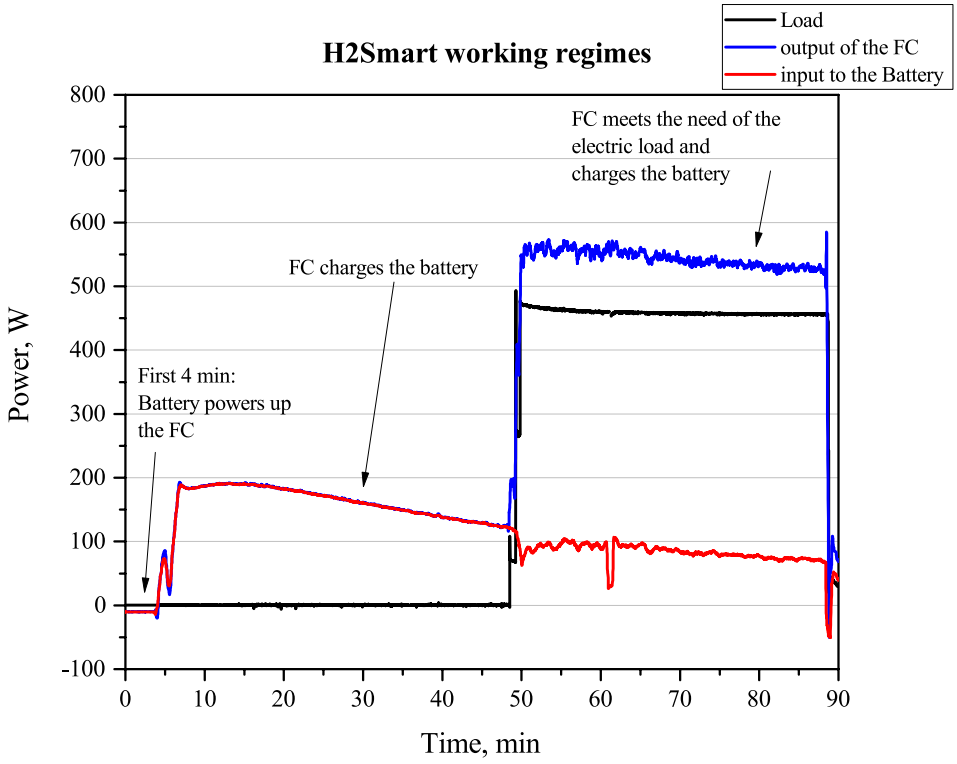

Figure 63. Power distribution during different working regimes

The black line indicates the power requested and received by the load; the red line shows the power received by the battery; the blue line signifies the power *output* of the fuel cell. The power output is positive on the graph, but the concept of output can be perceived as negative and stand for the sum of both loads (battery and the demand). On the first part of the picture, the blue line and the red line are identical due to the absence of the demand load. In case the FC shuts down or experience a low pressure of hydrogen from the MH back-up battery meets the demand of the load ensuring the reliability of the supply.

5.6 Experimental results, system response

The power distribution for the second part of experimental investigations is shown in Figure 64. The same color indication is used with the previous graph. For the first 17 minutes, enough pressure was supplied to the FC, and the load was increasing in a step-by-step process: 300W, 500W, and 700W. Then the pressure for FC was made below operational values of 0.055-0.083MPa gage pressure and the FC shut down can be noted in the 20th minute. The red lower line indicates that backup battery supply met the demand of the load. The same backup supply performance can be noted in the 125th minute, where FC again experienced a shutdown.

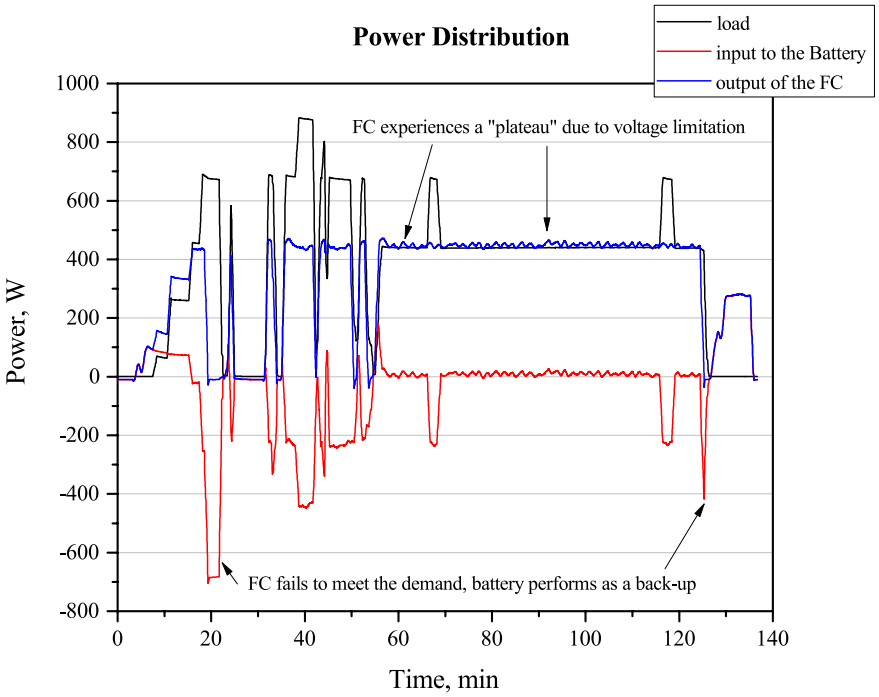

Figure 64. Power distribution during FC shut down and a system response

On the 22nd minute, rapid peak demand of the load was tested; FC started the operation and met the required power level of the demand. The lower red peak in the 22nd minute indicates the nuance we have noticed further on during the operation of the FC. Given different load levels higher and lower than 450W, the plateau of the FC was noted. After multiple additional experiments, we can assume that the voltage level of the battery limits the output of the FC. This nuance needs to be further investigated to draw any conclusions.

On the side of the power, the battery backup supplies FC start-up procedures, crisis shutdowns. The FC charges the battery as a regular load until it is charged completely.

During the experiment, the FC met the demand of the load as well as charged the battery. If the load exceeds the amount of power FC can provide, the battery stops the charging process automatically and meets the remaining demand of the load.

5.7 Experimental results, demand response

The concept described in this thesis has been proved to be feasible by the experimental test below. The H2Smart system starting temperature was around 5-8^{o}C. FC exhaust heat was supplied to the water inside the system and sent to the reactor. Figure 65 shows temperature measurements across the system: inside the fuel cell, inside the system, and inside the reactor. The purple line on the graph indicates temperature measurements inside the fuel cell, which increased to maximum 29^{o}C, then slowly decreased to 25^{o}C. Red and black lines indicate the temperature of the water inside the system before and after the reactor respectively. The blue line shows the temperature inside the reactor that increased to the maximum of 23^{o}C and then stayed relatively constant.

Throughout the experiment, the fuel cell met the demand of the load that slowly decreased. A power output of the fuel cell is shown in the Figure 66.

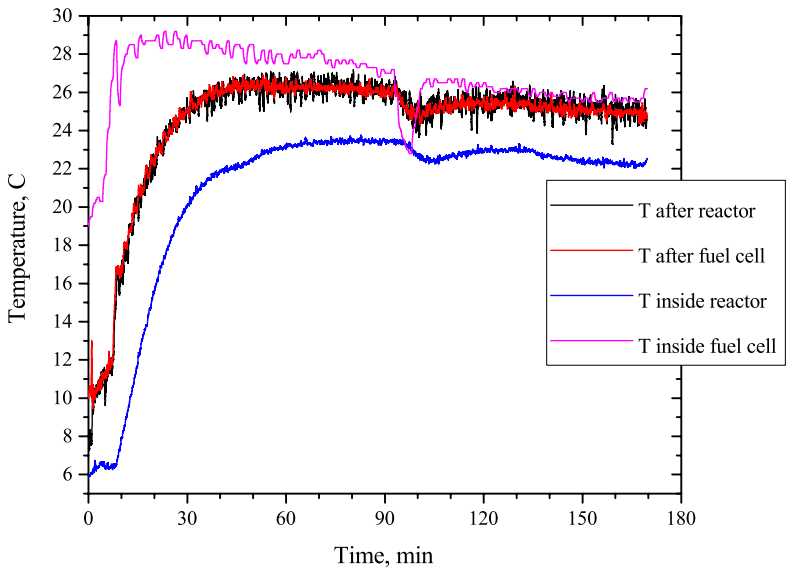

Figure 65. Temperature measurements across the system: inside the fuel cell, inside the system, and inside the reactor

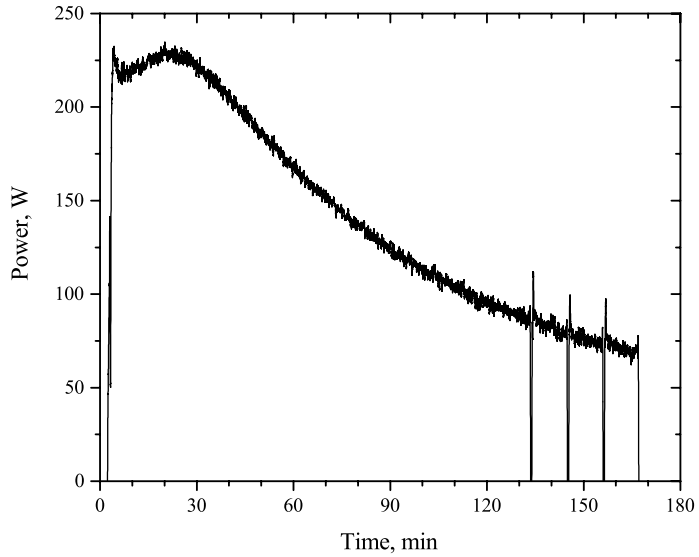

Figure 66. Power output of the FC

In the Figure 67, a pressure demand from the fuel cell is shown (red line). The measurements were taken after a reducer to 0.16 MPa; this is the needed pressure for the fuel cell performance.

Hydrogen output pressure from the MH reactor is shown in Figure 67 (black line). Throughout the experiment, MH reactor produced enough hydrogen pressure to supply successful fuel cell performance.

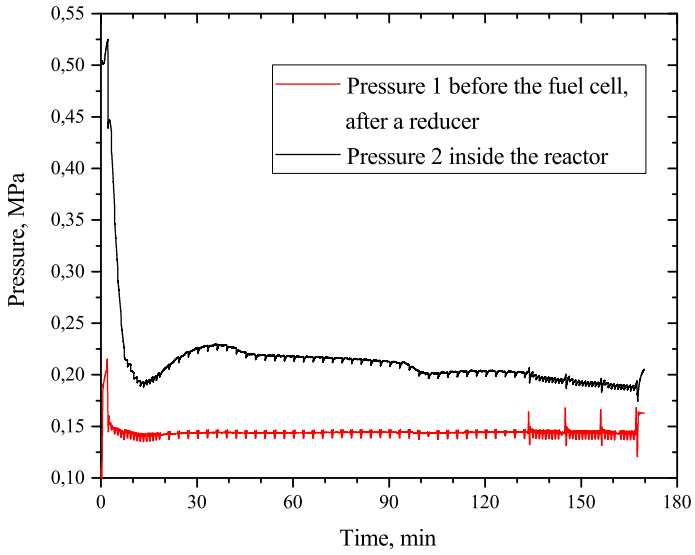

Figure 67. Pressure levels in MH reactor and FC inlet

On the next experiment, a similar concept but a longer period of time was tested. In Figure 68, the outcomes of the experiment are presented. MH reactor was able to

maintain the needed pressure level and supply FC with enough hydrogen flow to meet the demand throughout the experiment. On the temperature graph Figure 68a, the lowering of the temperature inside the reactor show that the volume of hydrogen was declining inside the reactor. The further experiment continues, the bigger is the difference between the temperatures after the FC and inside the reactor, which constitutes to the drawbacks of heat transfer after a long desorption process.

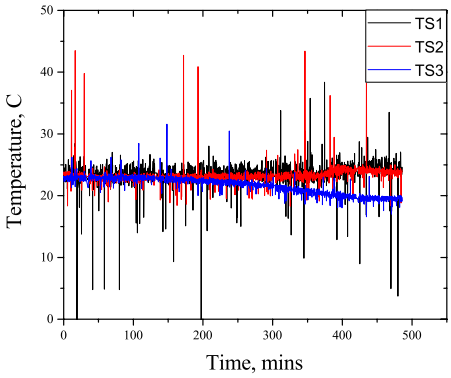

(a) - temperature after the reactor (black), after the FC (red), inside the reactor (blue)

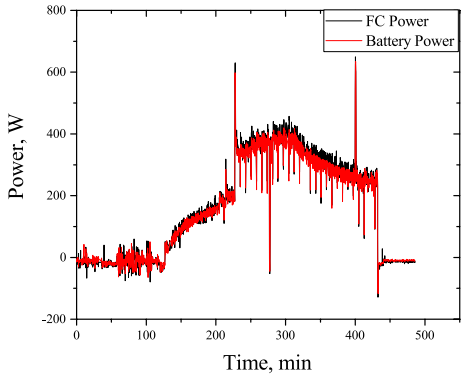

(b) – output power on the FC (black), input power on the battery (red)

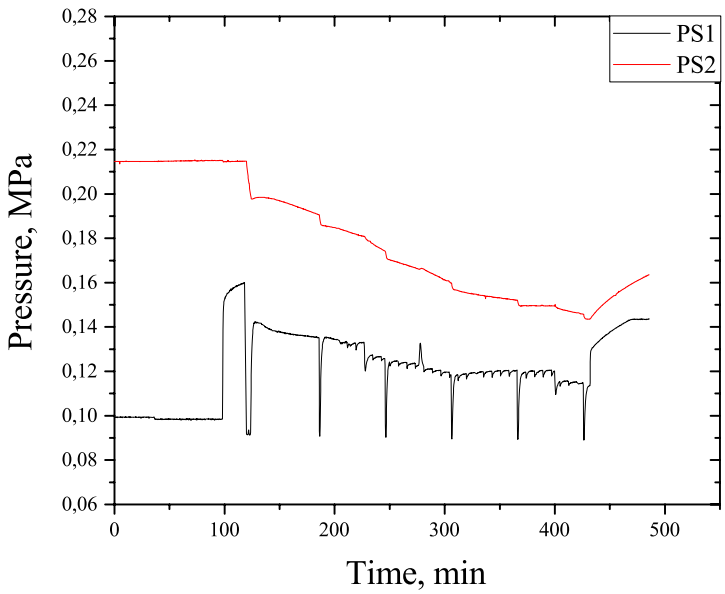

(c) – pressure inside the reactor (red), after the reducer and before the FC (black)

Figure 68. Experimental results H2Smart: (a) temperature, (b) power, (c) pressure

5.8 Chapter 5 conclusions

A novel type of hydrogen storage system with low-pressure MH hydrogen storage reactor, low-temperature PEM FC, electrolyzer, and an inverter is designed and developed. The system functions at the safe low-pressure operation levels. The PCT diagram of intermetallic compound with design requirements from Chapter 4 was obtained experimentally.

The results prove the possibility of technical realization of the proposed concept and study multiple working regimes, system and demand response, investigate the pressure levels depending on the temperature differences inside the system. H2Smart experimental set-up utilizes a novel type of MH reactor using exhaust heat inside the system and avoids external heat agents that previously eliminated the possibility of using MH hydrogen storage in an autonomous power supply.

The proposed system has significantly opened the possibility of creating a novel air-heated MH storage reactor and provided valuable kW scale experimental results for the further development of theoretical investigations in electrochemical investigations of MH storage in a bigger scale.

Chapter 6 Economic evaluation of the proposed concept

6.1 Test case description

The framework of economic evaluation of the project is based on the real case – Batamai village in Yakutia region where renewable energy sources were integrated in 2012. Batamai is a small village with a population of 233 people. Since 2012 the installed capacity of solar PVs was doubled and formed 60 kW of output power. The performance of RES system is justified by high solar insolation in Yakutia climate zone. The implementation of solar PVs leads to significant diesel fuel economy (i.e., 14,4 tones in 2015). Average power generation in 2015 is shown in Figure 69.

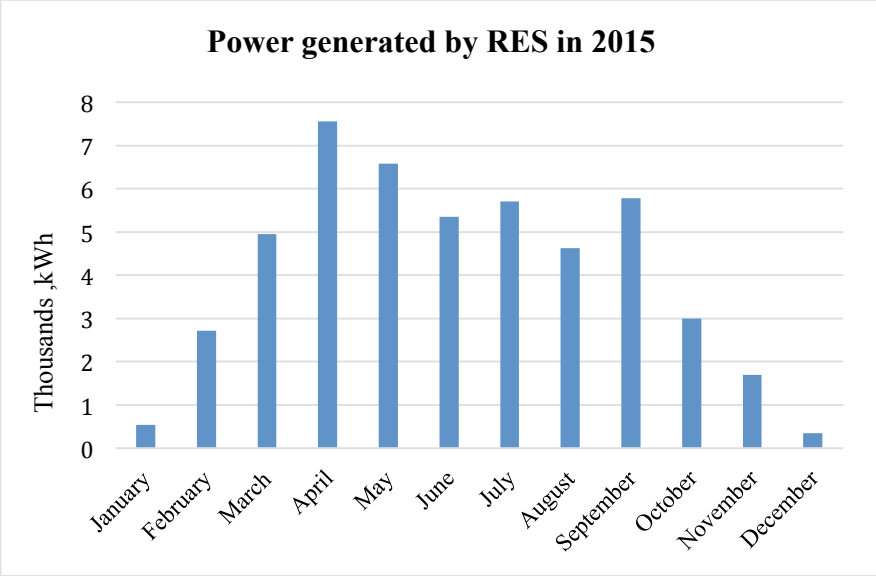

Figure 69. Power generated by RES in 2015

There real storage system, operating in Batamai, consists of 90 Lead Acid batteries and associated equipment such as inverters, controllers, etc. The installed capacity of the storage system is 27,6 kW. The assumption of current analysis states that the average number of operating hours is 200 hours per year while average autonomy time is 2 hours. When the backup storage system operates independently, it provides around 6% of total diesel fuel economy.

The goal of the economic evaluation is the comparison of hybrid hydrogen energy storage and the existing lead-acid energy storage system. The total costs of Lead Acid energy storage will be compared with five different economic scenarios of total costs of hybrid hydrogen energy storage. These scenarios present different prices for fuel cell and electrolyzer per kWh as well as prices for a kilogram of MH.

6.2 Methodology and data [219]

The 27,6 kW hydrogen system with 2 hours autonomy is proposed to be designed in the Batamai village for the economic comparison with an existing energy storage system. A simple model for estimation of capital, operational, and total costs for 15 years of ownership was created to compare the hybrid hydrogen backup system with conventional Lead Acid batteries. Hybrid hydrogen/batteries backup system (H2BS) combines Lead Acid batteries of a substantially lower capacity and hydrogen subsystem, including water electrolysis, fuel cells, and metal hydride hydrogen storage. As the technology is rather young, several price scenarios were estimated.

In the framework of this economic evaluation, NPV and IRR analyses are not provided rather focusing on real economic benefits (diesel fuel economy) of the system implementation. There are at least two critical factors such as infrastructural (smooth integration of solar PVs) and socio-economical (resilient power supply in the remote area) which could not be assumed or estimated. The goal of the economic investigation is to calculate and compare the costs of the existing system with the H2BS system. Moreover, discount rates are difficult to estimate due to the frequent changes of refinancing rate and bank interest rates. Thus it is hard to predict discount rates for the chosen long term, as well as currency exchange rates. Life-cycle cost-benefit analysis is not useful due to the frequent changes in state policy and legislation in the field of energy efficiency and RES.

The assumption is that the Total Costs of the system is the sum of Capital Expenditures (CAPEX) and Operational Expenditures (OPEX) from zero years (the year when CAPEX are invested) to the year which corresponds to the last one in the framework of the comparison (T):

$$TCO = \sum_{j=0}^{T} CAPEX + \sum_{j=1}^{T} OPEX \tag{6.1}$$

Table 17 presents necessary data for the model. It includes retail prices of equipment in US dollars, production and service prices in rubles. All the prices correspond to the years 2015-2017 prices for equipment, service, and production.

6.3 Lead-acid batteries

CAPEX are the expenditures for the system creation and installation, includes also a necessary infrastructure, such as invertors, controllers, etc. Thus the equation contains

additional 20% for this equipment and assembly:

$$CAPEX^0{}_{BAT} = 1.2 N_{BAT} PR_{BAT} \quad (6.2)$$

Number of batteries scheduled for utilization is

$$N^j{}_{util} = N_{BAT} / t_{BAT} + N^{j-1}{}_{util} / t_{BAT},\ N^0{}_{util} = 0 \quad (6.3)$$

Replacement cost for the year j:

$$CAPEX^j{}_{BAT} = CAPEX^0{}_{BAT} / t_{BAT} + CAPEX^{j-1}{}_{BAT} / t_{BAT} \quad (6.4)$$

Operating expenditures for the year j are combined from the costs of electricity, utilization, and testing:

$$OPEX^j{}_{BAT} = PR_{kWh} t_{out} P_{nom} / \eta_{BAT} / C_{loss} + N^j{}_{util} PR_{util} + PR_{test} \quad (6.5)$$

Table 17. Data for the model

Backup power system requirements			**Lead Acid Batteries**		
Nominal power, kW	P_{nom}	27,6	Capacity, Ah	C_{BAT}	300
Nominal DC voltage, V	U_{nom}	48	Nominal voltage, V	U_{BAT}	3,2
Autonomy time, h	t_{nom}	2	Battery testing, RUB/year	PR_{test}	60,000
Total annual power outage, h/year	t_{out}	200	Battery efficiency, %	η_{BAT}	80
Comparison term, years	T	15	Nominal depth of discharge, %	DOD_{BAT}	80
Metal hydride reactor RS-L			Self-discharge, %/year	C_{loss}	30
Reactor price, RUB	PR_{RSL}	100,000	Battery mass, kg	m_{BAT}	48
Alloy mass per reactor, kg	m_{MH}	100	Retail price, USD	PR_{BAT}	435
Alloy price, RUB/kg	PR_{MH}	6000	Battery lifespan, years	t_{BAT}	4
Nominal alloy capacity, %wt.	C_{H2}	1.1	Utilization, USD/kg	RR_{util}	1.4
Nominal RS-L H_2 capacity, st.m^3	V_{H2}	12.25			
Fuel cell			**Other data**		
Nominal power, kW	P_{FC}	10	H_2 density, g/st.m^3	ρ_{H2}	89.8
FC price, USD/kW	PR_{FC}	5000	H_2 lowest heating value, MJ/kg	LHV_{H2}	119.91
FC efficiency	η_{FC}	50	H_2 99.999% per 40L cylinder (6 st.m^3), RUB	PR_{H2}	11,000
FC maintenance, RUB/year	PR^{FC}_m	10,000	H_2 99.98% per 40L cylinder (6 st.m^3), RUB	PR_{H2}	1800
Electrolyzer			H2BS maintenance, RUB/year	PR_{H2BS}	30,000
EL productivity, st.m^3/h	q_{EL}	0.2	Electricity price,	PR_{kWh}	15

			RUB/kWh		
EL price, USD/kW	PR_{EL}	5000	RUB/USD (Apr 2016)	PR_{USD}	62
EL efficiency, %	η_{EL}	65	RUB/EUR (Dec 2016)	PR_{EUR}	64

6.4 H2BS Hybrid Hydrogen Energy Storage

As Hybrid hydrogen energy system H2BS contains Lead Acid batteries for the startup process, the specification of the percentage of batteries in the system is necessary. The parameter K is the part of the load, which is covered by a fuel cell. Thus the number of RS-L metal hydride reactors might be calculated as:

$$N_{MH} = P_{nom} t_{nom} R / V_{ном} / LHV_{H_2} / \rho_{H_2} / \eta_{FC} \tag{6.6}$$

Additional 20% for the system balance and assembly are part of the H2BS CAPEX equation, which includes the costs of FCs, MH, batteries, and electrolyzer:

$$CAPEX_{H2BS} = 1.2(RN_{MH}(PR_{RSL} + m_{MH} PR_{MH}) + RP_{nom} PR_{FC} + q_{EL} LHV_{H_2} \rho_{H_2} PR_{EL} / \eta_{EL}) + \\ +(1-R) CAPEX_{BAT} \tag{6.7}$$

Operating expenditures:

$$OPEX^{j}{}_{H2BS} = PR_{kWh} t_{out} P_{nom}(R / \eta_{EL} + (1-R) / \eta_{LAB} / C_{loss}) + (1-R) N^{j}{}_{util} PR_{util} + PR_{H2BS} \tag{6.8}$$

6.5 Results and conclusions

Results of the comparison are presented in the Figure 70. The conservative scenario for H2BS storage system is **'H2BS: Electrolyzer&Fuel cell ($5000/kW) + MH ($100/kg)'** as the technology is considerably new with high costs. It could be noticed that H2BS system has more significant Capital Cost than the Lead Acid batteries have. However, this cost doesn't change significantly during the lifetime, while conventional battery systems are suffering from rather substantial Operational Costs and the need for replacement due to the loss of capacity, which make the H2BS system cheaper in a long-term span (10 years and more).

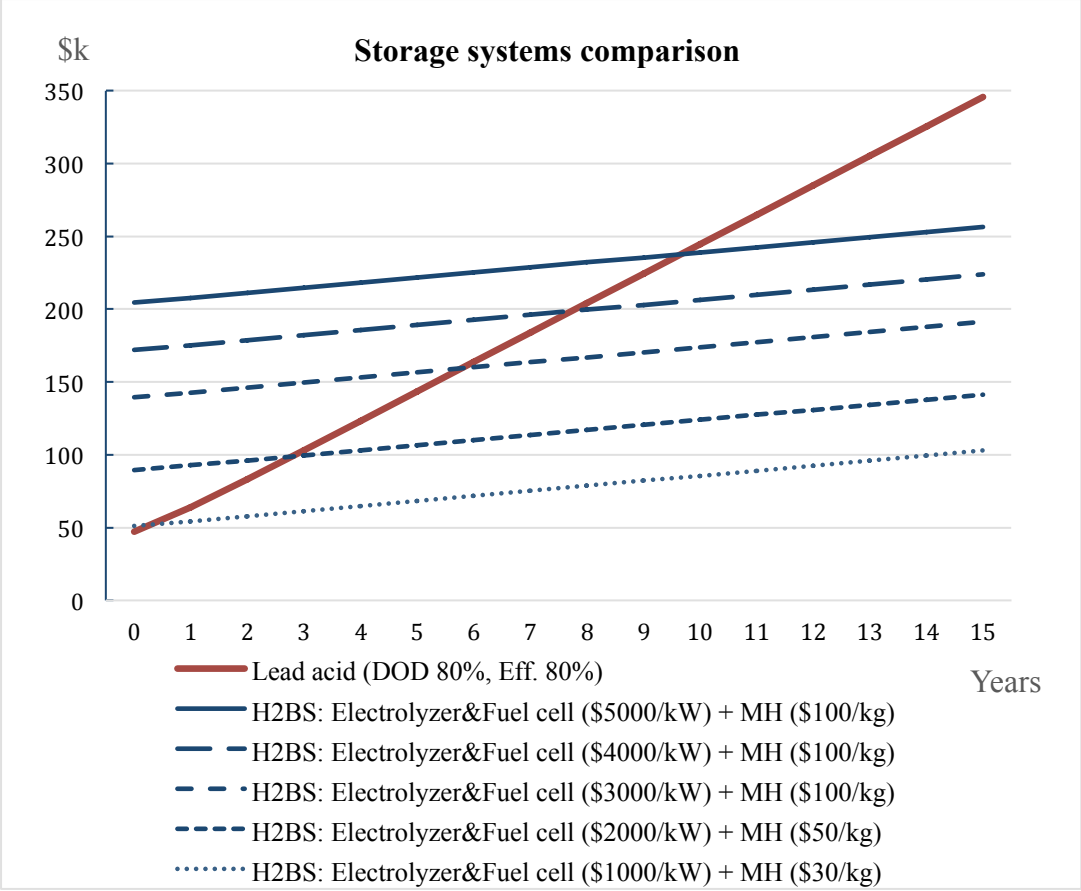

Figure 70. Comparison of the technologies in terms of cost

Lead-acid batteries technology is well developed with established supply chain; however the issues of this technology are also well known. The new technologies are required to provide valuable advantages to compete and overtake customer inertia. If the assumption would be that the same development level of hybrid hydrogen energy systems is already on the market, a new estimation of the costs is needed with the new lower prices for electrolyzer, fuel cell, and/or metal hydride. Total costs have a linear dependence on the mentioned prices (Figure 70) – the lower the prices are, the smaller system's CAPEX and thus the more competitive is H2BS system.

Major conclusions

In this dissertation, the design of four different energy storage technologies has been presented, including two novel experimental systems that can be considered as a "proof-of-concept" and one novel simulation methodology. The development and experimental investigations of these systems comprise the basis for MH storage system integration, intermetallic compounds composition, and heat and mass transfer intensification in the future.

Thereby the following statements are concluded from the current thesis:

- The H2Bio system was designed and developed to serve as a low power proof-of-concept for the proposed technology.

H2Bio is a 175W output power system that integrates MH reactor and PEM FC. Two MH reactors 140 l each can store and purify hydrogen due to the metallic alloy selectively absorbing hydrogen. System integration of the reactors suggest using free space in the next design of the reactor or installing a buffer before the FC to provide necessary volume of hydrogen for the impulsive manner of FC intake. The set of obtained system working regimes suggests that a commercial FC requires an energy source to start the system and support as a backup supply. The presence of excessive heat from the air cooling system in the FC has a potential to be utilized for the sorption process in the reactor. The increased ambient temperature and decreased relative humidity result in a significant power output decrease of the FC. The efficiency of an FC increases with increased humidity and decreased outlet temperature insignificantly.

- With the purpose of selecting a backup supply for the FC, a hardware-in-the-loop simulation methodology has been designed and developed.

A conventional battery model created by Tremblay Dessaint was integrated to the battery emulator and was connected to a Triphase controller with FC demand current profile from a real experiment (H2Bio working regimes, Chapter 2) programmed into it. SOC graphs of four types of batteries are responding to suggested current profiles were obtained and analyzed. The outcome suggests that a rapid response together with a smooth recovery of the battery is necessary for the performance with an FC. Even though all the batteries have met the demand and recovered quite fast the Lead Acid battery had the smoothest operation regime. Also, the integrated model has few limitations, including the absence of battery degradation. The mathematical model was

updated with fitted efficiency and degradation models to investigate the relation of costs and capacity level of the battery. It was concluded that lower SOC operation leads to lower loss of capacity but higher energy losses. Even though lower SOC lead to lower loss of capacity, for the case of Batamai, a reliable electricity generation system is required thus keeping the battery around the same SOC is a complex task. The outcome of this section suggests automatically charging the battery when excessive electricity is produced.

- Preliminary experimental investigations studied the possibility of FC exhaust heat utilization in a 1 kW system.

Preliminary investigations were designed to experimentally explore the possibility of supplying excessive heat from the FC to MH storage desorption. With this purpose, an internal and external temperature of the FC were measured, first integration and working regimes of PEM FC and MH were shown. The temperature experiments resulted in obtaining an average temperature of the exhaust air from the FC - 30^{o}C. The qualitative experiment proved that output hydrogen flow is enough to maintain required levels of hydrogen flow for 1.1 kW power output system. The 2.5 kW system requirements, however, were not met. The experiment also had great potential for better results as no thermal insulation was used and additional water was present in the reactor. Successful results of the preliminary investigations resulted in a design and development of a system that utilizes the proposed concept.

- IMC was selected depending on the outcomes of preliminary investigations, design requirements, technical requirements.

The variety of IMCs was studied to show satisfactory desorption pressure at 20-30 ^{o}C. The samples of IMCs were melted in an electric arc furnace from Cianflone Model 2701 with a non-consumable tungsten electrode on a water-cooled copper crystallizer in an argon atmosphere. The PCT diagram of a chosen IMC was obtained experimentally and showed satisfactory pressure levels even at the temperatures 10 ^{o}C below needed.

- The H2Smart system was designed and developed to utilize a proposed technology as well as a concept of FC exhaust heat utilization for the MH desorption process.

A novel type of hydrogen storage system with low-pressure MH hydrogen storage reactor, low-temperature PEM FC, electrolyzer, and an inverter was designed and developed to be autonomous from additional heat supplied to the system. The initial

scheme of the system was updated with a radiator that collects FC output heat and intensifies the desorption process in the MH reactor. The experimental results showed that the concept of heat utilization from the FC is feasible to be used for 1 kW hydrogen storage systems.

- Economical comparison of the proposed system with lead-acid batteries for the case of Far East settlements of Russia showed that the proposed system has an economic advantage over the batteries in the 10-15 year period due to no loss of capacity.

The primary outcome proves the possibility of creating an autonomous power generation unit based on low-pressure MH energy storage systems. It has also provided valuable kW scale experimental results for the further development of theoretical investigations of bigger scale MH storage and justified the need for creating a novel air-heated MH storage reactor. As a future outlook, a novel 30 kW MH storage system should be designed and developed for the field tests in the Batamai village.

Bibliography

[1] MacKay. SustainableEnergy–withoutthehotair.*UIT Cambridge*, 2009. ISBN 978-0-9544529-3-3. Available free online from www.withouthotair.com

[2] Lee K, Son KM, Gilsoo J. Smart storage system for seamless transition of customers with intermittent renewable energy sources into microgrid. In: *31st International telecommunications energy conference*; 2009. p. 1–5.

[3] Asmus P. Microgrids distributed energy systems for campus, military, remote, community, and commercial & industrial power applications: market analysis and forecasts. *Pike Report*; 2012.

[4] Mclarnon F, Cairns E. Energy storage. *Ann Rev Energy* 1989;14:241–71

[5] Pickard W, Shen Q, Hansing N. Parking the power: Strategies and physical limitations for bulk energy storage in supply-demand matching on a grid whose input power is provided by intermittent sources. *Renewable and Sustainable Energy Reviews* 2009;13:1934–45.

[6] H. Ibrahim. and others "Energy storage systems—Characteristics and comparisons", Renewable and Sustainable Energy Reviews 12 (2008) 1221–1250

[7] Chen H, Cong T, Yang W, Tan C, Li Y, Ding Y. Progress in electrical energy storage system: A critical review. *Progress in Natural Science* 19 (2009) 291–312

[8] Huggins R. Energy storage. Stanford, California, USA: Springer Science & Business Media; 2010.

[9] Abdrahamane Traore, Allan Taylor, M. A. Zohdy, F. Z. Peng "Modeling and Simulation of a Hybrid Energy Storage System for Residential Grid-Tied Solar Microgrid Systems" Journal of Power and Energy Engineering, (2017) 5, 28-39

[10] Report by Edison Electric Institute "Harnessing the Potential of Energy Storage" http://www.eei.org/issuesandpolicy/generation/Documents/EEI_HarnessingStorage_Final.pdf, May 2017

[11] Grid Energy Storage. U.S. Department of Energy https://www.sandia.gov/ess-ssl/docs/other/Grid_Energy_Storage_Dec_2013.pdf, December 2013

[12] Linden S. Bulk energy storage potential in the USA, current developments and future prospects. *Energy*. (2006) 31:3446–57.

[13] Makansi J, Abboud J. Energy storage: the missing link in the electricity value chain-An ESC White Paper. *Energy storage Council*. (2002) p.1-23

[14] Moore T, Douglas J. Energy storage, big opportunities on a smaller scale. *EPRI J* (2006) Spring Issue pp.16-23

[15] Styczynski ZA, Lombardi P, Seethapathy R et al. Electric energy storage and its tasks in the integration of wide-scale renewable resources. In: *GIGRE/IEEE PES joint symp*. (2009) pp. 1-11

[16] Li W, Joós G. Comparison of energy storage system technologies and configurations in a wind farm. In: *IEEE power electronics specialists conference*, Orlando, FL, USA, (2007) pp. 1280–1285.

[17]Kook KS, McKenzie K, Liu Y et al. A study on applications of energy storage for the wind power operation in power systems. In: *IEEE Power engineering society general meeting,* Montreal, QC, Canada, (2006) pp. 1–5.

[18]W. A. Braunecker, B. K. Hughes. Effect of Glass Transition Temperature on the Energy Storage Properties of Nitroxide Radical Containing Polymers. Conference, Phoenix, Arizona, 2015.

[19]Leou Rong-Cen. An economic analysis model for the energy storage system applied to a distribution substation. *Int J Electrical Power Energy Syst* 2012;34(1):132–7.

[20] Rodriguez GD. A utility perspective of the role of energy storage in the smart grid. In: *IEEE power and energy society general meeting*; (2010) pp. 1–2.

[21] Available from: http://www.sandia.gov/ess/esselect.html.

[22] Available from: http://www.kema.com/services/consulting/etd/es/PLATOS.aspx.

[23] Xingguo T, Qingmin L, Hui W, et al. Advances and trends of energy storage technology in Microgrid. *Electrical Power and Energy Systems* 44 (2013) 179–191

[24] Georgescu M, Barote L, Marinescu C, Clotea L. Smart electrical energy storage system for small power wind turbines. In: *12th International conference on optimization of electrical and electronic equipment*; (2010). p. 1191–197.

[25] Tan X, Lu S. Study on smart energy storage technology and control strategy in micro-grid. *Lecture notes in electrical engineering*. Vol. 138. (2011) p. 189–96.

[26] Hoffman MG, Sadovsky A, Kintner-Meyer MC et al. Analysis tools for sizing and placement of energy storage in grid applications: a literature review. *Pacific Northwest National Laboratory*; 2010.

[27] Kusko A, DeDad J. Stored energy-short-term and long-term energy storage methods for standby electric power systems. *IEEE Trans Ind Appl* 13 no. 4 (2007) pp.66-72

[28] Available from: http://www.beaconpower.com/products/EnergyStorageSystems/DocsPresentations.htm

[29] Available from: http://www.electricitystorage.org/ESA/applications/.

[30] Jewitt J. Impact of CAES on Wind in Tx, OK and NM, In: *Annual peer review meeting of DOE energy storage systems research*. San Francisco, USA (2005) pp. 1-16

[31] Karpinski A, Makovetski B, Russell S, et al. Silver-zinc: status of technology and applications. *J Power Sources 80* (1999) pp, 53-60

[32] McDowall JA. High power batteries for utilities – the world's most powerful battery and other developments, In: *Power engineering society general meeting*. IEEE, Denver, USA (2004)

[33] Available from: http://www.saftbatteries.com/

[34] Yeleti Sandeep, Fu Yong. Impacts of energy storage on the future power system. In: *North American power, symposium*; 2010.

[35] Dti Report. Review of electrical energy storage technologies and systems and of their potential for the UK

[36] Available from: http://www.fuelcelltoday.com/

[37] Electric Mobility Canada. Preliminary analysis of eVionyx Ni–Zn battery and Zn–Air fuel cell. Available on http://www.mec.ceveq.qc.ca/

[38] Available from: http://www.zbbenergy.com/technology.htm

[39] Steinfeld A, Meier A. Solar thermochemical process technology. In: *Encycl Energy. Elsevier Inc* Academic Press, Vol. 15, (2001) pp. 237-256

[40] Steinfeld A, Kuhn P, Reller A, et al. Solar-processed metals as clean energy carriers and water-splitters. *Int J Hydrogen Energy*

[41] Lovegrove K, Luzzi A, McCann M, et al. Exergy analysis of ammonia-based thermochemical solar power systems. *Sol Energy*

[42] Chen H, Ding Y. A cryogenic energy system using liquid/slush air as the energy carrier and waste heat and waste cold to maximise efficiency, specifically it does not use combustion in the expansion process. UK Patent G042226PT,

[43] Mclarnon FR, Cairns EJ. Energy storage. *Ann Rev Energy*

[44] Available: http://government.ru/en/department/85/events/ 2016

[45] Available: http://www.hevelsolar.com 2016

[46] Ustinov A., Khayrullina A., Borzenko V., Khmelik M., Sveshnikova A. Development method of Hybrid Energy Storage System, including PEM fuel cell and a battery. *Journal of Physics: Conference Series.* 2016. 745. p.032152.

[47] Efimov A. The experience of Solar PV installation in the Northern States of Russia. *SakhaEnergo presentation*, 2016

[48] Varkaraki E, Lymberopoulos N, Zoulias E, Guichardot D, Poli G. Hydrogen-based uninterruptible power supply. *Int J Hydrogen Energy* 32 (2007) 1589–1596.

[49] Mykhaylo V. Lototskyy, Moegamat Wafeeq Davids, Ivan Tolj, Yevgeniy V. Klochko, Bhogilla Satya Sekhar, Stanford Chidziva, Fahmida Smith, Dana Swanepoel, Bruno G. Pollet. Metal hydride systems for hydrogen storage and supply for stationary and automotive low temperature PEM fuel cell power modules. *Int J Hydrogen Energy* 40 (2015) 11491–11497.

[50] Borzenko V and Dunikov D Feasibility analysis of a hydrogen backup power system for Russian telecom market *J. Phys.: Conf. Ser*. 891 012077 (2017)

[51] Hydrogen, Fuel cell & Infrastructure Technologies Program. Multi-Year Research Development and Demonstration Plan. Planned program activities for 2003-2010. US Department of Energy, Energy Efficiency and Renewable Energy, Draft (June 3, 2003).

[52] Winter C. Hydrogen energy — Abundant, efficient, clean: A debate over the energy-system-of-change. *International Journal of Hydrogen Energy 34* (2009) S1-S52.

[53] Elam C.C. Realizing the hydrogen future: the International Energy Agency's efforts to advance hydrogen energy technologies *International Journal of Hydrogen Energy 28(6)* (2003) pp. 601-607.

[54] Baykara S.Z. Hydrogen as fuel: a critical technology? *Int. J. Hydrogen Energy 30* (2005) p. 545—553.

[55] Shpilrain E, Malyshenko S, Kuleshov G. Introduction to Hydrogen Energy. *M: Energoizdat*, (1984)

[56] Malyshenko S, Nazarova O.V. Hydrogen storage. *Nuclear-hydrogen energy and technology, M: Energoizdat,* (1988)

[57] Hydrogen in Metals. T.2. Applications. Alefelc G, Felkl I. Moscow. Mir (1981)

[58] Gamburg D, Semenov V, Dubovkin N, Smirnova L. Hydrogen. Characteristics, generation, storage, transportation, applications. M.: Chemistry, (1989) 672 p.

[59] Mishenko A, Application of hudrogen for automotive engines. Kiev: *Наукова дум-ка*, (1984)

[60] Irani R.S. Hydrogen Storage: High-Pressure Gas Containment. MRS Bulletin September 27 (2002) pp 680-682.

[61] Tarasov B, Lototsky M, Yartys V. The issues of hydrogen storage and the future of hydride application for hydrogen storage. *Russian chemical J*. L, №6 (2006) pp. 34-48.

[62] Encyclopedia of the Gas industry. 4th. Editor: Basnieva K. *«Tvant»,* 884 p.

[63] Zuttel A. Materials for hydrogen storage *Materials Today*, Volume 6, Issue 9, September (2003) pp. 24-33.

[64] Nijkamp, M. G., et al. *Appl. Phys*. A 72 (2001) p. 619.

[65] Isaeva V, Kustov L. Metallorganic structures – new materials for hydrogen storage. *Russian chemical J*, т. L, №6 (2006) pp. 56 - 72.

[66] Mao W.L, Mao H., Goncharov A.F., Struzhkin V.V., Guo Q, Hu J., Shu J., Hembley R.J., Somayaazulu M., Zhao Y. Hydrogen Clusters in Clathrate Hydrate *Science* v.297, (2002) pp. 2247 – 2249.

[67] Florusse L. J., Peters C. J. Schoonman J., Heister K. C., Koh C.A., Dec S.F., Marsh K.N., Sloan E.D. *Science*, 2004, v.306, p. 469-471

[68] Chahine R., Bose T.K., Veziroglu T.N., Derive C., Pottier J. //9th World Hydrogen Energy Conference. Hydrogen Energy Progress IX, 1993, v.2.

[69] Young K. S. *Proc. Society of Automotive Engineers*, 911703 (P-245), (1991) pp. 69-72.

[70] Young K. S. *Int. J. Hydrogen Energy*, v.17, # 7 (1992) pp.505-507.

[71] Tarasov B, Goldshleger N, Moravsky A. Carbon nanostructures. *Успехи химии*, 70, № 2 (2001) pp.149 -166.

[72] Schur D.V, Tarasov B.P., Zaginaichenko S. Yu. et.al. *Int. J. of Hydrogen* Energy, v. 27, N 10 (2002) p. 1063-1069.

[73] Schur D.V., Tarasov B.P., Shul'ga Y.M., Zaginaichenko S.Yu., Matysina Z.A., Pomytkin A.P. *Carbon*, v. 41, is. 7, (2003) pp. 1331-1342.

[74] Panella B., Hirscher M., Roth S. *Carbon*, v. 43, is. 10, (2005) pp. 2209-2214

[75] Rosi N.L., Eckert J., Eddaoudi M., Vodak D.T., Kim J., O'Keeffe M., Yaghi O.M. *Science*, v. 300, (2003) pp. 1127-1129

[76] James S. L. *Chem. Soc. Rev*., v. 32, (2003) pp. 276-288.

[77] Papaefstathiou G. S., MacGillivray L. R. *Coord. Chem. Rev*., v. 246, (2003) pp. 169-184.

[78] Nijkamp M. G., Raayamakers J. E. M. J., Dillen A. J., Jong K. P. *Appl. Phys*. A, v. 72, (2001) pp. 619-623

[79] Rowsell J. L. C., Millward A. R., Park K. S. Yaghi O. M. *J. Am. Chem. Soc*., v. 126, N 18, (2004) pp. 5666-5667.

[80] Tarasov B.P., Fokin V.N., Moravsky A.P., Shul'ga Yu.M., Yartys' v.A. *J. of Alloys and Compounds*, v. 253-254, (1997) pp. 25-28.

[81] Tarasov B.P. Hydrogen Materials Science and Chemistry of Metal Hydrides. *NATO Science Series II. Eds*. N. Veziroglu et. al. The Netherlands: Kluwer Academic Publishers, v. 71, (2002) pp. 283-290.

[82] M. Markiewicz, Y.Q. Zhang, A. Bösmann, N. Brückner, J. Thöming, P. Wasserscheid, S. Stolte, Environmental and health impact assessment of Liquid Organic Hydrogen Carrier (LOHC) systems – challenges and preliminary results, Energy Environ. Sci. 8 (2015) 1035–1045.

[83] C. Jensen, D. Brayton, S. Jorgensen, Development of a Practical Hydrogen Storage System Based on Liquid Organic Hydrogen Carriers and a Homogeneous Catalyst (IV.E.2) vol. 1, (2013), pp. 135–139.

[84] Päivi T. Aakko-Saksa, Chris Cook, Jari Kiviaho, Timo Repo. Liquid organic hydrogen carriers for transportation and storing of renewable energy – Review and discussion. Journal of Power Sources 396 (2018) pp. 803–823

[85] D. Teichmann, W. Arlt, P. Wasserscheid, Liquid Organic Hydrogen Carriers as an efficient vector for the transport and storage of renewable energy, Int. J. Hydrogen Energy 37 (2012) pp. 18118–18132

[86] M.J. Schneider, Hydrogen Storage and Distribution via Liquid Organic Carriers, (2015)

[87] Tarasov B.P., Shul'ga Yu.M., Fokin v.N., Vasilets v.N., Shul'ga N.Yu., Schur D.V., Yartys V.A. *J. of Alloys and Compounds*, v. 314, N 1-2, (2001) pp. 296-300.

[88] Verbetsky V.N., Malyshenko S.P., Mitrokhin S.V., Solovey V.V., Shmal'ko Yu.F. Metal Hydrides: Properties and practical applications. Review of the works in CIS-countries. *International Journal of Hydrogen Energy*. V.23. No 12. (1998) pp.1165-1177.

[89] Sandrock G., A panoramic overview of hydrogen storage alloys from a gas reaction point of view. *Journal of Alloys and Compounds* 293-295, (1999) pp. 877-888

[90] Uehara I., Sakai T., Ishikawa H. The state of research and development for applications of metal hydrides in *Japan. Journ. of Alloys and Compounds*. v. 253-254 (1997) pp.635-641

[91] Kolacheva B, Shalin R, Ilin A. Alloys for hydrogen storage. — M.: *Metallurgy*, (1995)

[92] Tarasov B, Burnasheva V, Lototsky M, Yartys V. Hydrogen storage methods and the opportunities for metal hydride materials application. *Alternative energy and ecology* 12 (2005) pp. 14-37.

[93] Rudman, P.S., Sandrock, G.D., Goodell, P.D. Hydrogen separation from gas mixtures using LaNi5 pellets. *Journal of the Less Common Metals* 89, (1983) pp. 437-446

[94] Huston E.L., Sandrock G.D. Engineering properits of metal hydrides. *J. Less–Common Met*, 74, (1980) p. 435-443.

[95] Zhao Shuang*, Lin Qin, Chen Ning, Ma Li, Ye Wen. Calculation and prediction for the hydriding properties of $LaNi_{5-x}$ Mx alloys. *Journal of Alloys and Compounds* 287, (1999) pp. 57–61.

[96] Achard J.C., Percheron-Guegan A., Dias H., Briacourt F. Rare earth ternary hydrides. Hydrogen strage applications. 2nd int. Congress on hydrogen in metals (Paris, 6-11 june 1977): *Proc.-Pergamon Press*., Oxford: 1978.

[97] Van Vucht J.H.N., Kuijpers F.A., Bruning H.C.A.M. Reversible room-temperature absorbtion of large quantities of hydrogen by intermetallic compounds. *Phlips Res. Repts* 25, (1970) pp.133-140.

[98] Kuijpers F.A., Van Mal H.H. Sorption hysteresis in the $LaNi_5$-H and SmCo5-H systems. *J. Less–Common Met*, V.23, (1971) pp.395-398.

[99] Bushcow K.H.J., Velge W.A.J.J. Phase relation and hydrogen absorbtion in the lanthanum-nickel system. *J. Less–Common Met* V.29 (1972) pp.203-210.

[100] Masahiro K. Hydrogen absorbtion and desorption by $LaNi_4$. Jap. *J.Appl. Phys*, V.16, №8, (1977) pp.1477-1478.

[101] Van Mal H.H. Stability of ternary hydrides and some applications. *Philips Res. Repts.Suppl,* V.1, (1976) pp.1-88.

[102] Van Mal H.H., Bushcow K.H..J., Miedema A.R. Hydrogen absorption in $LaNi_5$ and related compounds: experimental observation and their explanation. *J. Less–Common Met* V.35, (1974) pp.65-76.

[103] Bushcow K.H.J., Van Mal H.H., Miedema A.R. Hydrogen absorption in intermetallic compounds of thorium.J. *Less–Common Met* V.42, (1975) pp.163-178.

[104] Hydrogen storage. *Nuclear-hydrogen energy and technology.* 8. — M.: *Энергоатомиздат*, (1988) pp. 155—205.

[105] Au M., Chen C., Ye Z., Fang T., Wu J., Wang O. The recovery, purification, storage and transport of hydrogen separated from industrial purge gas by means of mobile hydride containers. *International Journal of Hydrogen Energy* 21 (1996) pp 33-37.

[106]Sandrock G.D., Goodell P.D. Cyclic life of metal hydrides with impure hydrogen: Overview and engineering considerations. *Journal of the Less Common Metals* 104 (1984) pp. 159-173.

[107] Tarasov B, Shilkin B. Interaction of intermetallic compounds $LaNi_5$ и $CeCo_3$ with hydrogen in the presence of Ar, CH_4 и CO_2. *Chemistry J*. T. 39. № 1. (1994) pp.18-22

[108] Artemov V, Lazarev D, Yankov G, Borzenko V, Dunikov D, Malyshenko S. Influence of unabsorbed gas impurities on the processes of heat and mass transfer in metal hydride devices for the accumulation and purification of hydrogen. *Thermophysics of high temperatures*.. T. 42. № 6. (2004) p. 972

[109] Tarasov B, Shilkin S. Influence of O_2, CO и SO_2 for hydrogen sorbtion characteristics of $LaNi_5$ и $CeCo_3$. *Chemistry J*. T. 40. № 5. (1995) pp 736-742

[110] Sandrock G.D., Goodell P.D., Surface poisoning of LaNi5, FeTi and (Fe,Mn)Ti by O2, Co and H2O. *Journal of the Less Common Metals*, 73 (1980) 161-168

[111] Lee M., et al. Thermal conductivity measurements of copper-coated metal hydrides (LaNi5, Ca0.6Mm0.4Ni5, and LaNi4.75Al0.25) for use in metal hydride

hydrogen compression systems. *International Journal of Hydrogen Energy*. V. 34. № 7. (2009) p. 3185.

[112] Borzenko V I, Dunikov D O, Malyshenko S P Reversible solid-state hydrogen storage systems and their integration with PEM FC. *Second Rus-Tai Symp on Hydrogen and FC Tecp App* (2009)

[113] Blinov DV, Borzenko VI, Dunikov DO, Romanov IA. Experimental investigations and a simple balance model of a metal hydride reactor. *Int J Hydrogen Energy* **39**: (2014) pp. 19361-19368

[114] Lototskyy M V, Yartys V A et al. Metal hydride hydrogen compressors: A review. *Int J Hydrogen Energy* **39** (2014) pp. 5818-5851

[115] Shilov AL, Efremenko NE. Effect of sloping pressure "plateau" in two-phase regions of hydride systems. *Russ J Phys Chem* 60 (1986) pp.3024-8.

[116] Larsen JW, Livesay BR. Hydriding kinetics of $SmCo_5$. *J Less- Common Met* 73 (1980) pp.79-88.

[117] Fujitani S, Nakamura H, Furukawa A, Nasako K, Satoh K, Imoto T, et al. A method for numerical expressions of P-C isotherms of hydrogen-absorbing alloys. *Z Phys Chem* 179 (1993) pp.27-33.

[118] Lototsky MV. A modification of the LachereKierstead theory for simulation of PCT diagrams of real "hydrogenehydride- forming material" systems. Kharkov Univ Bull/No. 477: *Chem Ser* 5(28), (2000) pp.45-53.

[119] Lototsky MV, Yartys VA, Marinin VS, Lototsky NM. Modelling of phase equilibria in metalehydrogen systems. *J Alloys Compds* (2003) 356-357:27-31.

[120] Park CN, Luo S, Flanagan TB. Analysis of sloping plateaux in alloys and intermetallic hydrides. I. Diagnostic features. *J Alloys Compds* (2004) 384:203-7.

[121] Lacher JR. A theoretical formula for the solubility of hydrogen in palladium. *Proc Roy Soc (Lond*) (1937) A161:525-45.

[122] Kierstead HA. A theory of multiplateau hydrogen absorption isotherms. J *Less-Common Met* (1980) 71:303-9.

[123] Brodowsky H, Yasuda K, Itagaki K. From partition function to phase diagramestatistical thermodynamics of the $LaNi_5eH$ system. *Z Phys Chem* (1993) 179:45-55.

[124] Beeri O, Cohen D, Gavra Z, Johnson JR, Mintz MH. Thermodynamic characterization and statistical thermodynamics of the TiCrMneH (D) system. *J Alloys Compds* (2000) 299:217-26.

[125] Murthy SS. Heat and mass transfer in solid state hydrogen storage: a review. J *Heat Transf* (2012) 134:031020.

[126] Goodell PD. Thermal conductivity of hydriding alloy powders and comparisons of reactor systems. *J Less- Common Met* (1980) 74:175-84.

[127] Sandrock G. A panoramic overview of hydrogen storage alloys from a gas reaction point of view. *J Alloys Compds* (1999) 293e295:877-88.

[128] Førde T, Maehlen JP, Yartys VA, Lototsky MV, Uchida H. Influence of intrinsic hydrogenation/dehydrogenation kinetics on the dynamic behaviour of metal hydrides: a semi-empirical model and its verification. *Int J Hydrogen Energy* (2007) 32:1041-9.

[129] Førde T, Næss E, Yartys VA. Modelling and experimental results of heat transfer in a metal hydride store during hydrogen charge and discharge. *Int J Hydrogen Energy* (2009) 34:5121-30.

[130] Friedlmeier G, Manthey A, Wanner M, Groll M. Cyclic stability of various application-relevant metal hydrides. *J Alloys Compds* (1995) 231:880-7.

[131] Wanner M, Friedlmeier G, Hoffmann G, Groll M. Thermodynamic and structural changes of various intermetallic compounds during extended cycling in closed systems. *J Alloys Compds* (1997) 253-254:692-7.

[132] Yartys V, Lototskyy M, Maehlen JP, Halldors H, Vik A, Strandm A. Continuously-operated metal hydride hydrogen compressor, and method of operating the same. Patent application WO (2010) 087723 A1, 2010.

[133] Lototskyy M, Klochko Ye, Linkov VM. Metal hydride hydrogen compressor. Patent application WO (2012) 114229 Al, 2012.

[134] Golben PM. Multi-stage hydride-hydrogen compressor. In: Proceedings of the eighteenth intersociety energy conversion engineering conference, Orlando, FL, August 21e26, 1983. Volume 4 (A84-30169 13-44). *New York: American Institute of Chemical Engineers;* (1983) pp. 1746-53.

[135] DaCosta DH. Advanced thermal hydrogen compression. Proc 2000 *hydrogen program review, NREL/CP*-570-28890 (2000)

[136] Murthy SS. Heat and mass transfer in solid state hydrogen storage: a review. J *Heat Transf* (2012) 134:031020.

[137] Dantzer P. Metal-hydride technology: a critical review. In: Wipf H, editor. Hydrogen in metals III. Properties and applications. *Berlin-Heidelberg: Springer-Verlag* (1997) pp. 279-340.

[138] Smith KC, Fisher TS. Models for metal hydride particle shape, packing, and heat transfer. *Int J Hydrogen Energy* (2012) 37:13417e-8.

[139] Visaria M, Mudawar I. Experimental investigation and theoretical modeling of dehydriding process in high- pressure metal hydride hydrogen storage systems. *Int J Hydrogen Energy* (2012) 37:5735-49.

[140] Garrison SL, Hardy BJ, Gorbounov MB, Tamburello DA, Corgnale C, vanHassel BA, et al. Optimization of internal heat exchangers for hydrogen storage tanks utilizing metal hydrides. *Int J Hydrogen Energy* (2012) 37:2850-61.

[141] Wang H, Prasad AK, Advani SG. Hydrogen storage systems based on hydride materials with enhanced thermal conductivity. *Int J Hydrogen Energy* (2012) 37:290-8.

[142] Talaganis BA, Meyer GO, Aguirre PA. Modeling and simulation of absorptionedesorption cyclic processes for hydrogen storage-compression using metal hydrides. *Int J Hydrogen Energy* (2011) 36:13621-31.

[143] Bhouri M, Goyette J, Hardy BJ, Anton DL. Honeycomb metallic structure for improving heat exchange in hydrogen storage system. *Int J Hydrogen Energy* (2011) 36:6723-38.

[144] Baichtok YK, Avetisov AK, Baranov YM, Telyashev RG, Mordkovich VZ, Suvorkin SV, et al. Shell and tube module for a hydride thermosorption hydrogen separator and compressor. Patent Application WO 2013/006091 A1 (PCT/RU20121000522) (2013)

[145] Hu X, Qi Z, Yang M, Chen J. A 38 MPa compressor based on metal hydrides. *J Shanghai Jiaotong Univ* (Sci) (2012) 17(1):53-7.

[146] Lototsky M, Halldors H, Klochko Ye, Ren J, Linkov V. 7-200 bar/60 L/h continuously operated metal hydride hydrogen compressor. In: Schur DV, Zaginaichenko SYu, Veziroglu TN, Skorokhod VV, editors. *Hydrogen materials science and chemistry of carbon nanomaterials: ICHMS'2009* XI Int Conf, Yalta Crimea Ukraine, August 25-31, 2009. Kiev: AHEU Publ (2009) pp. 298-9.

[147] Bocharnikov MS, Yanenko YuV, Tarasov BP. Metal hydride thermosorption compressor of hydrogen high pressure. *Int Sci J Altern Energy Ecol* ISJAEE (2012) 12(116):18-23.

[148] Wang H, Prasad AK, Advani SG. Hydrogen storage systems based on hydride materials with enhanced thermal conductivity. *Int J Hydrogen Energy* (2012) 37:290-8.

[149] Krokos CA, Nikolic D, Kikkinides ES, Georgiadis MC, Stubos AK. Modeling and optimization of multi-tubular metal hydride beds for efficient hydrogen storage. *Int J Hydrogen Energy* (2009) 34:9128-40

[150] Voss MG, Stevenson JR, Mross GA. Hydrogen storage and release device. Patent US 7455723 B2; (2008)

[151] Kelly NA, Girdwood R. Evaluation of a thermally-driven metal-hydride-based hydrogen compressor. *Int J Hydrogen Energy* (2012) 37:10898-916.

[152] Ivanovsky AI, Kolosov VI, Lototsky MV, Solovey VV, Shmal'ko YF, Kennedy LA. Metal hydride thermosorption compressors with improved dynamic characteristics. *Int J Hydrogen Energy* (1996) 21:1053-5.

[153] Lototsky M, Halldors H, Klochko Ye, Ren J, Linkov V. 7e200 bar/60 L/h continuously operated metal hydride hydrogen compressor. In: Schur DV,

Zaginaichenko SYu, Veziroglu TN, Skorokhod VV, editors. *Hydrogen materials science and chemistry of carbon nanomaterials*: ICHMS'2009 XI Int Conf, Yalta Crimea Ukraine, August 25e31, 2009. Kiev: AHEU Publ (2009) pp. 298-9.

[154] Ivanovsky AI, Kolosov VI, Lototsky MV, Solovey VV, Shmal'ko YF, Kennedy LA. Metal hydride thermosorption compressors with improved dynamic characteristics. *Int J Hydrogen Energy* (1996) 21:1053-5.

[155] Pearson D, Bowman R, Prina M, Wilson P. The Planck sorption cooler: using metal hydrides to produce 20K. J Alloys Compds (2007) 446-447:718-22.

[156] Morgante G, Pearson D, Melot F, Stassi P, Terenzi L, Wilson P, et al. Cryogenic characterization of the Planck sorption cooler system flight model. *JINST* 2009;4:T1(2016) http://iopscience.iop.org/1748-0221/4/12/T12016.

[157] Yartys V, Lototskyy M, Maehlen JP, Halldors H, Vik A, Strandm A. Continuously-operated metal hydride hydrogen compressor, and method of operating the same. Patent application WO 2010/087723 A1, (2010)

[158] Halene C. Method and apparatus for compressing hydrogen gas, Patent US 4995235 (1991)

[159] Ovshinsky SR, Young RT, Li Y, Myasnikov V, Sobolev V. Hydrogen storage bed system including an integrated thermal management system. Patent US 6833118 B2, (2004)

[160] Ovshinsky SR, Young RT, Li Y, Myasnikov V, Sobolev V, Bavarian F. Hydrogen storage bed system including an integrated thermal management system. Patent US 6878353 B2, (2005)

[161] Da Silva EP. Industrial prototype of a hydrogen compressor based on metallic hydride technology. *Int J Hydrogen Energy* (1993) 18(4):307-11.

[162] Shmal'ko YuF, Ivanovsky AI, Lototsky MV, Kolosov VI, Volosnikov DV. Sample pilot plant of industrial metal- hydride compressor. *Int J Hydrogen Energy* (1999) 24:645-8.

[163] Tamhankar S, Boyd T, Gulamhusein A, Golben M, DaCosta D. Integrated hydrogen production, purification and compression system. DoE hydrogen program, project PDP29, http://www.hydrogen.energy.gov/pdfs/review09/ pdp_29_tamhankar.pdf; (2009)

[164] Mykhaylo V. Lototskyy, Ivan Tolj, Lydia Pickering, Cordellia Sita, Frano Barbir, Volodymyr Yartys, "The use of metal hydrides in fuel cell applications", Progress in Natural Science: Materials International 27 (2017) 3–20

[165] R. Mohta1 and S. Orimo, "The renaissance of hydrides as energy materials", Nature Reviews, Materials, vol.2, №16091 (2016)

[166] M. Lototskyy, I. Tolj, M.W. Davids, P. Bujlo, F. Smith, B.G. Pollet, J. ''Distributed hybrid'' MH–CGH2 system for hydrogen storage and its supply to LT PEMFC power modules" Alloys Compds 645 (2015) S329–S333

[167] F. Gonzatti, V. Nizolli, F.Z. Ferrigolo, F.A. Farret, M.A. Silva de Mello, "Experimental Hydrogen Plant with Metal Hydrides to Store and Generate Electrical Power" *Int. J. Emerg. Electr. Power Syst. 17* (1) (2016) 59–67.

[168] G. Kyriakarakos, A.I. Dounis, S. Rozakis, K.G. Arvanitis, G. Papadakis, "Polygeneration microgrids: A viable solution in remote areas for supplying power, potable water and hydrogen as transportation fuel", *Appl. Energy 88* (2011) 4517–4526.

[169] J. Fernández-Moreno, G. Guelbenzu, A.J. Martín, M.A. Folgado, P. Ferreira-Aparicio, A.M. Chaparro, "A portable system powered with hydrogen and one single air-breathing PEM fuel cell" *Appl. Energy 109* (2013) 60–66.

[170] Borzenko V I, Dunikov D O, Malyshenko S P. Reversible solid-state hydrogen storage systems and their integration with PEM FC. *Second Rus-Tai Symp on Hydrogen and FC Tecp App* (2009)

[171] Blinov D V, Borzenko V I, Dunikov D O, Romanov I A. Experimental investigations and a simple balance model of a metal hydride reactor. *Int J Hydrogen Energy 39* (2014) 19361-19368

[172] Malyshenko S P, Borzenko V I, Dunikov D O, Nazarova O V Metal hydride technologies of hydrogen energy storage for independent power supply systems constructed on the basis of renewable sources of energy. *Thermal Engineering* 59 (6) (2012) pp 468 – 478

[173] Kim S and Hong I, "Effects of humidity and temperature on a proton exchange membrane fuel cell (PEMFC) stack," *J. Ind. Eng. Chem*. 14 (2008) 357–364

[174] Tolj I, Bezmalinovic D, and Barbir F, "Maintaining desired level of relative humidity throughout a fuel cell with spatially variable heat removal rates," *Int. J. Hydrogen Energy* 36, (2011) 13105–13113

[175] Jeon D, Kim K, Baek S, and Nam J, "The effect of relative humidity of the cathode on the performance and the uniformity of PEM fuel cells," *Int. J. Hydrogen Energy* 36(19) (2011) 12499–12511.

[176] Yan W, Wang X, Lee D, Zhang X, Guo Y, and Su A, "Experimental study of commercial size proton exchange membrane fuel cell performance," *Appl. Energy* 88, (2011) 392–396

[177] Hottinen T, Noponen M, Mennola T, Himanen O, Mikkola M, and Lund P, "Effect of ambient conditions on performance and current distribution of a polymer electrolyte membrane fuel cell," *J. Appl. Electrochem*. 33 (2003) 265–271

[178] Noorkami M, J et al., "Effect of temperature uncertainty on polymer electrolyte fuel cell performance," *Int. J. Hydrogen* 39 (2014) 1439–1448

[179] Lee P and Hwang S, "Performance characteristics of a PEM fuel cell with parallel flow channels at different cathode relative humidity levels," *Sensors* (Basel) 9 (2009) 9104–9121

[180] NurOzen D, Timurkutluk B, and Altinisik K, "Effects of operation temperature and reactant gas humidity levels on performance of PEM fuel cells," *Renewable Sustainable Energy* Rev. 59 (2016) 1298–1306

[181] Lin B, "The hydrogen fuel cell power system," in Conceptual Design and

Modeling of a Fuel Cell Scooter for Urban Asia, *Elsevier*, New York, (1999), Chap. 3, pp. 85–120.

[182] Svechnikova A, Abrosimov K, Khayrullina A, Ustinov A. *J of Ren. and Sust. E* 9 (2017) 044301

[183] Design and specification for safe and reliable battery systems for large ups. [Online]. Available: http://www.apcmedia.com/ (2016)

[184] Lelie M et al *Intelec conf* (2013)

[185] Bu-107: Comparison table of secondary batteries. [Online]. Available: http://batteryuniversity.com/learn/article/secondary batteries (2016)

[186] Design and testing of a fuel-cell- powered battery charging station. [Online]. Available: http://vtb.engr.sc.edu/vtbwebsite/downloads/publications/design and testing of a fuel- cellpowered battery charging station.pdf (2016)

[187] Ciez R E and Whitacre *J Energy Conversion and Management*, 112 (2016) pp. 435–444

[188] Tremblay O, Dessaint L A, and Dekkiche A I. A Generic Battery Model for the Dynamic Simulation of Hybrid Electric Vehicles. *Vehicle power and propulsion conf, VPPC 2007. IEEE.* (2007) pp. 284–289.

[189] Du¨rr M et al *J. of Pow Sources*, 161, no. 2, (2006) pp. 1400–1411

[190] Kuhn E et al *J. of Pow Sources*, 158, no. 2, (2006) pp. 1490–1497

[191] A. Shafiei A et al *Proc. Vehicle Power and Propulsion Conf. (VPPC) IEEE* (2011) pp. 1–5

[192] New dynamic battery model for hybrid vehicles. [Online]. Available: http://www.ijetae.com/files/Volume4Issue4/IJETAE 041E4 108.pdf (2016)

[193] Patsios, C.,Wu, B., Chatzinikolaou, E., Rogers, D. J., Wade, N., Brandon, N., Taylor, P. C., An integrated approach for the analysis and control of grid connected energy storage systems, *In Journal of Energy Storage*, Volume 5 (2016) pp. 48-61, ISSN 2352-152X

[194] Blinov D.V., Borzenko V.I., Dunikov D.O., Romanov I.A. Experimental investigations and a simple balance model of a metal hydride reactor. *Int J Hydrogen Energy*; 39 (2014) 19361-19368

[195] V. Borzenko, «The reserch of processes, design and development of a metal hydride system for storage and purification of hydrogen for the power plants based on the 1kW PEM FC», Dissertation, [in Russian] (2012)

[196] Askri F., Jemni A., Ben Nasrallah S. Prediction of transient heat and mass transfer in a closed metal—hydride reactor, *International Journal of Hydrogen Energy* (2004) 29. p. 195—208

[197] Askri F., Jemni A., Ben Nasrallah S. Dynamic behavior of metal–hydrogen reactor during hydriding process. *Int. J. Hydrogen Energy* (2004) 29, p. 635—647.

[198] Nakagawa T., Inomata A., Aoki H., Miura T. Numerical analysis of heat and mass transfer characteristics in the metal hydride bed. *International Journal of Hydrogen Energy* (2000) 25, p. 339—350

[199] Inomata A., Aoki H., Miura T. Measurements and modeling of hydriding and dehydriding kinetics // Journal of Alloys and Compounds (1998) 278 pp.103—109

[200] Borzenko V, Dunikov D, Lazarev D. Study of heat and mass transfer processes in experimental metal hydride reactors. *In: Proceedings of Problems of gas dynamics and heat and mass transfer in power plants. XV School-Seminar of Young Scientists and Specialists under the guidance of Academician RAS A.I. Leontiev T.2* (2005) pp. 231-234

[201] Lazarev D. Mathematical and numerical modeling of heat and mass transfer processes in metal hydride storage and purification of hydrogen. PhD thesis. M. (2006)

[202] Artemov V, Borovskih O, Lazarev D, Yankov G. Numerical analysis of heat and mass transfer processes in a shell-and-tube metal hydride hydrogen accumulator based on a mathematical model of porous media. *Vestnik MEI 1* (2008) pp.63-73

[203] Artemov V, Borovskih O, Lazarev D, Yankov G. The main factors limiting the rate of hydrogen sorption in metal hydride storage systems. *In Proceedings: International Symposium on Hydrogen Energy* (2005) pp. 121-126

[204] Artemov V, Borovskih O. et al. Evaluating the effectiveness of the finning of the active volume of a metal hydride reactor. *XVI School-Seminar for Young Scientists and Specialists. Acad. RAS A.I. Leontiev, "Problems of gas dynamics and heat and mass transfer in power plants"* (2007) in 2 volumes

[205] Borzenko V, Dunikov D, Malyshenko S. Crisis phenomena in metal hydride hydrogen storage facilities. *High Temp*;49(2) (2011) 249 – 256

[206] Malyshenko S, Borzenko V, Dunikov D, Nazarova O. Metal hydride technologies of hydrogen energy storage for independent power supply systems constructed on the basis of renewable sources of energy. *Thermal Engineering*; 59 (6) (2012) pp. 468 – 478

[207] Borzenko V, Eronin A. The use of air as a heating agent in hydrogen metal hydride storage coupled with PEM fuel cell. *Int Jof Hydrogen Energy*. V. 41, Issue 48, (2016) pp.23120–23124

[208] Züttel A. Materials for hydrogen storage. *Materials Today* (2003) pp.24–33.

[209] Mitrokhin S, Zotov T, Movlaev E, Verbetsky V. Hydrogen interaction with intermetallic compounds and alloys at high pressure. *J of Alloys and Compounds*; 580: (2013) pp.590-593

[210] Sandrock G. A panoramic overview of hydrogen storage alloys from a gas reaction point of view. *Journal of Alloys and Compounds*; 293-295 (1999) 877-888

[211] Uehara I., Sakai T., Ishikawa H. The state of research and development for applications of metal hydrides in Japan. *J Alloys and Compounds*; 253-254 (1997) 635-641

[212] Sakintuna B, Lamari-Darkrim F, Hirscher H, Metal hydride materials for solid hydrogen storage: A review. *Int J Hydrogen Energy*; 32 (2007) 1121-1140

[213] Malyshenko S, Borzenko V, Dunikov D, Nazarova O. Metal hydride technologies of hydrogen energy storage for independent power supply systems constructed on the basis of renewable sources of energy. *Thermal Engineering*; 59 (6)

(2012) 468 – 478

[214] Muller V., Blackledge D. Metal hydrides. M. : *Атомиздат*,. 432 (1973)

[215] Hemmes H., Driessen A., Griessen R. Thermodynamic properties of hydrogen between 100 and 1000 K at pressures up to 1 Mbar. *Physica* B+C. Т. 139–140. № 0. С. 116-118 (1986)

[216] Vargaftik N. Handbook of thermophysical properties of gases and liquids M. : *Science*, 721 (1972)

[217] McCarty R.D. Hydrogen Technological Survey. *Thermophysical Properties*. Washington, D.C. : NASA (1975)

[218] Dunikov D, Borzenko V, Blinov D, Kazakov A, Lin CY, Wu SY, Chu CY. Biohydrogen purification using metal hydride technologies. Int J Hydrogen Energy 41 (2016) 21787-21794

[219] Borzenko V and Dunikov D Feasibility analysis of a hydrogen backup power system for Russian telecom market *J. Phys.: Conf. Ser*. 891 (2017) 012077